UNIVERSITY OF CALIFORNIA,
IRVINE

Condensed-Phase Photochemical Processes in Secondary Organic Aerosols from Biogenic and Anthropogenic Sources

DISSERTATION

submitted in partial satisfaction of the requirements
for the degree of

DOCTOR OF PHILOSOPHY

in Chemistry

by

Kurtis Timothy Malecha

Dissertation Committee:
Professor Sergey A. Nizkorodov, Chair
Professor Barbara J. Finlayson-Pitts
Assistant Professor Craig Murray

2018

Chapter 2 © 2016 American Chemical Society
Chapter 3 © 2017 American Chemical Society
Chapter 4 © 2017 American Chemical Society
All other Materials © 2018 Kurtis Timothy Malecha

Dedication

To my Parents: Tim and Sue
For always putting up with my inquisitiveness, rambunctiousness, and stubbornness

~

"I have not failed. I've just found 10,000 ways that won't work."

"Many of life's failures are people who did not realize how close they were to success when they gave up."

-Thomas A. Edison

~

"All young people, regardless of sexual orientation or identity, deserve a safe and supportive environment in which to achieve their full potential."

-Harvey Milk

Table of Contents

TABLE OF CONTENTS ..... **III**

LIST OF ABBREVIATIONS ..... **V**

LIST OF FIGURES ..... **VII**

LIST OF TABLES ..... **XIII**

ACKNOWLEDGEMENTS ..... **XV**

CURRICULUM VITAE ..... **XIX**

ABSTRACT OF THE DISSERTATION ..... **XXV**

CHAPTER 1: INTRODUCTION **1**

1.1 BACKGROUND 2
1.1.1 Brief Context of Atmospheric Chemistry *2*
1.1.2 Atmospheric Aerosols *3*
1.1.3 Secondary Organic Aerosol Complexity *5*
1.2 AEROSOL AGING PROCESSES 7
1.2.1 Condensed-Phase Aerosol Photochemical Aging Techniques *10*
1.2.2 Photosensitization Reactions *12*
1.3 AEROSOL VOC PRECURSORS STUDIED 13
1.4 GENERAL METHODS OF THE DISSERTATION 15
1.4.1 SOA Generation and Collection from Smog Chamber *15*
1.4.2 SOA Generation and Collection from Aerosol Flow Tube *17*
1.4.3 Proton Transfer Reaction Time-of-Flight Mass Spectrometer *19*
1.4.4 Quartz Crystal Microbalance *20*
1.5 STRUCTURE OF THE DISSERTATION 20

CHAPTER 2: PHOTODEGRADATION OF SECONDARY ORGANIC AEROSOL PARTICLES AS A SOURCE OF SMALL, OXYGENATED VOLATILE ORGANIC COMPOUNDS **22**

2.1 ABSTRACT 23
2.2 INTRODUCTION 23
2.3 EXPERIMENTAL SECTION 26
2.4 RESULTS AND DISCUSSION 33
2.4.1 Photoproduction of OVOCs *33*
2.4.2 Control Experiments *37*
2.4.3 Mass Correlations to Photoproduction of OVOCs *38*
2.4.4 Discussion of Mass-Normalized Data across SOA Types *40*
2.4.5 Atmospheric Implications *42*
2.5 CONCLUSIONS 47

CHAPTER 3: PHOTODEGRADATION OF SECONDARY ORGANIC AEROSOL MATERIAL QUANTIFIED WITH A QUARTZ CRYSTAL MICROBALANCE **49**

3.1 ABSTRACT 50
3.2 INTRODUCTION 50
3.3 EXPERIMENTAL SECTION 52
3.4 RESULTS AND DISCUSSION 58

3.4.1 Observations of Photodegradation *58*
3.4.2 Comparing the PTR-ToF-MS and QCM Data *60*
3.4.3 Control Experiments *63*
3.4.4 Oxidation Flow Reactor Implications *64*
3.4.5 Atmospheric Implications *64*

CHAPTER 4: FEASIBILITY OF PHOTOSENSITIZED REACTIONS WITH SECONDARY ORGANIC AEROSOL PARTICLES IN THE PRESENCE OF VOLATILE ORGANIC COMPOUNDS 69

4.1 ABSTRACT 70
4.2 INTRODUCTION 71
4.3 EXPERIMENTAL SECTION 72
4.4 RESULTS AND DISCUSSION 80
4.4.1 Loss of Limonene and Formation of OVOCs *80*
4.4.2 Uptake Coefficients *82*
4.4.3 Absorption Spectra of Limonene Reaction Products *88*
4.4.4 Control Experiments *89*
4.4.5 Atmospheric Implications *91*
4.5 CONCLUSIONS 97

CHAPTER 5: PHOTOCHEMICAL REACTIONS ON TREE SURFACES 99

5.1 ABSTRACT 100
5.2 INTRODUCTION 100
5.3 EXPERIMENTAL SECTION 101
5.4 RESULTS AND DISCUSSION 108

REFERENCES 112

List of Abbreviations

Abbreviation	Meaning
APIN	α-pinene
APIN/NO_x	α-pinene oxidized by OH under high NO_x conditions
APIN/O_3	α-pinene oxidized by ozone
APIN/OH	α-pinene oxidized by OH under low NO_x conditions
BP	Benzophenone
CIMS	Chemical Ionization Mass Spectrometer
CRDS	Cavity Ring Down Spectroscopy
FMLR	Fractional Mass Loss Rate
FTIR	Fourier Transform Mass Spectroscopy
GC	Gas Chromatography
GUA	Guaiacol
GUA/NO_x	Guaiacol oxidized by OH under high NO_x conditions
GUA/OH	Guaiacol oxidized by OH under low NO_x conditions
IC	Imidazole-2-carboxyaldehyde
IPCC	Intergovernmental Panel on Climate Change
ISO	Isoprene
ISO/NO_x	Isoprene oxidized by OH under high NO_x conditions
ISO/O_3	Isoprene oxidized by ozone
ISO/OH	Isoprene oxidized by OH under low NO_x conditions
LIM	d-limonene
MOUDI	Micro Orifice Uniform Deposit Impactor
NAP	Naphthalene
NAP/NO_x	Naphthalene oxidized by OH under high NO_x conditions
NAP/OH	Naphthalene oxidized by OH under low NO_x conditions
OA	Organic Aerosol
OFR	Oxidation Flow Reactor
OVOCs	Oxygenated Volatile Organic Compounds
$PM_{2.5}$	Particulate Matter smaller than 2.5 micrometers in diameter
POA	Primary Organic Aerosol
ppbv	Parts per Billion by Volume
ppmv	Parts per Million by Volume
PTR-ToF-MS	Proton Transfer Reaction Time-of-Flight Mass Spectrometer
QCM	Quartz Crystal Microbalance
RH	Relative Humidity
SA	Succinic Acid
sccm	Standard Cubic Centimeters per Minute
SLM	Standard Liters per Minute

SMPS	Scanning Mobility Particle Sizer
SOA	Secondary Organic Aerosol
SVOC	Semivolatile Organic Compound
TET	Tetradecane
TET/NO_x	Tetradecane oxidized by OH under high NO_x conditions
TET/OH	Tetradecane oxidized by OH under low NO_x conditions
TMB	1,3,5-trimethylbenzene
TMB/NO_x	1,3,5-trimethylbenzene oxidized by OH under high NO_x conditions
TMB/OH	1,3,5-trimethylbenzene oxidized by OH under low NO_x conditions
UV-LED	Ultraviolet Light Emitting Diode
VOCs	Volatile Organic Compounds

List of Figures

Figure 1.1. Commonly-used methods for production of VOCs from aged OA. The blue circles correspond to the OA particles dispersed in a gaseous phase or collected on a substrate, while hν corresponds to photons of light inducing chemical aging often accompanied by the production of VOCs. 11

Figure 1.2. A diagram of the smog chamber utilized for this work. The constituents in parentheses were used as needed for specific experiments. 17

Figure 1.3. The aerosol flow tube setup. The VOC is injected and mixed with ozone at the entrance of the flow tube. After leaving the flow tube, the SOA is run through a charcoal denuder to remove ozone and other gasses. The HEPA filter provides makeup air for the MOUDI. 18

Figure 2.1. A diagram of SOA photodegradation experiments. The SOA is prepared in the chamber and monitored with the instruments on the left of the diagram. After a maximum particle concentration is achieved, the particles are collected, annealed, and thereafter irradiated with a UV-LED directly on the substrate. The resulting OVOCs are monitored with the PTR-ToF-MS. 27

Figure 2.2. The PTR-ToF-MS calibration plots for (A) acetaldehyde, (B) acetone, (C) acetic acid, and (D) formic acid. The horizontal axis is the PTR-ToF-MS measured mixing ratio and the vertical axis is the known amount that was injected into the chamber. Each data point has vertical and horizontal error bars corresponding to 95% confidence intervals of the amount of OVOC present and measured, respectively. The vertical error bars increase with the OVOC amount because of the accumulation of errors in the successive injections of the OVOC in the chamber. 32

Figure 2.3. A time profile of the PTR-ToF-MS run for the photoproduction of various VOCs from the ISO/O_3 SOA system. The UV-LED was turned on at 20 min and turned off at 115 min in this example. 34

Figure 2.4. The PTR-ToF-MS counts observed versus the mass collected for the various α-pinene SOA systems for the production of acetone. Production of other OVOCs also correlated with the mass of SOA for all the SOA samples analyzed in this study. 39

Figure 2.5. A bar plot showing the OVOC mixing ratios divided by the SOA mass collected for all SOA types. The error bars correspond to a 95% confidence interval range. The formic acid values are divided by 5 because its mixing ratios are much higher than for other OVOCs. 41

Figure 2.6. A plot comparing the spectral flux densities of the UV-LED and that of the sun at a solar zenith angle of 0°. 44

Figure 3.1. Incoming zero air at a flow of 150 sccm flows over the QCM crystal, and the OVOCs emitted as a result of irradiation are detected by the PTR-ToF-MS. The modified sample holder screws into the existing crystal holder, creating a sealed environment. Above the sealed mixing space (volume = 6.6 cm^3) is a 2.54 cm CaF_2 window compressed with o-rings to allow the UV light to irradiate the SOA particles on the QCM crystal. 53

Figure 3.2. The sensitivity factor C_S for each SOA type is compared with the theoretical value of 56.6 Hz cm^2 μg^{-1} (dashed horizontal line). The factors are not very dependent on the mass loading until they are less than 1 mg. 55

Figure 3.3. The spectral flux densities over the range of the electromagnetic spectrum of the pen-ray lamp (in green), 305 nm LED (in gray), and 365 nm LED (in orange), and the sun at both 40 km and 0 km (in red and blue, respectively) on the summer solstice in Los

Angeles, California. The left axis corresponds to the lamps, and the right axis (logarithmic scale) represents the sun's spectral flux density. 57

Figure 3.4. (a) Photoproduction of OVOCs observed during 254 nm irradiation of LIM/O_3 SOA. The lamp is turned on at ~10 min and turned off at ~85 min for this sample. (b) The baseline-corrected QCM frequency increases during irradiation because of the SOA material is losing mass. (c) The QCM frequency's mass loss rate, which was determined by taking the derivative of the frequency change with respect to time and then divided by C_f (Eq. 3.1), is also plotted..... 59

Figure 3.5. (a) The QCM- and PTR-ToF-MS mass loss rates are roughly linearly proportional to one another for all SOA types in this study with the slope being ~0.5. (b) The log-log plot of the same data to zoom in on smaller values. 62

Figure 3.6. The efficiency factor is plotted for the (a) APIN/O_3 and (b) LIM/O_3 data. Each curve is fit to an exponential decay (solid line). 66

Figure 3.7. The present of mass lost for the APIN/O_3 SOA during long 254 nm irradiation. Nearly all the APIN/O_3 SOA sample mass was lost during this long irradiation period.. 68

Figure 4.1. An overview of the SOA photosensitization experiments. (a) The SOA is prepared in the chamber, collected on an inert substrate, and annealed to remove volatile SOA components. (b) The sample is irradiated with a UV-LED directly on the substrate in a photolysis flow cell. A collapsible Teflon bag provides either purge air or air containing a known mixing ratio of limonene. The limonene and photoproduced OVOCs are monitored with the PTR-ToF-MS with an inlet flow of 0.2 SLM. 73

Figure 4.2. Schematic diagram of the flow cell. 77

Figure 4.3. The PTR-ToF-MS calibration plots for (A) acetaldehyde, (B) acetone, (C) acetic acid, and (D) d-limonene. The horizontal axis is the PTR-ToF-MS measured mixing ratio and the vertical axis is the known amount that was injected into the chamber. Each data point has vertical and horizontal error bars corresponding to 95% confidence intervals of the amount of VOC present and measured, respectively. The vertical error bars increase with the VOC amount because of the accumulation of errors in the successive injections of the VOC in the chamber. 79

Figure 4.4. An example of photoinduced uptake of limonene and photoproduction of various OVOCs from the NAP/NO_x SOA observed with the PTR-ToF-MS. The UV-LED was turned on at ~8 min and turned off at ~30 min. 81

Figure 4.5. A comparison of the absorption spectra of the BP/SA reference system after irradiation for samples irradiated in the presence of limonene and without the presence of limonene. 89

Figure 4.6. A regression plot of the limonene PTR-ToF-MS signal versus the UV-LED power for the high-NO_x SOA systems. Error bars correspond to the 95% confidence level for the ion counts of protonated limonene. The reduction in the ion counts is linear with respect to the power of the UV-LED. 90

Figure 4.7. The spectral flux densities over the near-UV range of the electromagnetic spectrum of the LED (in blue) and the sun (in red) on the summer solstice in Los Angeles, California. The left axis corresponds to the LED, and the right axis represents the sun's flux density. 92

Figure 5.1. The irradiance of the set of UV-B lamps (in blue), UV-A lamps (in red), and the solar irradiance at noon on the Summer solstice in Kuopio, Finland are compared between 250 and 400 nm. 103

Figure 5.2. An overview of the experimental setup used for the scots pine saplings. A stream of humidified air that can optionally contain ozone is fed to the Teflon bag containing the tree. Relative humidity and temperature are also measured in real time with a probe. UV-B lamps are turned on during specific stages of the experiment to initiate either stress of the tree or photochemistry of the SOA. Visible lamps are on at all times. A variety of instruments on the right-hand side of this figure are used for detection of species. The PTR-ToF-MS is connected directly to the bottom of the bag for reasons mentioned in the main text. The tree branch image is from the public domain. 105

Figure 5.3. A photograph of the experimental setup wherein a tree sapling is placed inside the Teflon bag. The visible lights are turned on in this example. 106

Figure 5.4. The PTR-ToF-MS traces for a typical experiment. The normalized (to the hydronium reagent ion) counts per second are presented on the y-axis and the time (in hr) is presented on the x-axis. Colored background shading corresponds to different experimental parameters. The initial bag and then plant background are presented with green shading. The first UV exposure is shown with blue shading. The next background is presented with no shading. Note that this time was shorter than other backgrounds for reasons mentioned in the experimental section. The ozone exposure is shown in pink shading. The second UV exposure is shown in purple shading. Finally, the background of the plant is shown in white shading at the end of the experiment. 109

Figure 5.5. The SMPS particle concentration data for two separate days of experiments. The ozone is fed to the bag right after the 0 hr mark. The ozone is stopped at the 1.5 hr mark for each of these days. On June 18, the UV-B lamps were turned on at the 2.5 hr mark, and for June 20, they were turned on at the 4.25 hr mark..... 110

List of Tables

Table 1.1. The VOCs used in this work to generate SOA. Column 1 lists the common name followed by the IUPAC name, and finally the abbreviation used in this dissertation. Column 2 shows the structure of each of the molecules. Column 3 categorizes which type of precursor each molecule is, and then it lists some common sources for each. 13

Table 2.1. Summary of the SOA samples prepared in this work.[a] 29

Table 2.2. The resulting calibration factors for each OVOC. For the SOA photodegradation experiments, we multiplied the mixing ratios measured by PTR-ToF-MS by this factor for each OVOC in the main text analysis. The subscripted digits correspond to the first nonsignificant digit. 33

Table 2.3. The top 10 increasing peaks (labeled by their nominal *m/z* values) during irradiation for each SOA system analyzed. The peaks are listed in descending order of the relative intensity change, with the peaks that increased the most appearing at the top.[a]..... 36

Table 2.4. The list of the high resolution *m/z* values for the PTR-ToF-MS peaks for the APIN/O_3 SOA system. The peaks are listed are in descending order for the overall intensity increase during irradiation. 37

Table 3.1. All the SOA samples examined in this study. Colum 3 contains the integrated photon fluxes for each sample. The 254 nm data's integrated flux only contains the emission line at 254 nm (other lines assumed to contribute little to photochemistry). Column 4 contains the mass collected on the QCM crystal after the annealing step mentioned in the main text. The masses were taken in triplicate and averaged. C_f was calculated as per the main text (the product of the mass collected and C_f is equal to the change in QCM frequency between the loaded crystal and clean crystal). The mass loss rates for this study were

taken during the initial part of the photodegradation, where the frequency change was linear. The PTR Mass Loss Rate was determined by summing up each of the 4 OVOCs' mass loss rates as discussed in the main text. 61

Table 4.1. Summary of the SOA Samples Prepared for This Work.[a] 75

Table 4.2 The reagents used for this study, their CAS registry numbers, their source, and their stated purity. 76

Table 4.3. The resulting calibration factors for each VOC. For the SOA photodegradation experiments, we multiplied the mixing ratios measured by the PTR-ToF-MS by this factor for each VOC in the main text analysis. The subscripts show the first digit that is not significant. 80

Table 4.4. Summary of the results of the photosensitization experiments.[a] 86

Table 4.5. The lifetimes of limonene with respect to different atmospheric sinks.[a] 93

Table 5.1. An overview of the experimental parameters used for these experiments. The X in each column corresponds to which parameters were employed at the given section of the experiment. The experiment progresses from top to bottom of this table. 107

Acknowledgements

I still recall the moment Professor Sergey Nizkorodov called to congratulate me on getting into UCI's Chemistry PhD program. I was suffering from strep throat, had lost my voice, and was rather bummed after doing poorly on a biochemistry exam. He left a very excited voicemail saying congratulations, pronounced my last name correctly (that's huge!), and even remembered bumping into me on the 3rd floor of Rowland Hall the previous summer. (That was when I did the Chem-SURF REU program with Professor Kenneth Janda.) I was thrilled about going to UCI for a PhD, and after arriving and rotating with excellent faculty, I chose to work in Sergey's lab. I have loved every moment of being in his lab. He allowed me to explore pretty much anything I wanted to. He gave me the independence I needed to work at my own pace, but he was always there to offer advice or mentoring when I needed it. Additionally, he always told me exactly what he thought about my (sometimes crazy) ideas, which I have really, truly appreciated. When things weren't going well, he always knew exactly what to say to get me on the right track again. Sergey really does care about his students, and this became increasingly evident as I progressed in this program. Thank you, Sergey, for providing me with so many amazing opportunities and a fantastic mentorship. I'm honored to be graduating from your group.

A very large thank you to my other committee members, Professor Barbara J. Finlayson-Pitts and Professor Craig Murray. Coming into graduate school, I had only limited experience with Atmospheric Chemistry. I knew I wanted to learn as much as possible in my first few months, and Professor Finlayson-Pitts was nothing short of encouraging and supportive in her Atmospheric Chemistry course and beyond. I especially appreciated her feedback and

suggestions during my advancement exam. Those led to more of the work I did for my dissertation. She is someone I truly look up to, and have nothing but respect for.

Professor Murray has also been paramount to my success. During my rotation in his laboratory, he helped me get on the right track with courses and managing the stress of graduate school. He, too, provided excellent ideas during my advancement exam. Outside of all this, he has served as a fantastic mentor whom I can talk with about a wide variety of subjects.

I must thank Dr. Véronique Perraud for all of the help over the years. Her constant positive attitude is infectious. Even when we were at our wit's end in trying to fix the PTR-MS, she always had new, creative ideas about what we could do next to fix it. She has taught me so much about laboratory work and how to maintain instruments. We also learned that having a "good luck troll" or chicken figurine on an instrument was absolutely necessary to fixing it.

The UCI School of Physical Sciences machine shop has also been extremely helpful over the years. They could make pretty much anything I could dream up, even with a sketch from me that was nowhere near to scale (and poorly drawn!). They were always cheerful and willing to help with whatever it was I needed.

To the other Nizkorodov group members, past and present, – thank you for all of the support and friendships over the years. I seriously wouldn't be where I am now without you. And of course, thank you for putting up with my nagging about punctuation and grammar on PowerPoint slides! I will certainly miss the board game days (Hi, Amanda!), Olive Garden lunches (Hi, Lauren!), delicious baked goods (Hi, Mallory!), hour long chats about life (Hi, Julia!), beach outings (Hi, Paige!), bowling nights (Hi, Dian!), and group BBQs (Hi, Sandy!).

Thanks to our game night crew (Hi, Lauren, Josh, Tory, Nick, John, and Jared!) for a weekly night of fun. Also, thanks for putting up with me venting for hours at a time! Having this

crew has made graduate school more fun, and I certainly cherished all these moments we've had together. To all my other friends, thank you for the support through the years. You know who you are!

Of course, even getting into a PhD program would not have been possible without my undergraduate advisors at Minnesota State, Mankato. I entered into college as a first-generation student, and I was quite overwhelmed. Professor Marie Pomije-Miller was the first faculty member I met at MSU. I told her I was interested in possibly doing a Chemistry major, and from that moment forward, she took a personal interest in seeing me succeed. She saw things in me that I didn't even know about, and she constantly pushed me to do the absolute best work I could do.

Professor John Thoemke was another one of my chemistry advisors at MSU. He was the first person I did chemistry research with. His work on Reactive Oxygen Species that are photoproduced in natural waterways in many ways became foundational to my work on photochemical processes in atmospheric aerosols for my PhD. He taught me so many tips and techniques about research and life in general. To both of these fantastic professors, I must extend a very heartfelt thank you.

Also, a huge shout out to my family! Thanks for not only encouraging me to always do my best, but for supporting all my academic endeavors. My parents, Tim and Sue, always taught me that school comes first, and play comes second. They instilled a hardworking, pragmatic outlook in me from a very young age. I never saw the reason for picking up those sticks in the yard as a child, but now I see why. Also, working at the family business growing up has taught me a lot of skills that I didn't think I would need. I can confidently tear down a laboratory instrument and troubleshoot it because of these foundational skills I learned. I also learned how

to work on many tasks simultaneously in this setting. Again, it has served me well in my graduate school career and beyond. So, thanks, Mom and Dad! Thank you to my sister, Katelynn, for always being there for me when I needed to just “chat” or when I was overly stressed and needed a pep talk. And I can’t forget the memories we made on our international brother-sister trips!

Thank you to my partner, Jared, for standing by me as I went through all of this – through all the highs and lows of this stage of my life. You are someone whom I cherish. I can’t count the number of times you’ve helped and supported me. Whether it be bringing me dinner when I was working on a paper late at night at the office, or pulling me back into reality when I was far too deep into something that didn’t matter, I would not be finishing my PhD in this timeframe.

Thank you to my favorite bands for the amazing music you’ve put out in the past few years! Music is something that I live for, and it always provides me with the framework I need to get through each day. I would like to especially thank M83, Arcade Fire, Austra, Enya, The War on Drugs, Nina Simone, First Aid Kit, Radiohead, and Perfume Genius, among many other wonderful artists.

Finally, and certainly not least, I would like to thank the National Science Foundation for support through the AGS-1227579 photochemistry in organic aerosols grant, the MRI-0923323 grant for the acquisition of the PTR-ToF-MS instrument, and the Graduate Research Fellowship Program for supporting a large amount of my PhD work. Also thank you to *Environmental Science & Technology*, the *Journal of Physical Chemistry A*, and *Environmental Science & Technology Letters* for allowing me to reuse my published work as part of this dissertation.

Curriculum Vitae

Kurtis Timothy Malecha

EDUCATION:

Chemistry, Doctor of Philosophy 2018
University of California, Irvine, Irvine, CA

Chemistry, Master of Science 2015
University of California, Irvine, Irvine, CA

Major: Chemistry, Bachelor of Science 2013
American Chemical Society Approved Summa Cum Laude
Minors: German and Mathematics Honors Program
Minnesota State University, Mankato, Mankato, MN Dean's List

INSTRUMENTATION AND SOFTWARE EXPERIENCES:

- Proton Transfer Reaction Time-of-Flight Mass Spectrometry, Inductively Coupled Plasma Mass Spectrometry, Iodide Chemical Ionization Mass Spectrometry, Scanning Mobility Particle Sizer, Gas Chromatography Mass Spectrometry, Atomic Absorption Spectrometer, High Performance Liquid Chromatography, Infrared Spectroscopy, UV-Visible Spectroscopy, Fluorescence, Capillary Electrophoresis, Quartz Crystal Microbalance, CO Analyzer, NO_y Analyzer, Ozone Analyzer, ^{1}H and ^{13}C NMR, Light Emitting Diodes, Xe-Arc Lamps, flow tubes, aerosol chambers, and other common environmental, atmospheric, physical, and analytical chemistry techniques.

- Microsoft Office Suite, Igor Pro, Wolfram Mathematica, Python, HTML, EndNote, National Instruments LabVIEW, Custom Mass Spectrometer Analysis Software.

RESEARCH EXPERIENCES:

University of California, Irvine, Irvine, California 2014 – 2018
Professor Sergey A. Nizkorodov

- Dissertation work focusing on production and photosensitized uptake of volatile organic compounds (VOCs) during irradiation of condensed-phase secondary organic aerosols (SOA) utilizing proton transfer reaction mass spectrometry (PTR-MS) and a variety of other instrumental techniques. Funded through NSF Graduate Research Fellowship Program.

University of Eastern Finland, Kuopio, Finland June 2017
Professor Annele Virtanen

- Performed experiments on various coniferous trees to investigate reactive uptake and photoproduction of various VOCs. Utilized a variety of instrumentation techniques such as Iodide Chemical Ionization Mass Spectrometer (CIMS) and Scanning Mobility Particle Sizer (SMPS).

University of California, Irvine, Irvine, California Jan. – May 2017
Professors Michael T. Kleinman, James Smith, Sergey A. Nizkorodov, and Norbert Staimer

- Collaborative project focusing on chemical composition of waterpipe (hookah) smoke on-line for gas-phase, semivolatiles, and particulates. Employed instruments such as carbon monoxide detector, PTR-MS, and SMPS.

University of California, Irvine, Irvine, California June – August 2012
Dean Kenneth Janda

- Studied the thermodynamics of the bromine-xenon double clathrate hydrate. Funded through NSF's REU (Research Experiences for Undergraduates) Program.

Johannes Gutenberg Universität, Mainz, Germany May – July 2011
Professor-Doctor Tobias Reich

- Performed speciation studies in German on Np-237 utilizing Capillary Electrophoresis and ICP-MS at the Institut für Kernchemie with Nils Stöbener, a PhD student. Awarded through DAAD – RISE (German Academic Exchange Service – Research Internships in Science and Engineering). Publication followed.

Minnesota State University, Mankato Jan. 2011 – May 2013
Professor John D. Thoemke

- Determined correlations between optical characterization of Dissolved Organic Matter (DOM) and the photoproduction of Reactive Oxygen Species (ROS) from DOM. Awarded competitive grants from MSU and presented at Undergraduate Research Symposium. Presented at the 2013 spring ACS national meeting environmental and SCI-MIX poster sessions.

TEACHING EXPERIENCES:

Teaching Assistant Sep. 2013 – Jun. 2015
University of California, Irvine Department of Chemistry

- Conducted upper-division analytical and general chemistry laboratories and discussion sections for general chemistry
- Graded and provided feedback to student reports
- Created and graded quizzes for students

Chemistry Laboratory Assistant Aug. 2010 – May '13
Minnesota State University, Mankato Department of Chemistry

- Assisted professor in General Chemistry Laboratories with 48 students
- Conducted pre-lab procedures
- Taught students proper laboratory techniques common to General Chemistry

General Chemistry Recitation Sessions January – May 2012
Minnesota State University, Mankato Department of Chemistry

- Hosted optional, hour-long recitation sessions for General Chemistry students
- Created and made review materials for students, and lectured about chemistry concepts

SCIENCE MENTORING EXPERIENCES:

1. Stephanie Kim, UC Irvine Undergraduate (September 2014 – June 2016). 2016 Gebel undergraduate award winner. *Photolysis of cyclohexanedione in multiple phases.*
2. Emily Yen, Troy High School (Fullerton, CA) Student (Summer 2016). *Chamber photooxidation of guaiacol and PTR-ToF-MS calibrations.*
3. Tim Cai, UC Irvine Undergraduate (Summer 2016 – June 2017). Chemical engineering graduate student at Carnegie Melon University. *Mass loss from secondary organic aerosols measured by a quartz crystal microbalance.*

PUBLICATIONS:

- Malecha, K.T.; Cai, Z.; Nizkorodov, S.A. Photodegradation of Secondary Organic Aerosol Material Quantified with a Quartz Crystal Microbalance. *Environmental Science and Technology Letters* **2017** Submitted.

- Malecha, K. T.; Nizkorodov, S.A. The feasibility of photosensitized reactions with secondary organic aerosol particles in the presence of volatile organic compounds. *J. Phys. Chem. A.* **2017**, *121*, 4961-4967.

- Roskamp, K. W.; Montelongo, D. M.; Anorma, C. D.; Bandak, D. N.; Chua, J. A.; Malecha, K. T.; Martin, R. W. Multiple aggregation pathways in human yS-crystallin and its aggregation prone G18V-variant. *Invest. Ophthalmol. Visual Sci.* **2017,** *58*, 2397-2405.

- Malecha, K. T.; Nizkorodov, S. A. Photodegradation of secondary organic aerosol particles as a source of small, oxygenated volatile organic compounds. *Environ. Sci. Technol.* **2016**, *50*, 9900-9997.

- Stöbener, N.; Amayri, S.; Gehl, A.; Kaplan, U.; Malecha, K.; Reich, T. Sensitive redox speciation of neptunium by CE-ICP-MS. *Anal. Bioanal. Chem.* **2012**, *8*, 2143-2150.

PRESENTATIONS:

ORAL:

5. 254th ACS National Meeting & Exposition, August 2017, Washington, D.C., USA. Multi-Phase Environmental Chemistry of Aerosols Symposium. K. T. Malecha, S. A. Nizkorodov, J. Smith, C. L. Faiola, A. Ylisirniö, A. Virtanen, J. Holopainen, S. Schobesberger. *Photodegradation and photosensitization reactions of secondary organic aerosols on environmental surfaces.*

4. Science and Societal Impacts of Air Quality and Climate Issues: Past, Present, and Future, April 2017, Irvine, CA, USA. M. J. Lawler, K. T. Malecha, R. Johnson. *"Clean" tobacco: A water pipe dream?*

3. 253rd ACS National Meeting & Exposition, April 2017, San Francisco, CA, USA. LGBT Graduate Student and Postdoctoral Scholar Chemistry Research Symposium. K. T. Malecha, S. A. Nizkorodov. *Irradiation of secondary organic material in the presence of volatile organic compounds: The role of photosensitization*.

2. 35th Annual American Association for Aerosol Research Conference, October 2016, Portland, OR, USA. Aerosol Chemistry Session. K.T. Malecha, S. A. Nizkorodov. *Photolysis of secondary organic aerosol material in the presence of volatile organic compounds: The role of photosensitization.*

1. 249th ACS National Meeting & Exposition, March 2015, Denver, CO, USA. Chemical Processes at Environmental Interfaces Session. K. T. Malecha, S. A. Nizkorodov. *Photolysis of secondary organic aerosol material as a source of small oxygenated volatile organic compounds.*

POSTER:

7. NSF-GRFP Symposium: Training for Tomorrow, May 2017, Irvine, CA, USA. K. T. Malecha, S. A. Nizkorodov. *Irradiation of secondary organic aerosol material in the presence of volatile organic compounds: The role of photosensitization.*

6. 34th Annual Informal Symposium on Kinetics and Photochemical Processes in the Atmosphere, May 2017, San Diego, CA, USA. K. T. Malecha, S. A. Nizkorodov. *Irradiation of secondary organic aerosol material in the presence of volatile organic compounds: The role of photosensitization.*

5. 33rd Annual Informal Symposium on Kinetics and Photochemical Processes in the Atmosphere, March 2016, Irvine, CA, USA. K. T. Malecha, S. A. Nizkorodov. *Photolysis of secondary organic aerosol material as a source of small oxygenated volatile organic compounds.*

4. The International Chemical Congress of Pacific Basin Societies, December 2015, Honolulu, HI, USA. K. T. Malecha, S. A. Nizkorodov. *Photolysis of secondary organic aerosol material as a source of small oxygenated volatile organic compounds.*

3. 245th ACS National Meeting & Exposition, April 2013, New Orleans, LA, USA. K. T. Malecha, J. D. Thoemke. *Photoproduced reactive species in natural waters: Influence of chromophoric dissolved organic matter properties.*

2. 2013 Undergraduate Research Symposium, April 2013, Mankato, MN, USA. K. T. Malecha, J. D. Thoemke. *Photoproduced reactive species in natural waters: Influence of chromophoric dissolved organic matter properties.*

1. 2012 Undergraduate Research Symposium, April 2012, Mankato, MN, USA. K. T. Malecha, J. D. Thoemke. *Correlation of dissolved organic matter fluorescence properties and photoproduction of reactive oxygen species.*

AWARDS/HONORS:

NSF Graduate Research Fellowship Program Award 2015-2018
National Science Foundation
- Program recognizes and supports outstanding STEM graduate students
- Provides 3 years of financial support at $34,000 per year stipend plus tuition
- Selection criteria includes intellectual merit and broader impacts

Michael E. Gebel Award Spring 2017
AirUCI
- Recognizes a chemistry graduate student working in environmental chemistry with a broader set of life experiences.

Graduate Student Oral Presentation Award August 2017
ACS Environmental Chemistry Division
- Awarded for outstanding graduate student presentation at the 254th ACS National Meeting and Exposition in Washington, D.C.

- NSF GRFP Research Symposium Best Presentation Award May 2017
- Goldwater Scholar Program Nominee Spring 2012
- Television Commercial for MSU, Mankato Spring 2012
- MSU, Mankato URC Research Grant Spring 2012
- Phan To Su Memorial Chemistry Scholarship 2011-2013
- Maverick Momentum Scholarship Fall 2012
- Winston Grundmeier Chemistry Scholarship Fall 2010, Spring ‘11
- Kaufmanis German Scholarship Fall 2010
- Maverick Scholarship Fall 2009, Spring ‘10
- Lonsdale Lions Scholarship May 2009

WORK EXPERIENCE:

Mechanic and Delivery Assistant Jun. 2004 – Aug. '13
Tim's Small Engine, Lonsdale, MN

- Managed daily business activities independently
- Diagnosed problems with lawn and garden equipment
- Repaired, assembled, and delivered/picked up equipment
- Financed undergraduate education by working full time during Summer months

VOLUNTEER EXPERIENCE:

University of California, Irvine Chemistry Outreach Fall 2014 – Present
Irvine, CA

- Conducted experiments for inner city and local elementary school students
- Participated as a panelist for creating science fair projects
- Judged science fair projects

Safety on Site Representative Jan. 2014 – June 2016
University of California, Irvine, Irvine, California

- Served as the conduit between the UC Irvine department of Environmental Health and Safety and the Nizkorodov laboratory. Attended numerous safety training seminars. Identified best practices to ensure a safe working environment. Ensured lab member's safety training was consistently up to date.

Mankato Area Adaptive Ski Program Jan. 2010 – Mar. 2013
Mankato, MN

- Taught disabled skiers to ski in an adjusted environment
- Created and maintained website for program

PROFESSIONAL AFFILIATIONS:

- American Chemical Society (ACS), American Association for Aerosol Research (AAAR), Golden Key International Honour Society

Abstract of the Dissertation

Condensed-Phase Photochemical Processes in Secondary Organic Aerosols from Biogenic and Anthropogenic Sources

By

Kurtis Timothy Malecha

Doctor of Philosophy in Chemistry

University of California, Irvine, 2018

Professor Sergey A. Nizkorodov, Chair

The net climate effect of aerosols on Earth's atmosphere is highly uncertain. Secondary organic aerosols (SOA) heavily contribute to this uncertainty because they are chemically complex, and their chemical and physical properties have not been fully characterized. Various atmospheric chemical aging processes further complicate the interpretation of the climate effects of aerosols. The influence of the condensed-phase aging processes, which occur inside aerosol particles is an active, rapidly growing topic of research. Recently, a number of aerosol aging experiments have been discussed; however, a systematic evaluation of the role of the condensed-phase photochemical processes in aerosols has not been performed.

In this work, SOA was generated in a smog chamber or flow reactor from a variety of precursor types (anthropogenic and biogenic) and oxidant conditions. Additionally, experiments were performed on trees. Chapter 2 of this dissertation discusses the condensed-phase photodegradation experiments of the SOA material. The photodegradation is found to be efficient and atmospherically relevant. We detected a variety of volatile organic compounds (VOCs) that were produced during ultraviolet irradiation of SOA via proton transfer reaction

time-of-flight mass spectrometry (PTR-ToF-MS). Next, in Chapter 3, we quantify the rate of photodegradation of SOA material with a quartz crystal microbalance (QCM) that is connected in series with the PTR-ToF-MS. Additionally, we discuss that while the mass degradation is atmospherically relevant (1% per hour during the Los Angeles summer solstice), the mass loss is not likely to be a concern for oxidation flow reactors (OFRs) commonly used in atmospheric chemistry experiments.

Chapter 4 probes the possibility of photosensitized SOA reactions where a VOC is taken up into the condensed-phase aerosol material. While this reaction does occur, it is unlikely to compete with faster gas-phase reactions of VOCs. Finally, Chapter 5 explores preliminary experiments focusing on photochemical reactions on Scots pine tree surfaces. A given tree is isolated and coated with SOA generated by ozonolysis of its VOCs, and the tree is subjected to ultraviolet light to probe the photochemical reactions from the SOA coated tree. The results of Chapter 5 are not conclusive, but the photochemical reactions could still be important in the atmosphere.

Chapter 1: Introduction

1.1 Background

1.1.1 Brief Context of Atmospheric Chemistry

The Earth's atmosphere is comprised of different layers, all of which have unique features. From Earth's surface to about 15 km above the sea level is the layer known as the troposphere. The troposphere is characterized by decreasing temperature with altitude, and the air within this layer mixes fairly quickly in the vertical direction due to surface heating by incoming solar radiation.[1] The stratosphere lies above the troposphere and goes to heights of up to approximately 50 km. The stratosphere is characterized by increasing temperature with altitude resulting in much slower mixing than in the troposphere.[1] This temperature increase with altitude is driven by the ozone layer absorbing the incoming solar radiation.[1] The boundary between the stratosphere and troposphere is called the tropopause. Above the stratosphere, there are additional layers called the mesosphere, thermosphere, and exosphere. Most of the atmospheric chemistry that affects living species occurs in the troposphere, and to some extent in the stratosphere, because of convective processes, relatively warm temperatures, nearly all atmospheric water being in these regions, and their close proximity to the biosphere and hydrosphere.[2]

For the atmospheric chemistry community, considerable attention has been given to the fundamental mechanisms of tropospheric and stratospheric chemical reactions. The study of atmospheric chemistry has its modern beginnings in the study of photochemistry of small molecules.[3-7] Different areas of the atmosphere have access to varying wavelengths of solar radiation. For example, only light with wavelengths longer than 290 nm can penetrate into the troposphere because the ozone layer in the stratosphere strongly absorbs light with wavelengths between ~200 and ~290 nm.[8] Above the ozone layer in the stratosphere, wavelengths down to

200 nm are present.[1] Because the radiation present in the stratosphere reaches further into the ultraviolet region of the electromagnetic spectrum, the photochemistry of a given atmospheric species could be vastly different in the troposphere and stratosphere. For example, photochemistry of carbonyls is driven by a weak $n \rightarrow \pi^*$ transition at longer wavelengths in the troposphere, and by a much stronger $\pi \rightarrow \pi^*$ transition at shorter wavelengths in the stratosphere.[9]

In more recent years, instead of studying exclusively gas-phase reactions, attention has been shifting to studying multi-phase processes involving gases, particles, aqueous droplets and environmental surfaces.[10] This change in focus is partially driven by the inability to explain mixing ratios of atmospheric constituents without invoking atmospheric particles and aerosols. A few dramatic examples of chemistry that require multi-phase reactions include loss of N_2O_5 on aerosol particles,[11] reactions of HCl and $ClONO_2$ on polar stratospheric clouds,[12] and oxidation of SO_2 in fog droplets.[13]

1.1.2 Atmospheric Aerosols

An atmospheric aerosol, by definition, consists of liquid or solid particles (typical diameters of 10^{-9}-10^{-4} m) that are suspended in a gas.[14] Earth's atmosphere contains a number of different types of aerosols, which are typically classified into inorganic aerosols and organic aerosols (OAs). As the names suggest, OAs predominantly contain organic compounds (i.e., compounds consisting of carbon, hydrogen, oxygen, and nitrogen) whereas inorganic aerosols are dominated by inorganic compounds such as sulfuric acid and its salts, nitric acid and its salts, metal oxides, and black carbon.[15] In reality, compounds in particles mix, resulting in a continuum of aerosol types ranging in chemical composition from 100% inorganic to 100% organic and anything in between. A relatively small number of inorganic species actually

contribute to secondary inorganic aerosol formation, which include sulfur dioxide, oxides of nitrogen, and ammonia.[15] On the other hand, hundreds of organic species can form OAs that can readily react in the atmosphere because of the rich variety of species present in the aerosol that can easily undergo chemical reactions.[16]

OAs are further sub-divided into two major types based on the way they are produced: primary organic aerosol (POA) and secondary organic aerosol (SOA). POAs are emitted directly by individual sources, which include, for example, automobile exhaust or biomass burning.[16-18] Global estimates of POA emissions can be upwards of a 30 Tg yr^{-1}.[17] SOA is generally produced in the atmosphere when VOCs emitted from biogenic or anthropogenic sources react with atmospheric oxidants.[14-17, 19] Common oxidants in the atmosphere include the hydroxyl radical (OH), ozone (O_3), chlorine atom (Cl), and, during nighttime, the nitrate radical (NO_3).[14, 20] In more urban, anthropogenic-dominated environments, oxides of nitrogen (NO_x) are present[21] and can react along with other oxidants to form OA.[22-24] These products are successively oxidized to produce increasingly lower volatility compounds. After several oxidation cycles, the volatility is low enough that the oxidized VOCs can condense on pre-existing particles or assist in nucleating new particles.[25-26] Global estimates of SOA production per year are contested with numbers ranging from a few to hundreds of Tg yr^{-1}.[14, 27] Additionally, the differentiation between POA and SOA becomes difficult to ascertain in the atmosphere, as OA is known to be quite complex.[28] For example, gases from POA can evaporate once in the atmosphere, and these evaporated gases can further react and form SOA;[29] therefore, the distinction between POA and SOA begins to blur in the actual atmosphere. SOA was selected for study in this dissertation.

Aerosols can have negative effects on human health. Exposure to particulate matter that is smaller than 2.5 microns in diameter ($PM_{2.5}$) has been shown to have statistical links with lung

cancers,[30] cardiovascular disease,[31] decrease in overall life expectancy,[32-33] and several other air pollution-related illnesses.[34]

The physical properties of aerosol particles have implications for Earth's climate. The particles directly affect the climate by scattering or absorbing solar radiation, and this also contributes to reduced visibility.[14, 35-37] An indirect effect of particles is modification of cloud formation and cloud properties.[38] Because the chemical transformations of aerosol particles are still not fully characterized, their net effect on climate is highly uncertain.[39-41] For example, in the latest Intergovernmental Panel on Climate Change (IPCC) report, the radiative forcing (the net warming or cooling of the earth from an atmospheric constituent) of aerosols was between +0.23 and -0.77 W m^{-2}, indicating a highly uncertain net warming or cooling of the atmosphere from SOA.[39, 42] This uncertainty partially arises from the lack of understanding of the chemistry of aerosols in the atmosphere.

1.1.3 Secondary Organic Aerosol Complexity

SOA is distinguished by a high degree of chemical complexity. Even if SOA is produced by oxidation of a single VOC precursor, there can be thousands of unique chemical compounds in SOA.[43-48] Furthermore, the chemical composition of SOA strongly depends on the oxidant, concentration of VOC, presence of NO_x, and environmental conditions of oxidation, such as actinic flux or temperature.

SOA generated from a variety of aromatic hydrocarbons showed an overall higher yield for low NO_x conditions under hydroxyl radical oxidation relative to high-NO_x conditions,[49] and the benzene SOA produced more phenolic compounds generated under high NO_x conditions.[50] For biogenic SOA, isoprene epoxydiols (IEPOX), were formed in lower amounts in high NO_x

environments relative to methacrolein or methyl vinyl ketone for isoprene SOA.[51] Additionally, isoprene SOA generated separately from high- and low-NO_x oxidation conditions revealed more organic nitrates at high NO_x conditions relative to low NO_x, whereas low NO_x conditions contained >50% highly oxygenated C_5 compounds.[48] On the other hand, SOA formation from anthropogenic, aromatic precursors generated significant amounts of unsaturated anhydrides.[46] As another example, biogenic precursors formed much higher yields of lower volatility compounds under elevated ozone conditions relative to high-NO_x condition alone.[52] Therefore, because SOA from different oxidant conditions has highly variable chemical composition, it is worthwhile to study a variety of SOA types and oxidant conditions. Many different SOA types and oxidant conditions were selected for study in this dissertation.

The effect of seed particles for SOA generation can also strongly influence the SOA composition. Even though yields of SOA can be much higher for isoprene SOA generated with sulfate seed particles,[53] overall aerosol acidity may actually increase and an overestimation of the realistic aerosol yield could occur.[54] Indeed, by varying the seed particle type (and also acidity) for the α-pinene ozonolysis SOA system, the yield of high molecular weight oligomers was changed.[55] The sulfuric acid particles revealed a much higher yield of these oligomers relative to the ammonium sulfate particles. All SOA produced in this dissertation did not utilize seed particles.

High molecular weight oligomers (MW > 200 Da) can be formed in a variety of SOA types – in cloud reactions,[56] biogenic precursors under ozonolysis conditions,[57-58] or anthropogenic SOA to list a few vastly different examples.[59] Even though SOA is highly chemically complex, there are some patterns of functional groups present.[14] Organonitrates are found in SOA formed during high-NO_x events.[60] A large sum of biogenic and anthropogenic

SOA contains functional groups such as aldehydes, ketones, and carboxylic acids.[14] These groups of molecules all contain electronic transitions that are accessible at radiation wavelengths that are in the troposphere and the stratosphere.[9] All of this aforementioned SOA chemical complexity is further increased when so-called aging processes occur, as described below.

1.2 Aerosol Aging Processes

Aging of an aerosol can involve a variety of physical and chemical processes. Physical aging processes can include: gas-to-particle partitioning,[61] particle coagulation,[29] water uptake/loss,[62] and phase transitions.[63] Chemical aging processes can involve a variety of processes which change the overall chemical composition of the aerosol.[15, 64-75] The best known chemical aging reactions represent gas-phase oxidation of various semi-volatiles before their products partition into the particle. However, heterogeneous reactions on the particle surface and condensed-phase reactions inside the particle can also occur, and in some cases, they can be more important than gas-phase aging processes.[76] For example, sulfur dioxide can be efficiently oxidized in fog droplets to form sulfate and further sulfuric acid.[77] N_2O_5 (a reservoir for NO_x species) can be removed in large amounts by aerosols, thus significantly reducing its ozone forming potential.[78] Additionally, fatty acids, such as oleic acid, can be oxidized by ozone on the surface of particles.[79]

The chemical aging of organic aerosols is not well understood.[15] Historically, it was assumed that the aging of OA was largely driven by gas-phase processes followed by gas-to-particle partitioning,[80-81] heterogeneous uptake and reactions of oxidants,[69, 82-83] and aqueous reactions.[84-86] The gas-phase reactions implicated in aerosol aging are typically between a semivolatile VOC (SVOC) and an oxidant, which often yields successively lower volatility

species and can contribute to net aerosol growth.[80] As the name suggests, the heterogeneous reactions can be between a gas-phase component (usually an oxidant), and a condensed-phase component (usually a molecule that can be easily oxidized). After uptake of the oxidant, the chemical reactions within the OA can contribute to a change in particle density,[69] an increase in oxidation state,[82] and a change in the size of the OA particles[83] to name a few important effects.

Aging studies often involve taking an organic compound that is representative of environmental organic species and exposing it to an oxidant in a suitable reactor.[87-89] More recently, efforts have been put forth to try and understand the aging of an entire SOA sample, which consists of a number of different compounds and is more atmospherically realistic. For example, after being generated in a chamber, SOA from α-pinene,[64] toluene,[65] or polycyclic aromatic hydrocarbons[66] were subjected to further photooxidation from the hydroxyl radical and UV lights. As mentioned previously, the precursor and oxidant conditions strongly affect the aging processes. For example, the aging of naphthalene/low NO_x SOA in a chamber yielded insignificant changes in overall observed products in the aerosol phase when subjected to further OH and UV lights.[66] On the other hand, toluene/high NO_x yielded changes in identity of the products but little change in hygroscopicicity.[90] As another example, α-pinene ozonolysis SOA was aged with OH and separately with UV radiation.[67] The OH aging led to a net functionalization and increase in mass loading of the SOA whereas the UV radiation led to photolysis-driven degradation reactions. Clearly the chemistry occurring within the SOA during aging processes is complicated, so a more detailed understanding of the reactions occurring is important to study.

One way to help understand these photochemical aging processes is to separate the gaseous and particulate compounds and study aging processes in just the condensed-phase.

Indeed, these condensed-phase reactions appear to be quite important.[15, 27, 73, 91] For example, Hodzic et al. noted in a modeling study that just the particle phase photochemical reactions alone can efficiently degrade and remove SOA from the atmosphere in a time period of less than 7 days.[91] A more accurate picture of OA aging should therefore include condensed-phase photochemical reactions, which change the OA chemical composition and presumably physical properties.[73]

There are not too many studies in the literature where the condensed aerosol phase photolysis reactions in SOA have been investigated. Some of these studies have investigated photoproduction of VOCs during irradiation of SOA material collected on a substrate with techniques such as Cavity Ring-Down Spectroscopy (CRDS),[92] Chemical Ionization Mass Spectrometry (CIMS),[89] Gas Chromatography (GC),[93] and Fourier Transform Infrared Spectroscopy (FTIR).[94] Another study re-aerosolized α-pinene SOA extracted material into a small chamber and further aged them in a chamber with UV light.[95] Yet another study irradiated α-pinene/O_3 SOA that was sent from a chamber through a denuder train to strip away the oxidants and some VOCs.[73] The resulting particles were irradiated as they were sent through a flow tube. The mass loss resulting from the condensed-phase photochemical reactions was determined to be fast enough to consider in the atmospheric chemistry of SOA.

In the aqueous phase, several different types of SOA have been exposed to UV radiation, and the resulting photoproducts were investigated with high resolution mass spectrometry.[43] The resulting products were strongly correlated with the SOA precursors and the oxidation method (ozonolysis, high NO_x, etc.). For example, ozonolysis of biogenic monoterpenes showed a more drastic change in composition than that of the aromatic precursors under high NO_x conditions. In another study, aqueous organic aerosol was formed from phenolic compounds and thereafter

photochemically aged.[96] Initially, functionalization reactions dominated the aging processes. However, after a longer period of photochemical aging, photofragmentation reactions dominated. As another example, dimers formed during α-pinene ozonolysis were photooxidized in solution.[97] These compounds photodegraded rapidly. Knowledge of a variety of SOA types is necessary for better understanding of the resulting chemistry and products, especially during these aging processes.

While these previous studies suggested that condensed-phase photochemical reactions are important, they were qualitative in nature and also did not cover a wide-enough range of SOA types. Additionally, some of these studies relied on exposure of SOA to 254 nm radiation,[94] which is not a relevant wavelength in the troposphere. One of the main motivations for this dissertation is to systematically investigate this aging process of the condensed phase SOA material that is driven by tropospherically relevant UV irradiation. Chapters 2, 3, and 4 of this dissertation discuss some of these aging processes from laboratory-generated SOA.

1.2.1 Condensed-Phase Aerosol Photochemical Aging Techniques

Various methods to study condensed-phase photochemical reactions in OA particles are summarized below. These include a static chamber, a flow tube, and a substrate. Figure 1.1 provides a visualization of these three methods.

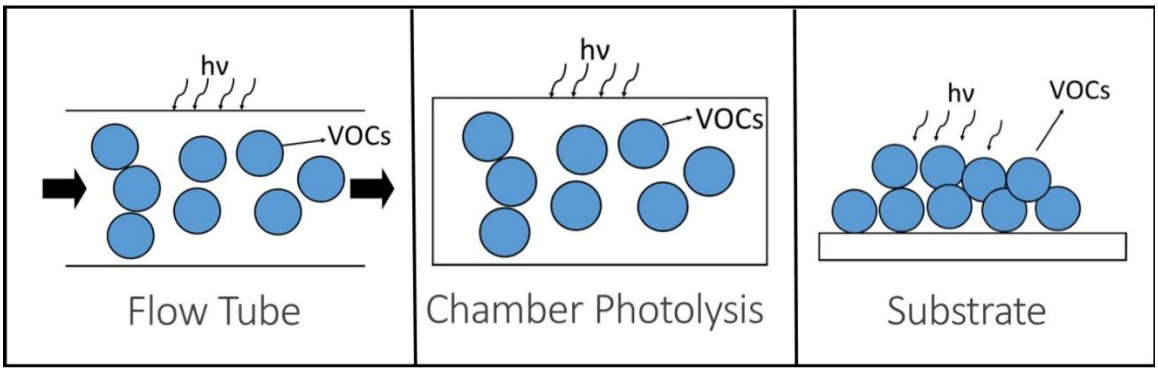

Figure 1.1. Commonly-used methods for production of VOCs from aged OA. The blue circles correspond to the OA particles dispersed in a gaseous phase or collected on a substrate, while hν corresponds to photons of light inducing chemical aging often accompanied by the production of VOCs.

In a static chamber, the SOA is either oxidized in the same chamber where it was generated,[66, 68, 98-99] or it is collected and extracted then re-aerosolized (in order to get rid of gaseous components of aerosol) and thereafter oxidized.[95] This method provides useful information about the SOA condensed-phase photochemical processes, but it suffers from strong interference from photochemistry involving gas-phase species surrounding the particles. Additionally, there may be possible artifacts from the collector and extraction process.

In a combined chamber - flow tube setup, the SOA formed in a chamber passes through a denuder to strip away gaseous components of aerosol and then sent through a quartz flow tube surrounded with UV lamps. This method offers advantages over the static chamber methods – it avoids secondary oxidation of the species from photoproduced oxidants and gases (due to its inherent non static flow conditions); however, it still suffers from interference from the re-evaporated gas-phase components of the aerosol.[73] For example, upon exiting the denuder, the particles can evaporate, thus re-populating the gas phase with photolyzable molecules.

Using a substrate to collect the condensed-phase particles is yet another method.[92-93, 100] This involves impacting the OA onto a photochemically inert substrate (a Teflon filter or a CaF_2 window) by an impactor (such as a Micro Orifice Uniform Deposit Impactor (MOUDI) or a slit

impactor). The irradiation of the SOA material is then done directly on the substrate. The main disadvantage of this method is that it can suffer from some mass-transfer limitations during photolysis.[101-105] Specifically, the thickness of the SOA material film is much larger than the diameter of a typical SOA particle making it difficult for the product molecules to diffuse out and/or oxygen (which often participates in photochemistry) and water to diffuse in. This method does offer the distinct advantage, though, of the lack of interfering gas-phase chemistry, which helps elucidate the influence of the condensed-phase photolysis of the OA. This dissertation work utilizes the substrate collection method.

1.2.2 Photosensitization Reactions

Molecules possessing photosensitization properties are potentially important for aging of SOA. A photosensitizer works by strongly absorbing radiation and transferring the excitation energy to another molecule that would not normally absorb at that wavelength.[106-107] This generally requires an efficient intersystem crossing of the photosensitizer to form a long-lived triplet electronic state.[107] Molecules that are good candidates for photosensitizers usually include molecules that have delocalized electrons,[107] which many aromatic species possess. Many identified molecules in POA and SOA contain aromatic molecules capable of photosensitization,[108] such as imidazoles[109] and benzophenones.[110] It has been suggested that photosensitized reactions between the excited photosensitizer and surrounding VOC molecules may be a driving force behind SOA growth in the atmosphere.[111] The majority of the previous experiments have involved single photosensitizer molecules such as PAHs and aromatic carbonyls dispersed in an inert organic matrix. Chapter 4 explores these photosensitized reactions with the full set of compounds found in the SOA material.

1.3 Aerosol VOC Precursors Studied

Several VOC precursors were used to make SOA for this work. They are from a variety of sources, including biogenic, biomass burning, and anthropogenic sources. Table 1.1 shows the names, structures, types of precursors, and some sources of these molecules.

Table 1.1. The VOCs used in this work to generate SOA. Column 1 lists the common name followed by the IUPAC name, and finally the abbreviation used in this dissertation. Column 2 shows the structure of each of the molecules. Column 3 categorizes which type of precursor each molecule is, and then it lists some common sources for each.

Names	**Structure**	**Type of Precursor/Source(s)**
α -Pinene (1*S*,5*S*)-2,6,6-Trimethylbicyclo[3.1.1]hept-2-ene APIN	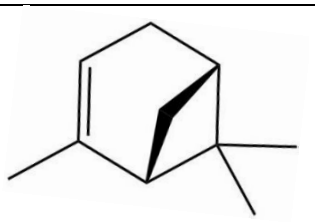	Biogenic Coniferous trees[112]
Isoprene 2-Methylbuta-1,3-diene ISO	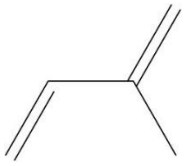	Biogenic Oak, Poplar, Eucalyptus Trees; Shrubs[113]
d-Limonene 1-Methyl-4-(1-methylethenyl)-cyclohexene LIM	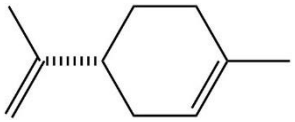	Biogenic Citrus Trees/Fruit[114]

Guaiacol 2-methoxyphenol GUA	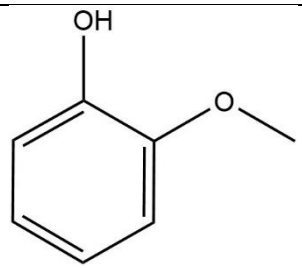	Biomass Burning Wood Smoke[115]
Naphthalene NAP	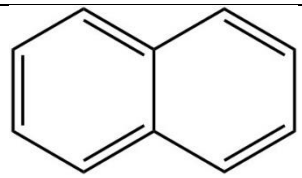	Anthropogenic Byproduct of Heating Coal Tar; Main Ingredient in Mothballs[116-117]
Tetradecane TET	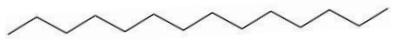	Anthropogenic Unburned Fuel[118]
Mesitylene 1,3,5-Trimethylbenzene TMB	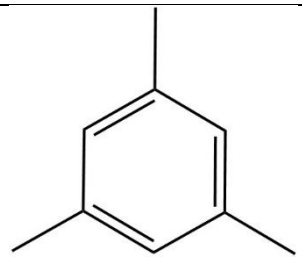	Anthropogenic Byproduct of Diesel and Gasoline Combustion, Coal Tar[117-118]

These SOA precursor molecules were selected because they represent a variety of types of molecules – from a conjugated ring system of naphthalene (the simplest polycyclic aromatic hydrocarbon[119]) to the linear alkane tetradecane. α-pinene and limonene were selected because they are quite common in the atmosphere.[120] Globally, monoterpenes (a class of molecules to which α-pinene and limonene belong) represent 11 % (by weight of carbon) of the total biogenic VOC emissions per year,[120] which is comparable to all anthropogenic VOC sources.[121-122] Additionally, α-pinene and limonene contain an endocyclic double bond, which can readily react with ozone to form SOA.[123-124] Monoterpenes are also known to have high SOA yields.[125] 1,3,5-

trimethylbenzene is a well-studied SOA precursor.[126-128] Isoprene is the most-emitted non-methane hydrocarbon in the atmosphere.[113, 120] Even though its SOA yield is relatively low,[125, 129] the high global emissions, which are over 600 Tg yr^{-1}, make isoprene an important precursor for atmospheric particulate matter.[130] Guaiacol was selected because of its biomass burning sources, and aerosol made from it was previously shown to be strongly light-absorbing.[43]

1.4 General Methods of the Dissertation

1.4.1 SOA Generation and Collection from Smog Chamber

SOA was generated in a smog chamber for the work presented in Chapters 2, 3, and 4. The general parameters of the chamber are described in this section, while specific details pertaining to each experiment are described in each corresponding chapter. The chamber is ~5 m^3 in volume with flexible FEP Teflon serving as the chamber walls. The chamber is enclosed with an opaque, rigid structure to support the chamber walls and to prevent UV light from escaping the chamber. Forty-two UV-B lamps (SolarcSystems, Inc. Model FS40T12/UBV) centered at 310 nm surround three sides of the chamber and are used to irradiate the sample and initiate photooxidation. Incoming purge air (Parker FT-IR purge gas generator) can be optionally humidified by a Nafion exchanger (Perma Pure model FC125-240) coupled to a heated water circulator (Julabo model HE-BASIS) at 30°C.

Various oxidation conditions were used for this work for the smog chamber. For OH/Low NO_x conditions, a measured volume (typical volume of tens of µL) of 30 wt% solution of H_2O_2 was added to the chamber via a glass trap with a stream of the zero air at approximately 10 SLM through a partially heated (70 °C) stainless steel tube. For OH/high NO_x conditions, before adding the peroxide solution, NO gas was delivered from a premixed gas cylinder (Praxair) with a calibrated mass flow controller operated for a set time period. For ozonolysis conditions, ozone

was generated by flowing UHP Oxygen (AirGas) at 6 SLM over an ozone generator lamp setup (Ozotech, model OZ2SS-V/SW). The pure SOA precursor was then added to the chamber in the same way as the peroxide solution (except in the case of naphthalene, which is discussed in further chapters). The oxidant(s) and the precursor were mixed via a fan inside the chamber for several minutes before the lamps were turned on (except for ozonolysis conditions) to initiate the photooxidation.

The generation of SOA can be monitored with several instruments and sensors. The temperature and relative humidity (RH) were monitored with a Vaisala HMT333 probe. The ozone and NO_y (nitrogen oxides plus compounds from the oxidation of these oxides) mixing ratios were monitored with Thermo Scientific 49i and 42i-Y monitors, respectively. Particle size distribution and number concentration were measured with a scanning mobility particle sizer (SMPS; TSI model 3936). The PTR-MS (discussed in another section in this chapter) was also used to track the precursor in selected experiments. After a maximum mass particle concentration was achieved in the SMPS readings (typically after 1-4 hours), the lamps were shut off (except for the dark ozonolysis experiments) and SOA collection began.

Several collection methods can be used from the chamber. For this work, the substrate collection was employed. The MOUDI cascade impactor[131] (MSP Corporation, model 110-R) was used to collect particles at a rate of 30 liters per minute, so a stream of makeup air from the purge air generator was introduced to the chamber at the same time. Before the MOUDI, a charcoal denuder was used to help strip away the gas-phase species. Typically stage 7 of the MOUDI (0.32-0.56 μm particle size range) collected the most aerosol mass for this work. Custom-built aluminum rings were used to hold the 2.54 cm CaF_2 windows in place in the

standard MOUDI substrates. A diagram of the chamber and collection setup is shown below in Figure 1.2.

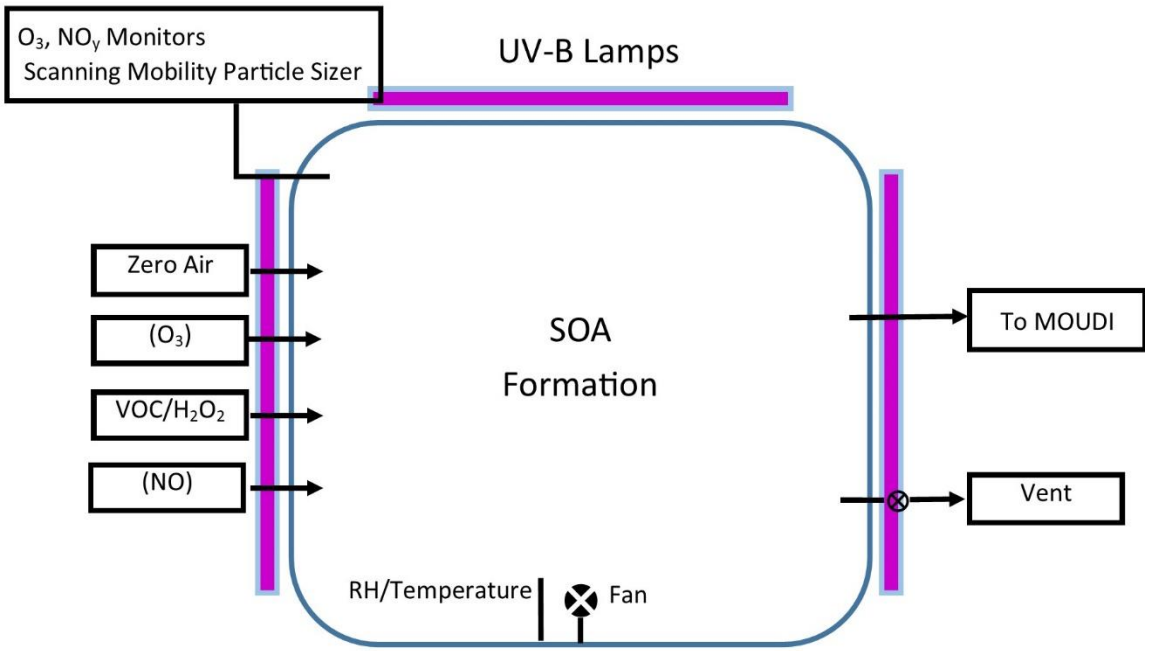

Figure 1.2. A diagram of the smog chamber utilized for this work. The constituents in parentheses were used as needed for specific experiments.

1.4.2 SOA Generation and Collection from Aerosol Flow Tube

SOA was also generated in an aerosol flow tube[132] for work involved with Chapter 2 (control studies) and Chapter 3. The flow tube is ~17 L in volume with ozone used as the VOC oxidant. The flow tube was kept at ambient temperature and pressure and the RH was kept <2%. Ozone was generated by flowing ~0.6 SLM of UHP oxygen over an ozone generator (Ozotech, model OZ2SS-V/SW). The ozone mixing ratio was determined with an ozone analyzer (AFX, model H1). This ozone was mixed with a VOC that is injected by a syringe (Hamilton GasTight) and syringe pump at a rate of 25 μL hr^{-1} (Fisher Scientific, model 14831200) through a septum and air flow of zero air at 5-7 SLM. This resulted in mixing ratios of 60-100 ppmv of ozone and

~5 ppmv of the VOC. Even though the residence time in the flow tube was a few minutes, sufficient SOA production was observed because of the high mixing ratios of the reactants. After the flow tube, the SOA passed through a 1 m long charcoal denuder to remove residual ozone and some VOCs. The MOUDI was used for collection of the SOA particles with the flow tube as well. A HEPA filter (TSI, model 1602051) tee was placed at the end of this denuder to admit particle-free make-up air from the lab; otherwise the high MOUDI flow rate (30 liters per minute) would collapse the flow tube. Much like the smog chamber, stage 7 of the MOUDI usually yielded the most mass, and SOA particles from this stage were usually used for analysis. Typical collection times ranged from 30 minutes to 2 hours. Figure 1.3 shows the flow tube setup.

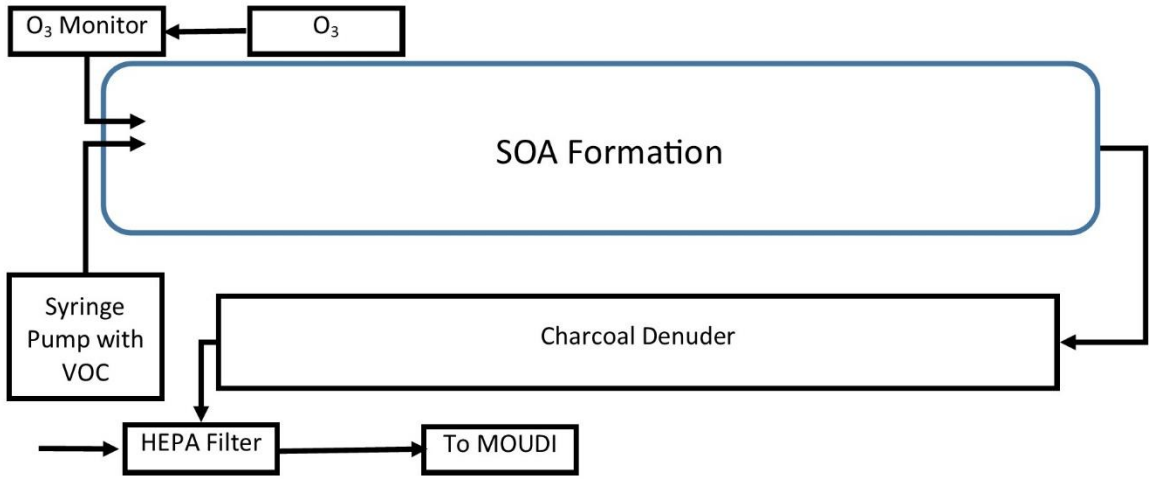

Figure 1.3. The aerosol flow tube setup. The VOC is injected and mixed with ozone at the entrance of the flow tube. After leaving the flow tube, the SOA is run through a charcoal denuder to remove ozone and other gasses. The HEPA filter provides makeup air for the MOUDI.

1.4.3 Proton Transfer Reaction Time-of-Flight Mass Spectrometer

For much of this dissertation work, PTR-ToF-MS was used to detect VOCs. PTR-MS relies on chemical ionization by hydronium ions (H_3O^+) as the ionization mechanism.[133-134] These hydronium ions transfer a proton to the analyte, and the resulting ionized species is detected – hence the name of this method. PTR-MS is a so-called "soft ionization" method of mass spectrometry; this means that there is relatively little fragmentation of the analytes relative to harder ionization methods (such as electron impact ionization). It is a highly sensitive technique that allows the user to detect as low as single digit part-per-trillion (ppt) levels of mixing ratios of analytes.

PTR-MS also allows for sampling at ambient pressures and temperatures with no pre-concentration of air samples necessary (other than assuring the measured VOC levels are below the ppmv level to prevent overwhelming this sensitive instrument). Because of the low levels of fragmentation, and ability to sample at ambient conditions, this method is ideal for detection of VOCs.

The basic (simplified) chemical reaction that PTR-MS relies on is:

$$H_3O^+ + R \rightarrow RH^+ + H_2O \qquad \textbf{(1.1)}$$

where R is the analyte of interest and RH^+ is the analyte with the transferred proton. In order for this reaction to be thermodynamically favorable, the proton affinity of R must be higher than that of water (7.22 eV). A particularly powerful advantage of PTR-MS is that the most common compounds found in air (e.g., nitrogen, oxygen, argon, and carbon dioxide) do not have high enough proton affinities to be ionized by this mechanism. Therefore, trace levels of VOCs can be detected without much interference from the common air molecules – something that would be hard to with a less selective electron impact ionization source.

1.4.4 Quartz Crystal Microbalance

The work presented in Chapter 3 utilized a Quartz Crystal Microbalance (QCM) to sensitively measure the mass of SOA samples during irradiation. A QCM is a piezoelectric resonator that can measure sub-microgram changes in mass in real time.[135-137] The underlying principle of operation is that the resonance frequency of a quartz crystal depends on the amount of mass that is deposited on its surface. The QCM used in this work operates at a frequency of ~5 MHz When material is added or removed from the crystal surface, the measured frequency is changed, which can be easily measured.

For this dissertation, SOA was collected directly onto the QCM crystals using the MOUDI particle collector. A QCM crystal was placed directly on top of a CaF_2 window in the MOUDI with the previously-mentioned custom-made rings to hold the window and QCM crystal in place. The QCM setup for this dissertation was from Stanford Research Systems (model QCM 200), and it was modified to allow the photoproduced VOCs to be detected by the PTR-ToF-MS (discussed in Chapter 3).

1.5 Structure of the Dissertation

Chapter 2 discusses the first set of photodegradation experiments we performed. This chapter focuses on the photoproduction of VOCs that are detected via PTR-ToF-MS during irradiation experiments with 305 nm light from a UV-LED. Four photoproduced VOCs were detected and quantified using PTR-ToF-MS across a range of SOA types. From this information, we scaled these measurements up to use “back of the envelope” calculations to determine how much formic acid could be produced as a result of photodegradation of SOA in the atmosphere per year, which was found to be significant. Additionally, we made conjectures about how much mass could be lost from the SOA particles over time during atmospheric aging.

Chapter 3 follows up Chapter 2 by utilizing a QCM in addition to the PTR-ToF-MS. This instrumental setup provides more direct information about the mass loss of SOA particles from photodegradation in real time. Additionally, we utilized 3 different irradiation wavelengths to determine the efficiency of photodegradation and thereafter more realistic photodegradation rates in the atmosphere.

Chapter 4 discusses the possibility of photoinduced uptake of VOCs into the SOA particles. This is the opposite effect of the photodegradation experiments – we wanted to see if it was possible for mass increases in the deposited SOA material to occur because of the photosensitized uptake of the VOC limonene. We determined that while there was some photoinduced uptake, the rate of this process was too slow, and it could not compete with the photodegradation that occurs simultaneously. We hypothesized at the end of this work that perhaps the photosensitized reactions would be more important near the leaf boundary layer.

In Chapter 5, we discuss preliminary work done at the University of Eastern Finland in Annele Virtanen's group. The photodegradation and photosensitization experiments of SOA produced on and near tree surfaces are described in this Chapter. The experiments utilized Scots Pine saplings isolated in Teflon bags. The trees were subjected to UVB light followed to stress the trees and have them emit more volatiles. Then the trees were subjected to ozone to produce SOA from the tree volatiles and to coat the needle surfaces with aerosol material. After this, the trees were once again treated with UVB radiation to see if the photodegradation or the photoinduced uptake would occur on atmospherically-relevant time scales.

Chapter 2: Photodegradation of Secondary Organic Aerosol Particles as a Source of Small, Oxygenated Volatile Organic Compounds

Portions of this chapter are reproduced with permission from Malecha, K. T.; Nizkorodov, S. A. "Photodegradation of Secondary Organic Aerosol Particles as a Source of Small, Oxygenated Volatile Organic Compounds." Environmental Science and Technology 2016, 50, 9990-9997; DOI: 10.1021/acs.est.6b02313.
Copyright 2016 by the American Chemical Society.

2.1 Abstract

We investigated the photodegradation of SOA particles by near-UV radiation and photoproduction of oxygenated volatile organic compounds (OVOCs) from various types of SOA. We used a smog chamber to generate SOA from α-pinene, guaiacol, isoprene, tetradecane, and 1,3,5-trimethylbenzene under high-NO_x, low-NO_x, or ozone oxidation conditions. The SOA particles were collected on a substrate, and the resulting material was exposed to several mW of near-UV radiation (λ~300 nm) from a light-emitting diode. Various OVOCs, including acetic acid, formic acid, acetaldehyde, and acetone were observed during photodegradation, and their SOA-mass-normalized fluxes were estimated with a PTR-ToF-MS. All the SOA, with the exception of guaiacol SOA, emitted OVOCs upon irradiation. Based on the measured OVOC emission rates, we estimate that SOA particles would lose at least ~1% of their mass over a 24 h period during summertime conditions in Los Angeles, California. This condensed-phase photochemical process may produce a few Tg/year of gaseous formic acid – the amount comparable to its primary sources. The condensed-phase SOA photodegradation processes could therefore measurably affect the budgets of both particulate and gaseous atmospheric organic compounds on a global scale.

2.2 Introduction

Aerosols directly affect climate by scattering and absorbing solar radiation and by modifying cloud properties.[42] Organic compounds represent the major aerosol component, occurring in comparable amounts to sulfates, nitrates, and other major inorganic species.[16] POA are emitted directly by their sources, whereas SOA are produced by atmospheric reactions of VOCs with oxidants.[16] Various atmospheric processes involving organic aerosols (OA) and their

components remain poorly understood, in part due to their complex chemical composition. A randomly selected OA particle could contain thousands of different compounds.[15]

Aging of an aerosol involves a change in composition and physical properties through various chemical and physical processes.[15] It is commonly assumed that the formation and chemical aging of SOA is driven by gas-to-particle uptake of low-volatility organics and by reactive uptake of oxidants by the particles' surfaces, with little, if any, chemistry occurring inside the particles. Recent evidence suggests that aging processes occurring in the condensed organic phase may be just as important.[15, 138] The condensed-phase photochemical reactions may not only change the SOA composition, but also change the volatility distribution of the SOA compounds resulting from photoinduced fragmentation of SOA compounds into more volatile products.[67] Indeed, a recent modeling study by Hodzic et al.[91] showed that inclusion of condensed-phase photolysis in a GEOS-Chem model can potentially result in ~50% of particle mass loss after 10 days of aging. This estimate is probably too high because Hodzic et al. made an unrealistic assumption that condensed-phase photolysis of organics occurs at the same rate as in the gas phase, disregarding matrix effects on photolysis. Absorption coefficient measurements of different types of SOA also suggested that lifetimes of SOA with respect to condensed-phase photochemistry could be quite short—assuming that every absorbed photon leads to a chemical reaction.[74] SOA mass loss, and consequently, decreases in particle size due to UV irradiation have been experimentally observed in several laboratory studies.[67, 73, 75, 95, 129, 139]

One way to study condensed-phase photochemical reactions in SOA particles is through irradiation of a model SOA prepared in a smog chamber or a flow reactor.[73] However, a potential issue with this approach is the difficulty of separating condensed-phase photochemical processes in particles from gas-phase photochemistry of volatile organics surrounding the particles. A way

to more selectively study condensed-phase photochemical aging is to do experiments with bulk SOA material after driving away the volatile constituents,[92-93, 100] for example, by depositing the SOA particles onto an inert substrate and carrying out UV irradiation directly on the substrate. This method offers a key advantage in that the photochemistry of gas-phase species (such as oxidant precursors and volatile organics present in chamber experiments) no longer interferes with the condensed-phase photochemistry occurring inside the SOA particles. A disadvantage of this method is that it can suffer from mass-transfer limitations during photolysis. Specifically, the time for the primary volatile products of photolysis to evaporate from the organic film (typical thickness >10 μm) may be too long compared to that for an isolated aerosol particle (typical diameter <0.5 μm), and as a result, the primary volatile products of photolysis may undergo secondary photochemical reactions before having a chance to escape from the film. For example, formic acid may actually be one of these secondary photoproducts, as suggested by Vlasenko et al.[101] In addition, the bulk film may be more depleted of oxygen during irradiation compared to aerosol particles. Previous experiments of this type in our laboratory demonstrated that condensed-phase photochemistry of SOA at $\lambda > 295$ nm produced formic acid, formaldehyde, and many other compounds, but we have not attempted to quantify the rate of photodegradation.[92-93, 100] Related experiments by Hung et al.[94] found a significant effect of 254 nm radiation on SOA prepared from isoprene and α-pinene. To the best of our knowledge, photodegradation of other types of SOA has not been studied, and the kinetics of these processes have not yet been investigated.

The rate and extent SOA material photodegradation can be evaluated indirectly from the amount of selected volatile products produced by the photodegradation. For example, carbon monoxide is a convenient tracer of photolysis of carbonyls.[93] In this study, we focus on the

photochemical production of several oxygenated VOCs (OVOCs), including formic acid, acetic acid, acetaldehyde, and acetone, in the photodegradation of different types of SOA. We find that these OVOCs are produced for a range of SOA types. We estimate that the SOA particles lose at least 1% of their mass per day under representative atmospheric conditions. Although the mass loss rate is modest, this photodegradation process can measurably affect the chemical composition of both particulate and gaseous components of aging SOA.

2.3 Experimental Section

An overview of the experimental methods is shown in Figure 2.1. SOA was generated in a ~5 m^3 Teflon™ chamber in the absence of seed particles. The SOA formation was tracked with an SMPS, an NO_y monitor (Thermo Scientific model 42i-Y), an ozone monitor (Thermo Scientific model 49i), and, for selected experiments, a PTR-ToF-MS (Ionicon model 8000).

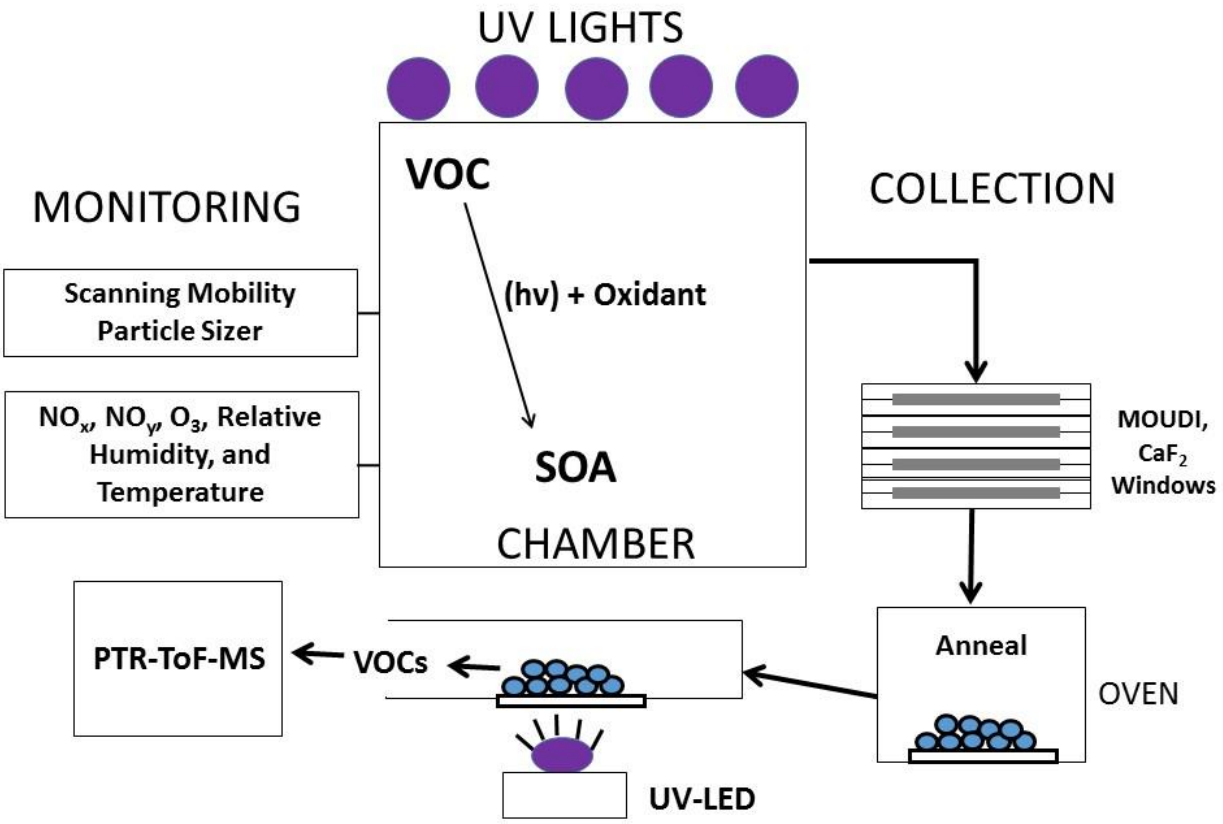

Figure 2.1. A diagram of SOA photodegradation experiments. The SOA is prepared in the chamber and monitored with the instruments on the left of the diagram. After a maximum particle concentration is achieved, the particles are collected, annealed, and thereafter irradiated with a UV-LED directly on the substrate. The resulting OVOCs are monitored with the PTR-ToF-MS.

Before SOA generation, the chamber walls were cleaned by exposure to high levels of OH and O_3 in humidified air to promote oxidation/removal of remaining species on the walls of the chamber and thereafter flushed with purge air. For a given experiment, the oxidants or their precursors were then added to the chamber; H_2O_2 served as an OH precursor in low NO_x and high NO_x photooxidation experiments; O_3 was used as an oxidant in dark experiments. The hydrogen peroxide was added by evaporating a measured volume of 30 wt% H_2O_2 solution from a glass trap under a stream of purge air at a rate of ~10 SLM, NO was added from a premixed

gas cylinder, and O_3 was added by passing oxygen through a commercial ozone generator. The VOC, which served as the SOA precursor, was injected into the chamber by evaporation into a flow of air, via the same method as H_2O_2. Ideally, these experiments should have probed a range of VOC concentrations to examine the effect of the concentration on SOA photochemistry; however, for this exploratory study, we had to use relatively high VOC mixing ratios, listed in Table 2.1, in order to collect sufficient amounts of SOA material for the experiments. A Teflon-coated fan mixed the precursor and oxidant(s) for several minutes before being shut off to reduce wall loss of particles. UV-B lamps (centered at 310 nm; FS40T12/UVB, Solar Tec Systems, Inc.) were turned on for all experiments, except for those performed with ozone as the oxidant. The aerosol was allowed to form for 1-5 hours (until a maximum particle mass concentration was achieved) before the collection. Table 2.1 lists the conditions used in all the experiments.

Table 2.1. Summary of the SOA samples prepared in this work.[a]

Pre-cursor	Oxidant(s)	# of repeat samples	Pre-cursor (ppmv)	H_2O_2 (ppmv)	NO (ppbv)	O_3 (ppmv)	Reaction Time (h)	Collection Time (h)
APIN	OH, Low NO_x	4	1	5	0	0	3	4
APIN	OH, High NO_x	5	1	5	400	0	3	3
APIN	O_3	4	0.5	0	0	3	1	6
GUA	OH, Low NO_x	3	0.5	2	0	0	3	4
GUA	OH, High NO_x	3	0.5	2	400	0	3	4
ISO	OH, Low NO_x	6	3	18	0	0	5	2.5
ISO	OH, High NO_x	5	2	12	600	0	3	4
ISO	O_3	3	4	0	0	4.5	2	3
TET	OH, Low NO_x	6	1	8	0	0	5	2.5
TET	OH, High NO_x	4	0.5	4	600	0	0.5	3.5
TMB	OH, Low NO_x	2	0.5	4	0	0	3	3
TMB	OH, High NO_x	2	0.5	4	0	0	3	1

[a]The oxidants correspond to "O_3" = Ozone, "OH, High NOx" = High NOx conditions, "OH, Low NOx" = Low NOx conditions. Columns 4-7 contain approximate starting mixing ratios of the precursors and oxidants.

SOA was collected with a MOUDI equipped with custom-made metal supporting rings to accommodate the uncoated CaF_2 windows as substrates instead of Teflon or foil filters. We typically collected hundreds of micrograms of SOA material per window; the largest amount was typically found on stage 7 of the MOUDI (0.32-0.56 μm particle size range). The window was then placed in a laboratory oven overnight at 40°C with ~10 SLM of purge air flowing over it in order to drive off higher volatility species and anneal the collected SOA particles into a more uniform film on the window. The typical material loss during this process was a few percent of

the collected total mass, as verified by weighing with a Sartorius ME5-F microbalance (1 μg precision).

The window was then placed into a custom-made glass flow cell with 550 sccm of purge air flowing over the window. A UV-light emitting diode (UV-LED; QPhotonics, Inc. UVClean 300-15) with a wavelength centered at ~305 nm, a full width half maximum of ~10 nm, and a power of ~3 mW at 0.8 A current (measured with a Coherent Powermax PS19Q power sensor) was used to irradiate the particles on the CaF_2 window. The actual spectral flux density experienced by the SOA sample was also measured using actinometry as described by Bunce et al.[140] The actinometry and direct power measurements agreed with each other to within a factor of 2.

The OVOCs resulting from the SOA photodegradation were detected with a PTR-ToF-MS (drift tube voltage of 600 V, field strength of ~120 Td, drift temperature 60 °C and resolving power of $m/\Delta m \sim 5\times10^3$). The OVOC mixing ratios in the air flowing over the irradiated sample were estimated using the built-in calculations of the PTR-ToF-MS Viewer software from Ionicon Analytik (v.3.1.0.31), transmission curves created from a calibrated "TO-14" aromatics mix (Linde), and rate constants between the hydronium ion and the OVOCs from Zhao and Zhang.[141] In order to verify the mixing ratios estimated by this method, a calibration of the PTR-ToF-MS was performed for selected OVOCs.

The PTR-ToF-MS was calibrated for the four OVOCs analyzed for this study (acetaldehyde, acetone, acetic acid, and formic acid) by evaporating a known amount of a given OVOC into the cleaned 5 m^3 chamber and monitoring the $[M+H]^+$ peak, corresponding to the protonated OVOC. The OVOC was added to the chamber in small increments, and the corresponding PTR-ToF-MS signal was measured after each successive addition. The inlet line

through which the OVOC was injected into the chamber was heated throughout the experiment to 60 °C, and the PTR-ToF-MS inlet line was also heated to the same temperature to prevent losses of OVOC on the steel surfaces of the inlets. We created a calibration plot for each OVOC comparing the actual amount of OVOC in the chamber with that reported by the PTR-ToF-MS instrument (Figure 2.2). The resulting calibration factors, representing the ratio of the measured to the actual OVOC concentrations, ranged from 1.1 to 4.9. Confidence intervals were calculated at the 95% level based on the uncertainty in the injection, the PTR-ToF-MS traces, and the resulting linear regression. These values are reported in Table 2.2.

We should point out that the calibration was done several months after the SOA photodegradation experiments, following a suggestion from the paper reviewers. To make the calibration as relevant as possible, the PTR-ToF-MS instrumental parameters were kept the same as when the photodegradation experiments were carried out. Nevertheless, because of the large time span between the experiments and the calibration, the conclusions reported in this chapter should be viewed as qualitative.

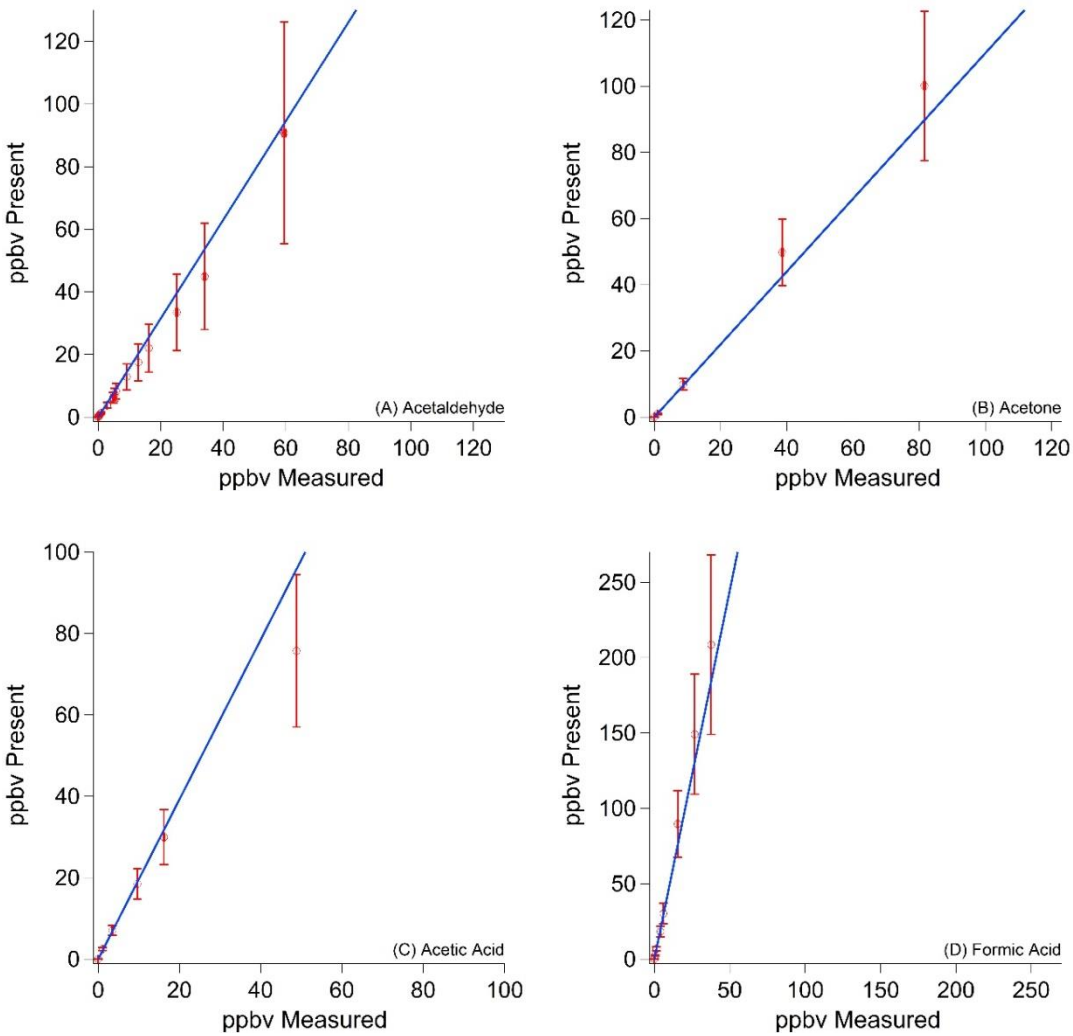

Figure 2.2. The PTR-ToF-MS calibration plots for (A) acetaldehyde, (B) acetone, (C) acetic acid, and (D) formic acid. The horizontal axis is the PTR-ToF-MS measured mixing ratio and the vertical axis is the known amount that was injected into the chamber. Each data point has vertical and horizontal error bars corresponding to 95% confidence intervals of the amount of OVOC present and measured, respectively. The vertical error bars increase with the OVOC amount because of the accumulation of errors in the successive injections of the OVOC in the chamber.

Table 2.2. The resulting calibration factors for each OVOC. For the SOA photodegradation experiments, we multiplied the mixing ratios measured by PTR-ToF-MS by this factor for each OVOC in the main text analysis. The subscripted digits correspond to the first nonsignificant digit.

OVOC	Calibration Factor	95% Confidence Interval
Acetaldehyde	1.5_8	0.2_3
Acetone	1.1_0	0.4_2
Acetic Acid	1.9_6	0.5_3
Formic Acid	4.8_9	0.9_7

2.4 Results and Discussion

2.4.1 Photoproduction of OVOCs

The result of a typical SOA irradiation experiment is shown in Figure 2.3 for an ISO/O_3 SOA sample, in which formic acid, acetic acid, acetaldehyde, and acetone are tracked by PTR-ToF-MS as a function of time. The window was inserted into the flow cell, and the UV-LED was turned on once the measured OVOC levels reached a steady state. Without the SOA sample annealing process, in which the more volatile components of SOA evaporated before the experiment, the background OVOC levels were significantly higher, and it took a long time (many hours) to achieve the steady state. This is likely due to outgassing of these OVOCs, which is accelerated when the annealing process is performed. In this figure, the window was placed in the flow cell just before the 0 min mark, and the irradiation began around 20 min. The resulting OVOCs were then allowed to reach a steady state count, which happened around 115 min for this run. Then the UV-LED was turned off and the counts were monitored until a baseline steady state is reached again for the next sample to be analyzed. Note that it took considerably less time for the acetaldehyde and acetone to reach the steady state levels compared to the acids, and less

time to decay back to the background level. This is due to the acids' sticky nature toward the walls of the flow cell and PTR-ToF-MS inlet line.

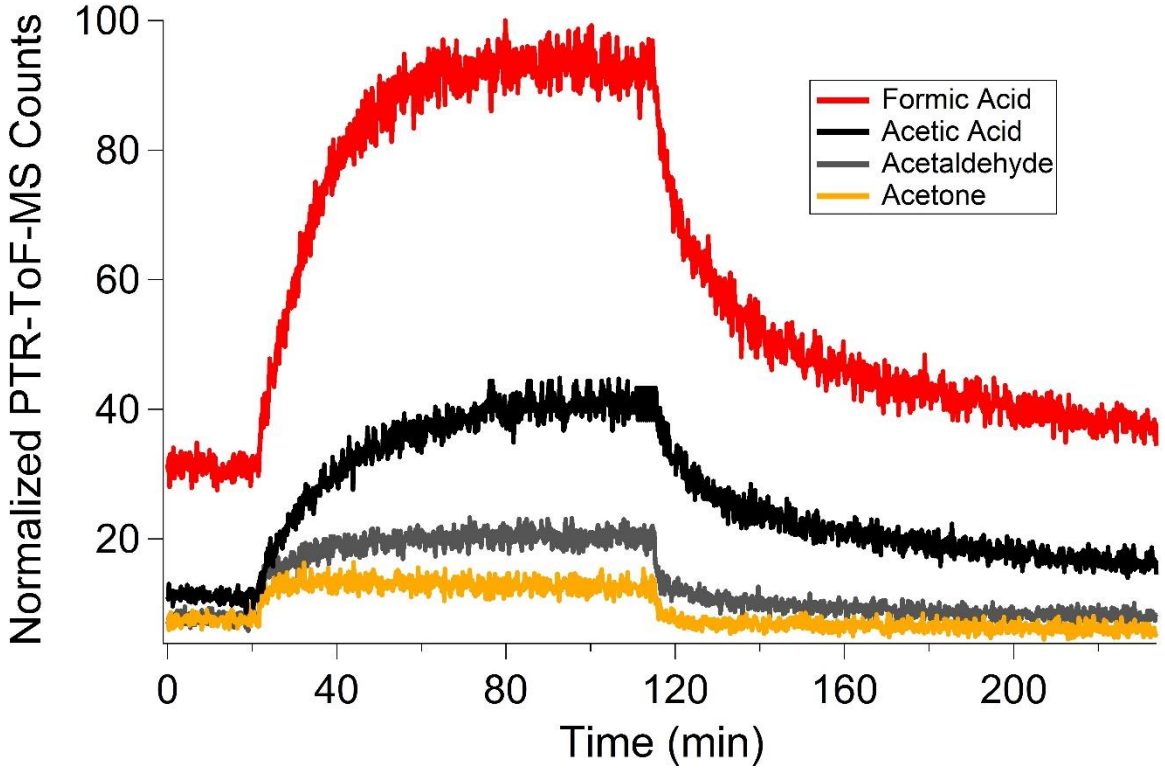

Figure 2.3. A time profile of the PTR-ToF-MS run for the photoproduction of various VOCs from the ISO/O_3 SOA system. The UV-LED was turned on at 20 min and turned off at 115 min in this example.

A number of peaks increased in the mass spectra of irradiated SOA; the list of the nominal masses of the peaks that increased the most can be found in Table 2.3. We focused our attention on the formic acid, acetic acid, acetaldehyde, and acetone peaks because of their efficient photoproduction in all the samples (with the exception of GUA SOA) and because these peaks could be assigned with a relatively high degree of confidence. We note that these were also the major OVOCs observed in photodegradation of limonene ozonolysis SOA by CIMS.[100] The assignments for many other observed peaks in the PTR-ToF-MS spectra were more

ambiguous, especially at higher *m/z* values, as demonstrated, for example, in Table 2.4 for APIN/O_3 SOA. Because of the fragmentation in PTR-ToF-MS, we cannot exclude the possibility that fragments from larger photoproducts contributed to the observed peaks of formic acid, acetic acid, acetaldehyde, and acetone; the amounts reported below could, therefore, be overestimated. Finally, we cannot exclude the possibility that multiple structural isomers could contribute to peaks at *m/z* 61.028 (acetic acid, glycolaldehyde or methyl formate) and *m/z* 59.049 (acetone, propanal or allyl alcohol).

We investigated which peaks increased the most in the PTR-ToF-MS spectra during irradiation of a given SOA sample. This was performed by analyzing the time traces of the spectra, subtracting the baseline spectrum count, and analyzing the peaks that grew the most in intensity during irradiation. The 10 peaks that appeared to increase the most were examined to ensure they were indeed increasing in response to the UV radiation and not just drifting in intensity. Table 2.3 lists all the SOA systems analyzed for this work and the top 10 increasing nominal *m/z* values below *m/z* 100.

Table 2.3. The top 10 increasing peaks (labeled by their nominal *m/z* values) during irradiation for each SOA system analyzed. The peaks are listed in descending order of the relative intensity change, with the peaks that increased the most appearing at the top.[a]

APIN/ High NO_x	**APIN/ Low NO_x**	**APIN/ O_3**	**ISO/ O_3**	**ISO/ High NO_x**	**ISO/ Low NO_x**	**TET/ High NO_x**	**TET/ Low NO_x**	**TMB/ High NO_x**	**TMB/ Low NO_x**
59	59	59	47	47	47	45	45	47	47
47	47	47	61	61	75	55	55	45	61
45	45	61	43	45	61	59	59	61	45
61	61	45	45	43	43	41	41	43	43
43	43	43	75	73	45	69	69	59	75
71	71	71	71	59	73	47	47	73	73
75	57	73	59	75	59	73	73	87	89
73	75	99	57	57	57	61	61	55	59
57	99	41	73	71	71	57	87	89	87
87	73	57	87	87	89	83	83	75	99

[a]The peaks corresponding to acetaldehyde (*m/z* 45, yellow), acetone (*m/z* 59, green), acetic acid (*m/z* 61, red), and formic acid (*m/z* 47, blue), which could be assigned with more certainty and for which the PTR-ToF-MS calibration was done, are color coded.

The PTR-ToF-MS spectrum of OVOC emitted by the irradiated APIN/O_3 SOA system was further analyzed to assign peaks to the top increasing nominal *m/z* values. This system was chosen because it was quite efficient at producing OVOCs under irradiation. Table 2.4 lists the measured *m/z* values, the expected *m/z* values, the potential chemical formula assignments, and possible assignments of the OVOCs. Because of the inability of PTR-ToF-MS to distinguish structural isomers the assignments cannot be made with certainty, especially at higher *m/z* values. However, chemical considerations help limit the assignments for the first four peaks to acetone, formic acid, acetic acid, and acetaldehyde.

Table 2.4. The list of the high resolution *m/z* values for the PTR-ToF-MS peaks for the APIN/O_3 SOA system. The peaks are listed are in descending order for the overall intensity increase during irradiation.

Measured *m/z*	**Theoretical *m/z* of the ion**	**Formula Assignment**	**Examples of OVOC that could match this formula**
59.049	59.04914	$C_3H_6OH^+$	**Acetone**, propanal, allyl alcohol
47.013	47.01276	$CH_2O_2H^+$	**Formic acid**
61.027	61.02841	$C_2H_4O_2H^+$	**Acetic acid**, glycolaldehyde, methyl formate
45.033	45.03349	$C_2H_4OH^+$	**Acetaldehyde**
43.018	43.01784	$C_2H_2OH^+$	Ketene, ethynol, oxirene
71.049	71.04914	$C_4H_6OH^+$	Cyclobutanone, crotonaldehyde, methyl vinyl ketone, dihydrofuran, many other possibilities
73.028	73.02841	$C_3H_4O_2H^+$	Methylglyoxal, acrylic acid, oxetanone, malondialdehyde, many other possibilities
99.080	99.08044	$C_6H_{10}OH^+$	Cyclohexanone, cyclopentylformaldehyde, mesityl oxide, many other possibilities
41.039	41.03858	$C_3H_5^+$	Propyne, allene, cyclopropene
57.033	57.03349	$C_3H_4OH^+$	Acrolein, cyclopropanone, methylketene, other possibilities

2.4.2 Control Experiments

Numerous controls were tested with these experiments. In order to verify that OVOCs were emitted in a photoinduced process and not as a result of evaporation from the SOA material, the window was heated to a higher temperature than what resulted from the exposure to the UV-LED radiation. The sample was irradiated at $\lambda = 310$ nm and separately at $\lambda > 450$ nm using a Xe-Arc lamp (Oriel PhotoMax 60100 housing and Oriel 6256 150 W lamp with a resulting output of ~1-6 mW) with the selected wavelength isolated with a monochromator

(Oriel Cornerstone 74000) to ensure that this process required near-UV radiation. Irradiation of a blank window (exposed to purge air in the MOUDI instead of the SOA) was performed to verify that no OVOCs came from contaminations in the MOUDI or the CaF_2 windows. Finally, we utilized a slit impactor (Sioutas, stage "D") for collection (as opposed to the MOUDI), and utilized an aerosol flow tube[132] for generation of the SOA instead of the chamber to test the level of sensitivity in the measurements to the method of generation and collection of SOA. The heating, visible wavelength irradiation, and blank window irradiation experiments did not produce any detectable OVOC emissions. The slit impactor and flow tube produced results consistent with the MOUDI-collected samples from the chamber. We note that the slit impactor samples took much longer (on the scale of many hours) to reach a steady state for counts observed in the PTR-ToF-MS. This is likely due to the impaction pattern being a thick "strip" as opposed to the more evenly-dispersed material collected with the MOUDI. The thicker the SOA material is on the substrate, the longer it takes for the photoproduced OVOCs to diffuse out of the material.[103] In our experiments with ~10 μm films of SOA material, the time scale for reaching the steady state was about 20 min (Figure 2.3). From Fick's law of diffusion, we estimate that for submicron ambient particles, the phoproducts will be able to diffuse out of submicron particles on a time scale of seconds.

2.4.3 Mass Correlations to Photoproduction of OVOCs

The optical extinction of the SOA was measured by placing the annealed SOA material on CaF_2 windows in a Shimadzu UV-2450 UV-Visible Spectrometer. It was found that the extinction was not correlated to counts observed in the PTR-ToF-MS. The measured extinction was likely dominated by the scattering from particles on the window, which did not contribute to

photochemistry. Furthermore, not all photons absorbed by SOA can lead to VOC production because of the chemical differences between different SOA types.

Although the PTR-ToF-MS signal did not correlate with the extinction for a given SOA type, there was good correlation with the SOA mass collected on the window. Figure 2.4 shows such correlations for the production of acetone from high-NO_x, low-NO_x, and ozonolysis SOA produced from α-pinene. Different slopes were observed for different SOA/OVOC combinations. For example, APIN/O_3 had a higher slope for the photoproduction of acetone than APIN/Low NO_x and APIN/High NO_x, which is consistent with results from Romonosky et al.,[43] who studied photodegradation of different types of SOA in aqueous solutions and concluded that ozonolysis SOA are on average more photolabile than high- or low-NO_x SOA.

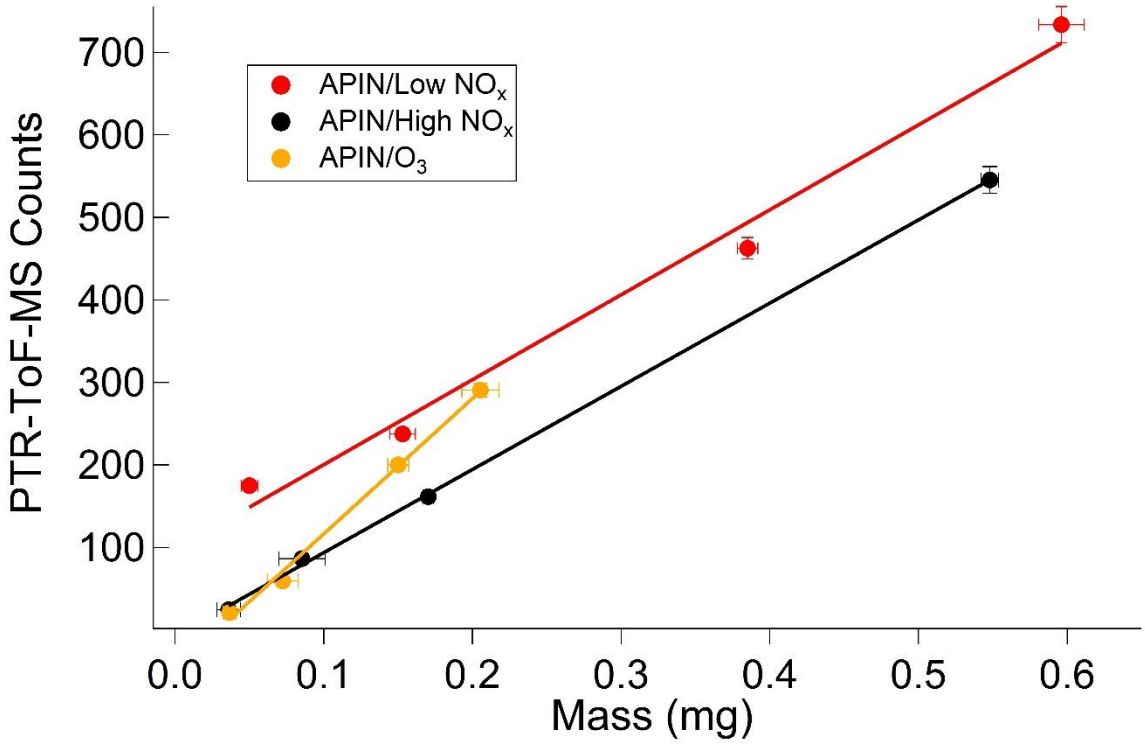

Figure 2.4. The PTR-ToF-MS counts observed versus the mass collected for the various α-pinene SOA systems for the production of acetone. Production of other OVOCs also correlated with the mass of SOA for all the SOA samples analyzed in this study.

2.4.4 Discussion of Mass-Normalized Data across SOA Types

Because the signals observed in the PTR-ToF-MS were linearly proportional to the SOA mass across all four analyzed OVOCs and across all SOA systems (with the exception of GUA, for which the OVOC signal was too small to stablish such a correlation), we normalized the estimated mixing ratios of each OVOC photoproduct by the SOA mass. This normalization made it possible to compare the relative rates of OVOC production in photodegradation of different types of SOA. A plot of the resulting normalized mixing ratios is presented in Figure 2.5 for the four chosen OVOCs: acetaldehyde, formic acid, acetone, and acetic acid. Confidence intervals were calculated at the 95% level which factored in the uncertainty in the mass of the SOA collected on the windows and the PTR-ToF-MS mixing ratio uncertainty. Each CaF_2 window was weighed in triplicate before and after collection of particles, and the PTR-ToF-MS uncertainty in mixing ratios employed the uncertainty in the baseline-subtracted signal and calibration factor uncertainty.

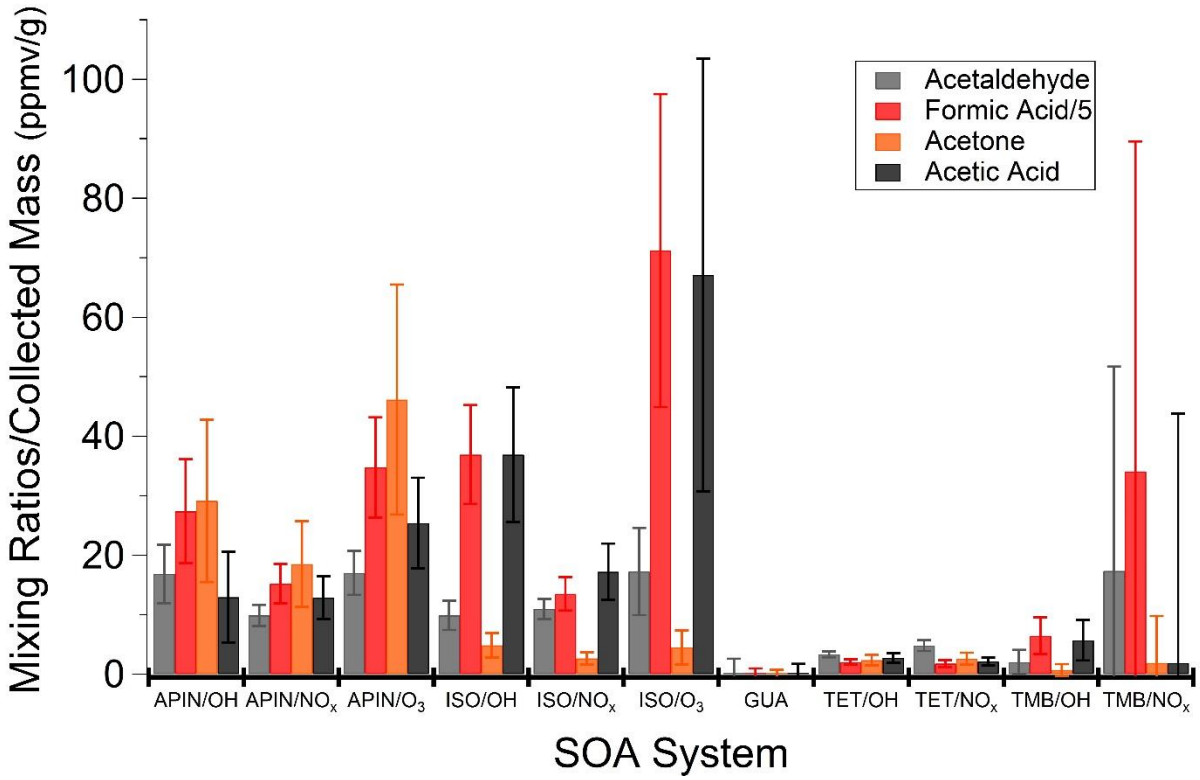

Figure 2.5. A bar plot showing the OVOC mixing ratios divided by the SOA mass collected for all SOA types. The error bars correspond to a 95% confidence interval range. The formic acid values are divided by 5 because its mixing ratios are much higher than for other OVOCs.

All SOA (with the exception of GUA) produced measurable amounts of OVOC photoproducts in these experiments. The relative amount of acetone photoproduct appeared to be higher for all three types of APIN SOA and lower for ISO SOA. Acetone could be a product of Norrish type-II splitting of methyl-terminated ketones, R-C(O)-CH_3, which are common among products of α-pinene oxidation.[93] Conversely, ISO SOA appeared to produce more acetic and formic acid than APIN SOA did, suggesting the secondary processes leading to these acids were more important in the ISO SOA systems. SOA from TET appeared to be less photoactive compared to SOA from APIN and ISO. SOA from saturated hydrocarbons tend to have a relatively low degree of oxidation,[142] which could contribute to their low photoactivity.

SOA from aromatic precursors TMB and GUA also produced much less photoproducts than SOA from APIN and ISO. In fact, guaiacol SOA did not produce any measurable OVOCs under irradiation for either high- or low NO_x SOA types. Wavelengths down to ~250 nm (from the previously-mentioned Xe-arc lamp and monochromator combination and output powers at ~2 mW) were tested for GUA SOA photodegradation with no apparent OVOC production. This lack of OVOC production from GUA SOA and reduced OVOC production from TMB SOA is most likely due to the formation of ring-substituted products during photooxidation in the chamber.[143] When these resulting products are irradiated they either form a triplet state via intersystem crossing and then form further ring substituted products (which are not volatile), or they efficiently relax.[9] Neither of these pathways provides OVOC production. Romonosky et al.[43] also noted that GUA and TMB SOA are more resistant to aqueous-phase photodegradation than other types of SOA.

2.4.5 Atmospheric Implications

The values in Figure 2.5 can be converted into the rate of mass loss from SOA material due to a given photoproduct. Under the steady state conditions of the experiment, the rate of production of a given molecule, Rate [molec s^{-1}], can be related to the concentration of this molecule in the flow, C [molec cm^{-3}], and the flow rate of the purge air, F = 9.17 cm^3 s^{-1}, as follows

$$Rate = F \times C \tag{2.1}$$

Normalizing this rate by the mass of SOA, m_{SOA} [g], and converting from concentration to volume mixing ratio, X [ppmv], and from molecules to the mass of the photoproduct, $m_{product}$ [g],

yields the following expression for the fraction of SOA mass lost per unit time due to a given volatile photoproduct

$$\frac{1}{m_{SOA}}\frac{dm_{product}}{dt} = F \times 2.46 \cdot 10^{13} \times \frac{MW}{N_A} \times \frac{X}{m_{SOA}} \quad \textbf{(2.2)}$$

where MW [g mol^{-1}] is the molecular mass of the photoproduct, N_A [molec mol^{-1}] is Avogadro's number, and the numeric factor ($2.46 \cdot 10^{13}$) accounts for the unit conversion from [ppmv] to [molec cm^{-3}] at 1 atm and 25 °C. The last term in this equation (X/m_{SOA}) is precisely the quantity plotted in Figure 2.5, which has a median value of ~13 ppmv/g for all detected OVOC compounds and examined SOA types (excluding GUA). Taking the average MW of a typical OVOC photoproduct (as analyzed for this study) as 50 g mol^{-1}, the median X/m_{SOA} translates into

$$\frac{1}{m_{SOA}}\frac{dm_{product}}{dt} = 2.4 \cdot 10^{-7} s^{-1} = 8.8 \cdot 10^{-4} h^{-1} \quad \textbf{(2.3)}$$

Based on this prediction, under the conditions of the experiment, the SOA sample would lose on average ~0.1% of its mass after one hour of irradiation from the UV-LED lamp as a result of a loss of a *single* volatile photoproduct. Considering that the photodegradation likely produces multiple volatile products (multiple compounds appeared in the PTR-ToF-MS spectra of the irradiated SOA, and compounds undetectable by the PTR-ToF-MS are also possible), the rate of overall mass loss could be considerably higher. To estimate the rate of the relative mass loss from SOA under ambient conditions, we can correct it by the ratio of the 24-hour average integrated flux from the sun and from our UV-LED.

$$Factor = \frac{\left\langle \int_{290nm}^{320nm} Flux(\lambda)_{sun} \cdot d\lambda \right\rangle_{24hr}}{\int_{290nm}^{320nm} Flux(\lambda)_{LED} \cdot d\lambda} \quad \textbf{(2.4)}$$

The integration extends over the wavelength where the UV-LED emits the most photons (Figure 2.6 compares the wavelength dependence of the UV-LED and the solar radiation). The 24-hour time averaging includes both the daytime, when most photochemistry takes place, and the nighttime, when the solar flux is minimal. The solar flux was calculated at each hour using the Quick TUV calculation[144] with the following parameters: Latitude/Longitude = N 34° W 118° (which corresponds to Los Angeles, California), Overhead Ozone = 300 du, Surface Albedo = 0.1, Ground and Measured Altitude = 0 km, and "pseudo-spherical discrete ordinate 4 streams" calculation methods. The resulting Factor is 0.053 on June 20 (the summer solstice); the value is smaller for other times of the year. For example, the Factor is 0.033 on April 1 (which is representative of the average earth-sun distance throughout the year).

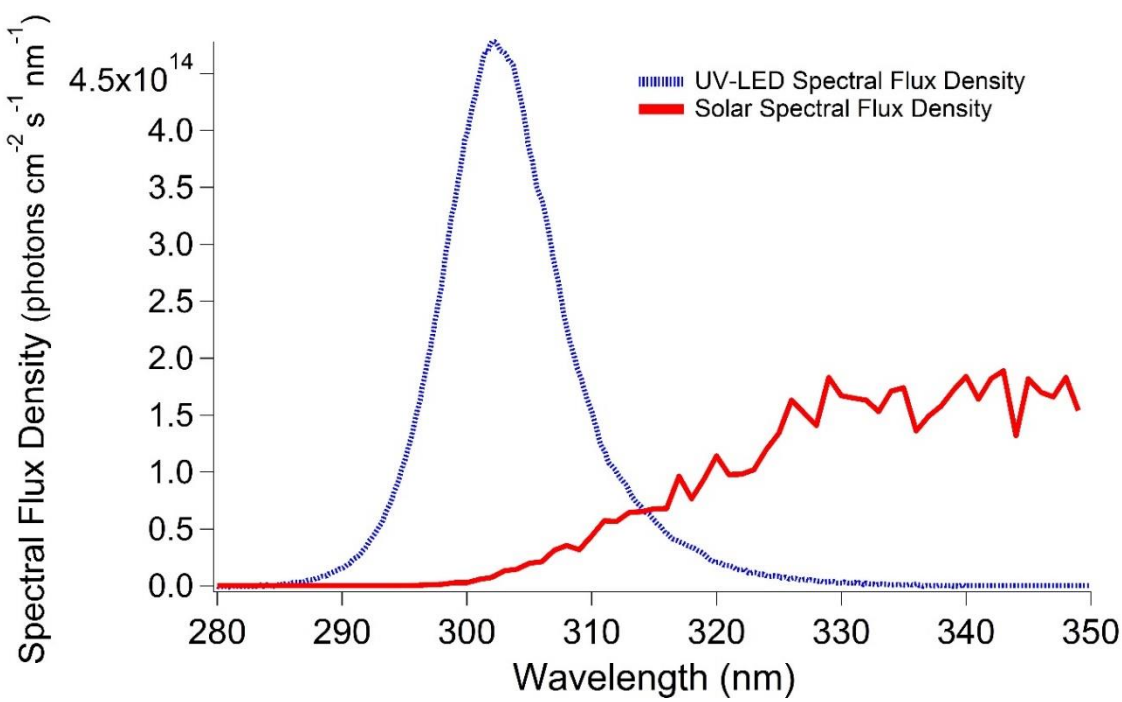

Figure 2.6. A plot comparing the spectral flux densities of the UV-LED and that of the sun at a solar zenith angle of 0°.

The number of OVOCs and other volatile photoproducts emitted during SOA photodegradation and detected by the PTR-ToF-MS was conservatively estimated to be $N \geq 10$ by examining the behavior of the *m/z* < 100 peaks before and during photodegradation. For example, Table 2.3 contains information about the top ten peaks that increased substantially upon irradiation of each SOA sample. This is a lower limit for the number of photoproducts because some of the major expected photoproducts, such as methane and carbon monoxide,[93] are not detectable by PTR-ToF-MS. If we scale the mass loss due to photoproduction of a single OVOC (equation 2.3) by the sun/LED factor (Factor = 0.053 for June 20 in Los Angeles, California) and an estimated lower limit for the number of photoproducts (N = 10), we arrive at the conservative mass loss of at least ~1.1 % after one day or 7.8% after one week. There are few measurements with which to compare this estimate, but our result is very close to the previous observations of Epstein et al.,[73] who estimated that the mobility-equivalent diameter of APIN/O_3 aerosol decreased by 3% over a week of solar radiation (implying a ~9% mass reduction over one week). Wong et al.[95] found that the mass loss rate of APIN/O_3 SOA was ~30% after only one hour of irradiation, which appears to be unrealistically high based on the present results. The high apparent mass loss in the Wong et al. experiments could be due to the loss of semivolatile compounds from the particles to the chamber walls or due to evaporative heating of particles by UV radiation. Despite the large spread in the existing experimental results, it is clear that the mass loss due to photodegradation could occur over atmospherically-relevant time scales for a range of SOA types. SOA particles spend days in the atmosphere before they are removed; the mass loss due to the photodegradation could be significant on this time scale.

Finally, we discuss the possibility that the photochemical reactions in SOA could serve as a source of certain OVOCs. We will focus our discussion on formic acid, since it appears to be a

common photoproduct for many types of SOA.[92-93, 100] Formic acid contributes measurably to the acidity of rain and fog, particularly in remote atmospheres.[145] It is produced in the atmosphere from a variety of primary and secondary sources. Primary sources include automobile exhaust, tree emissions, and biomass burning.[13] Secondary sources include ozonolysis of alkenes and photooxidation of monoterpenes. Models do not yet account for all sources of formic acid. The emissions of formic acid in the atmosphere are currently underpredicted by up to 90 Tg yr^{-1} (out of total yearly emissions of 120 Tg yr^{-1}).[146] Stavrakou et al.[146] noted the lack of laboratory experiments utilizing monoterpenes and isoprene, two major SOA precursors, for production of formic acid. They also noted that the existing models still failed to predict the measured amount of formic acid in the atmosphere, and that a large unidentified secondary biogenic source of formic acid may exist.

To predict the global average formic acid produced per year via the process described in this paper, we used Eq. (2.2) with MW set to the molecular mass of HCOOH (46 g/mol) and the last term equal to the median X/m_{SOA} value of 106 ppmv/g for the formic values shown in Figure 2.5. Accounting for the sun/LED factor of Eq. (2.4), with Factor = 0.033 for April 1 in Los Angeles, CA, this results in

$$\frac{1}{m_{SOA}}\frac{dm_{HCOOH}}{dt}\times Factor = 1.9\,yr^{-1} \qquad \textbf{(2.5)}$$

Hodzic et al.[27] recently discussed an updated model that predicts the SOA burden in the atmosphere as m_{SOA} = 0.95 Tg. The result shows that this process can produce ~1.8 Tg HCOOH yr^{-1}, a large value, which is close to the annual formic acid production from primary sources.[146] The photoproduction of formic acid from SOA particles could therefore contribute to the formic acid budget and help account for part of the discrepancy cited by Stavrakou et al. We note that

because of the potential fragmentation of larger OVOCs into the *m/z* corresponding to formic acid, we could overestimate its production rate from SOA. On the other hand, limiting the integration range of equation (2.4) only to the wavelengths over which UV-LED is emitting (290-320 nm, Figure 2.6) could lead to an underestimation of the production rate. SOA is known to absorb strongly over the entire UV region of the electromagnetic spectrum and into the visible as well.[74] Combined with the uncertainty in the PTR-ToF-MS calibration, the photoproduction rate quoted in this paper should be regarded as an order of magnitude estimate.

2.5 Conclusions

The results of this exploratory study show that photodegrdation of SOA can be efficieint and potentially lead to measureble mass loss from SOA particles and buildup of volatile products of SOA photodegrdation in the atmosphere. However, a number of questions have been left unaswered by this study: (a) What is the effect of RH on the rate of mass loss from SOA particles? Presence of water vapor makes the SOA matrix less viscous, and this could affect the photodegradation kinetics carried out at elevated RH.[147-148] (b) What is the effect of degree of oxidation of SOA on the rate of VOC production? Molecules with a higher degree of oxidation tend to fragment more efficiently in radical driven processes,[72] and the photodegradation mechanism could be similarly affected by the SOA degree of oxidation. (c) Do photosensitized processes play any role? In our experiments, various OVOCs were emitted by the SOA film upon irradiation. Experiments by Monge et al.[111] and Aregahegn et al.[149] observed an opposite process of uptake of VOCs by organic particles when an efficient photosensitizer was present on the surface. By design, our experiments could not probe the uptake resulting from such photosensitized reactions. (d) What is the role of primary vs. secondary photochemical reactions

in the SOA matrix? (e) How does the mechanism depend on the irradiation wavelength and power? While we did not have a chance to address these and many other questions in the present study, it will be important to do these experiments in the future to better understand the effect of these processes on SOA chemistry.

Chapter 3: Photodegradation of Secondary Organic Aerosol Material Quantified with a Quartz Crystal Microbalance

Portions of this chapter are reproduced with permission from Malecha, K. T.; Cai, Z.; Nizkorodov, S. A. "Photodegradation of Secondary Organic Aerosol Material Quantified with a Quartz Crystal Microbalance." Submitted to Environmental Science and Technology Letters, 2017
Unpublished Work Copyright 2017 by the American Chemical Society.

3.1 Abstract

We used a QCM to quantify the mass loss resulting from exposure of SOA particles deposited on the QCM crystal to 254, 305, and 365 nm radiation. The 305 and 365 nm experiments simulate tropospheric photodegradation of SOA, whereas the 254 nm irradiation is relevant for processes in the stratosphere and in OFRs. We coupled the QCM setup to a PTR-ToF-MS to chemically resolve the photoproduced VOCs responsible for the mass loss. The photoproduced VOCs detected by PTR-ToF-MS accounted for ~50% of the mass loss rates measured with QCM. Weakly-absorbing SOA produced by ozonolysis of α-pinene or d-limonene exhibited a much larger mass loss rate in both the QCM and PTR-ToF-MS data compared to strongly-absorbing SOA produced by photooxidation of guaiacol. We predict that the fractional mass loss rate of α-pinene ozonolysis SOA should be as high as ~1% per hour on the Summer solstice in Los Angeles in the lower troposphere, and ~4% per hour in the stratosphere. The mass loss rates for SOA particles crossing a typical 254 nm OFR are expected to be negligible because of the short residence time inside the reactor.

3.2 Introduction

Photodegradation of condensed-phase material in SOA has recently been shown to occur on atmospherically relevant time scales.[15, 67, 73, 95, 138-139, 150] However, all the previous experimental observations of SOA photodegradation have been qualitative, and at best, they reported only rough estimates for the rate of SOA photodegradation. For example, in our previous study, we could only estimate a lower limit of >1% mass loss per day for the photodegradation rate of SOA particles produced from common VOCs.[150] That study relied on a PTR-ToF-MS to observe small, OVOCs of SOA photodegradation, such as acetone, formic acid,

acetic acid and acetaldehyde, and likely missed volatile compounds that PTR-ToF-MS cannot detect such as saturated hydrocarbons, CO, and CO_2.[133]

The contribution of condensed-phase photochemistry to aging of SOA particles in Oxidation Flow Reactors (OFRs) is also uncertain. OFRs are increasingly used to achieve an equivalent of days or even weeks of atmospheric processing in seconds by exposing SOA to very high mixing ratios of OH.[151] OFRs rely on strong 254 nm or 185 nm radiation to produce high concentration of OH inside the reactor. This high concentration of radicals leads to functionalization followed by fragmentation of the molecules in particles.[82] In parallel with this fragmentation, direct photolysis of the SOA compounds may be possible. The effect of photolysis has been extensively modelled but has not been systematically tested by experiments.[152-153]

In this work, we are using a QCM to directly measure sub-microgram mass changes during photodegradation of SOA particles deposited on an inert substrate in real time. The powerful combination of QCM measurements with the PTR-ToF-MS analysis of the volatile OVOC photoproducts makes it possible to probe the chemical mechanisms for SOA undergoing photodegradation. QCM has a rich history of applications in atmospheric chemistry, for example, in studying SOA particle evaporation rates,[154] extent of water absorption on aerosols,[155-158] oxidative aging of organics[159], and photosensitized processes.[111] Our measurements demonstrate the utility of QCM for aerosol photodegradation experiments, and make it possible to quantify photodegradation rates of SOA at different wavelengths, including the 254 nm radiation used in OFRs as well as 305 and 365 nm radiation relevant in the tropospheric photochemistry. We show that photodegradation readily occurs for α-pinene and d-limonene ozonolysis SOA. In contrast, guaiacol/high NO_x SOA is found to be more photoresistant despite being more light-absorbing.

Our results support the conclusion that condensed-phase photochemistry can lead to measurable mass loss from SOA particles on time scale of hours, thus counteracting the aerosol particle growth from gas-to-particle partitioning.

3.3 Experimental Section

The SOA was generated by oxidation of select VOCs in either a smog chamber or aerosol flow tube. Three different types of SOA were investigated for this study: APIN/O_3, LIM/O_3, and GUA/NO_x. The ozonolysis experiments were performed in a flow tube, and the high-NO_x experiments were performed in a smog chamber with the same procedures and conditions as previously reported.[43, 150] All SOA samples were prepared in at least triplicate. The SOA particles were collected using a MOUDI for 1-4 hours with custom adapters to accommodate the 2.54 cm chrome/gold QCM crystals (Stanford Research Systems model O100RX1) as impaction substrates. The resulting SOA material collected on the QCM crystals was annealed as done previously, in order to remove the more volatile compounds and allow for the particles to merge in a continuous, although not uniform film.[150] The masses collected ranged from 0.4 to 2.8 mg, as determined by weighing the crystal before and after the collection with a Sartorius ME5-F microbalance (1 μg precision). Most of the material was distributed fairly evenly around the 2.54 cm crystal for each sample.

We modified a commercial QCM (Stanford Research Systems model QCM 200) holder to include a sealed space above the QCM crystal with a CaF_2 window on top. Details are shown in Figure 3.1. A flow of zero air (at 150 sccm) was sent through the space between the QCM crystal and the CaF_2 window, and a fraction of the outgoing air that was then fed into a PTR-

ToF-MS instrument (Ionicon model 8000) at 100 sccm. The PTR-ToF-MS was calibrated in the same manner as previously done.[150]

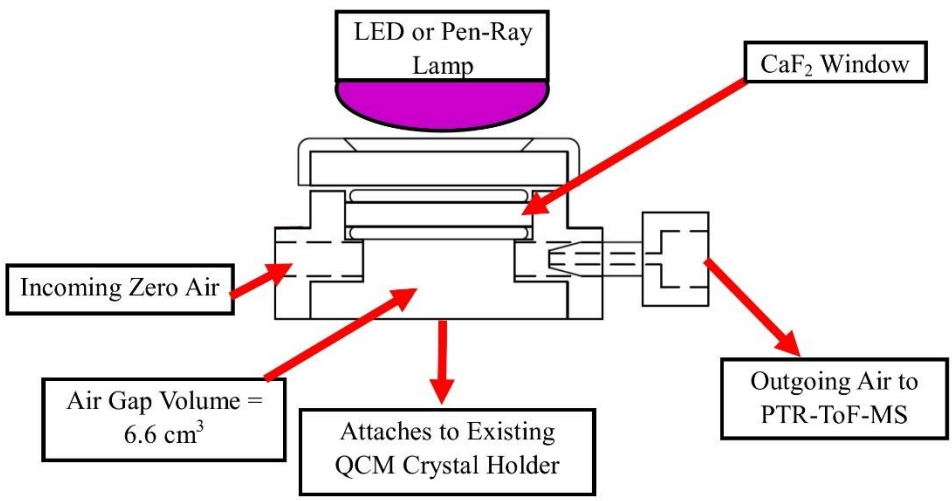

Figure 3.1. Incoming zero air at a flow of 150 sccm flows over the QCM crystal, and the OVOCs emitted as a result of irradiation are detected by the PTR-ToF-MS. The modified sample holder screws into the existing crystal holder, creating a sealed environment. Above the sealed mixing space (volume = 6.6 cm^3) is a 2.54 cm CaF_2 window compressed with o-rings to allow the UV light to irradiate the SOA particles on the QCM crystal.

Exposure to UV radiation reduced the mass of the SOA material remaining on the QCM crystal and increased its oscillation frequency. In order to convert the observed change in QCM frequency into SOA mass, a modified version of the Sauerbrey equation was used:[135]

$$\frac{dm}{dt} = -\frac{1}{C_f}\frac{df}{dt} \qquad \textbf{(3.1)}$$

where d*f*/dt is the rate of the frequency change during irradiation (in Hz/hr), C_f is the sensitivity factor (in Hz/μg), and *dm/dt* is the mass change rate (in μg/hr). Because the collected particles did not form a completely uniform thin film (for which the Sauerbrey equation was developed) C_f had to be determined from calibration experiments. This was done by measuring the

frequency for the clean crystal, collecting SOA on this crystal, determining the mass of SOA (Δm) collected with the Sartorius microbalance, and noting the frequency change (Δf) experienced by the QCM. The sensitivity factor was then calculated from Eq. (3.2) (the integrated form of Eq. (3.1)).

$$C_f = -\frac{\Delta f}{\Delta m} \tag{3.2}$$

Typical sensitivity factors for these experiments ranged between 5 and 14 Hz/μg, with the theoretical sensitivity factor being 11.2 Hz/μg, thus signifying good agreement with the experimental factor. More details are provided below. The sensitivity factors were approximately independent of the QCM mass loading and the type of SOA at higher mass loading (> 1 mg on the crystal) but started to deviate from the theoretical sensitivity factor at lower mass loading (Figure 3.2), presumably because there were not enough particles to form a continuous film on the surface.

In the commonly used form of the Sauerbrey equation, the sensitivity factor C_S has the units of Hz cm^2 μg^{-1} and is calculated as follows:

$$C_S = -\frac{\Delta f * area}{\Delta m} \tag{3.3}$$

where Δf is the frequency change resulting from uniformly distributing mass Δm over the QCM active area. For a rigid thin film of the same density as quartz, the theoretical sensitivity factor should be C_S = 56.6 Hz cm^2 μg^{-1}. We calculated the sensitivity factors for SOA films from the calibrated C_f values (defined in Equations 3.1 and listed in Table 3.1) assuming that the collected mass of SOA particles is uniformly distributed over the QCM substrate area of 5 cm^2 (confirmed by visual inspection). Figure 3.2 plots the sensitivity factor C_S versus the mass loading. The

calculated C_S value for SOA films is of the same order of magnitude as the theoretical value. The values appear to be systematically higher for APIN/O_3 SOA and increase with mass loading for GUA/NO_x SOA.

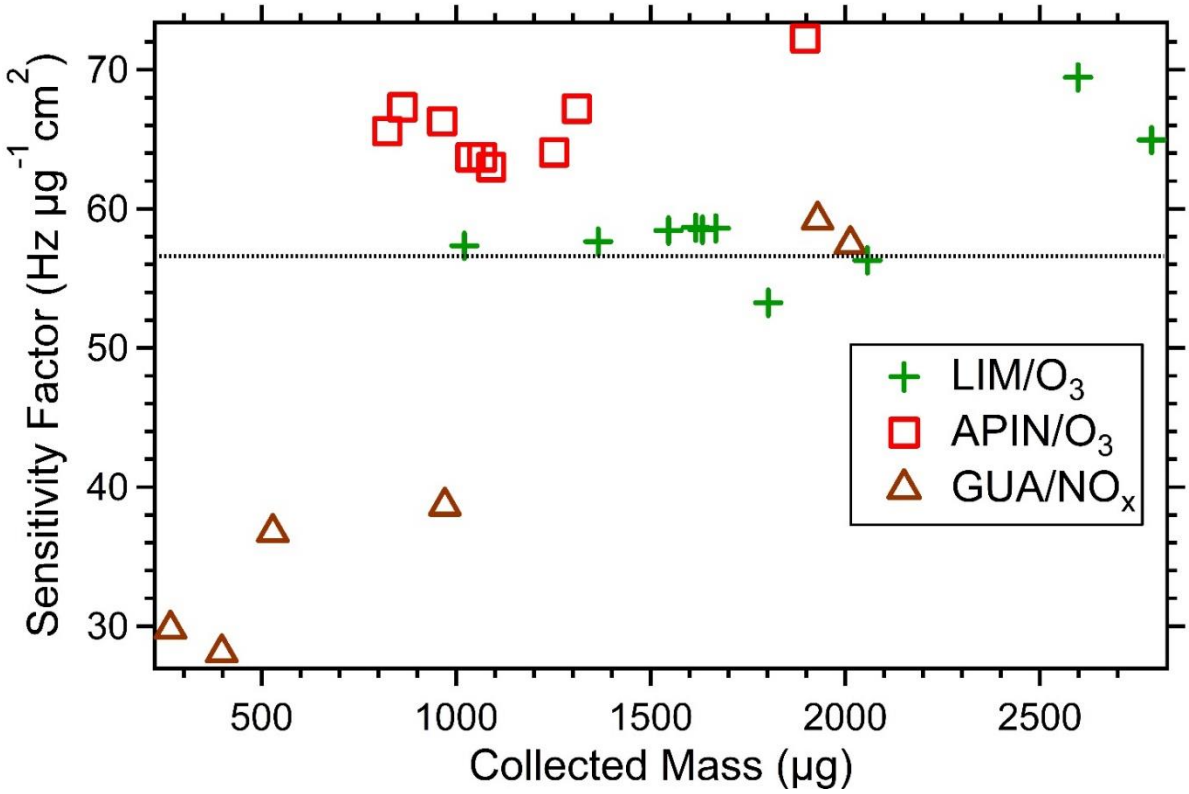

Figure 3.2. The sensitivity factor C_S for each SOA type is compared with the theoretical value of 56.6 Hz cm^2 μg^{-1} (dashed horizontal line). The factors are not very dependent on the mass loading until they are less than 1 mg.

The SOA material was irradiated directly on the QCM crystal with a suitable UV lamp. The lamps included a LED centered at 305 nm (Thorlabs, Inc. model M300L4), another LED centered at 365 nm (Thorlabs, Inc. model M365LP1) and a mercury pen ray lamp centered at 254 nm (Spectronics Corporation model Spectroline 11SC-1). The wavelength dependence of the spectra of the lamps is shown in Figure 3.3. The incident power of each lamp was measured with a Coherent PS19Q power meter in the same geometry that was experienced by the QCM crystal. The resulting powers were 3.7 mW, 2.5 mW, and 13.8 mW for the 254, 305, and 365 nm lamps,

respectively. With the 1 cm^2 area of the power meter, this corresponds to the spectral flux of radiation of $4.7 \cdot 10^{15}$, $3.8 \cdot 10^{15}$ and $2.5 \cdot 10^{15}$ photons cm^{-2} s^{-1}, respectively. The 254 nm lamp has several emission lines from 250-380 nm (Figure 3.3), and the spectral flux of radiation due to the 254 nm emission line was 2.5×10^{15} photons cm^{-2} s^{-1}. We previously showed that power meter measurements agree reasonably well with actinometry experiments (not presented here).[150, 160] The 245 nm spectral flux used in these experiments is comparable to that inside of a typical OFR. For example, Li et al. noted that the spectral flux of radiation in their OFR was $2.0 \cdot 10^{13}$ and $2.5 \cdot 10^{15}$ photons cm^{-2} s^{-1} for the 185 nm and 254 nm lamps, respectively.[161] We also compared the spectral flux densities of the lamps used in this work to that of the sun[144] at two different atmospheric altitudes (0 and 40 km). We utilized the following parameters for the TUV calculation:[144]

- Latitude/Longitude: 34°/-118°
- Date and Time: June 21, 2017, 19:00:00 GMT, representative of the summer solstice maximum flux in Los Angeles, CA
- Overhead Ozone: 300 du
- Surface Albedo: 0.1
- Ground Altitude: 0 km
- Measured Altitude: 0 km or 40 km
- Clouds Optical Depth/Base/Top: 0.00/4.00/5.00
- Aerosols Optical Depth/S-S Albedo/Alpha: 0.235/0.990/1.000
- Sunlight Direct Beam/Diffuse Down/Diffuse Up: 1.0/1.0/0.0
- 4 streams transfer model.

Figure 3.3 shows a comparison of the spectral flux densities for the sun and the lamps. Each flux density is integrated over this wavelength range, and the resulting fluxes are compared in the main text.

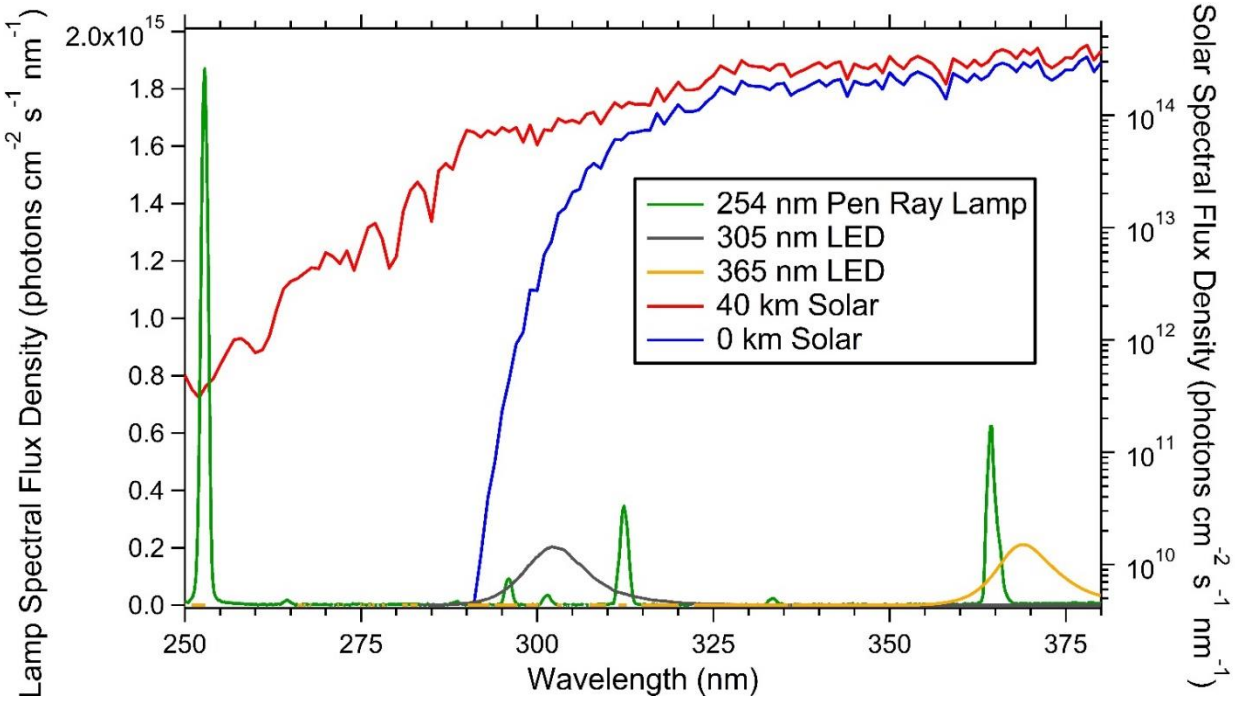

Figure 3.3. The spectral flux densities over the range of the electromagnetic spectrum of the pen-ray lamp (in green), 305 nm LED (in gray), and 365 nm LED (in orange), and the sun at both 40 km and 0 km (in red and blue, respectively) on the summer solstice in Los Angeles, California. The left axis corresponds to the lamps, and the right axis (logarithmic scale) represents the sun's spectral flux density.

The QCM crystals' masses were measured with the ME5-F microbalance before and after collection of the SOA, but due to the design of the QCM sample holder and its o-rings, it was not possible to accurately determine the mass loss during and after irradiation by weighing. We relied on Eq. (3.1) instead to calculate the mass loss from the measured QCM frequency. The QCM measurements were acquired simultaneously with the PTR-ToF-MS measurements. The PTR-ToF-MS data were analyzed based on a modified version of Eq. (2.2) from Chapter 2 to

determine the mass loss rate based on the four quantified photoproduced OVOCs (acetone, acetic acid, acetaldehyde, and formic acid).[150]

3.4 Results and Discussion

3.4.1 Observations of Photodegradation

Figure 3.4 shows results of a typical experiment in which the QCM frequency and selected OVOCs in the PTR-ToF-MS are observed during 254 nm irradiation of LIM/O_3 SOA. When the lamp is turned on, the QCM frequency starts to increase because the SOA material is losing mass from evaporation of the OVOC photoproducts. The rate of the mass loss from Eq. (3.1) is plotted in Figure 3.4c. The mass loss rate increases to a relatively constant value for ~15 minutes and then slowly decreases, replicating the measured trace of the major OVOC photoproduct, formic acid. When the lamp is turned off, the mass loss does not stop instantaneously because it takes some time the OVOC photoproducts to diffuse out of the SOA material and escape in the gas phase.

In most experiments, the QCM frequency was observed to increase at a small constant rate even without radiation due to slow evaporation of SOA material. To better visualize the extent of radiation-driven mass loss, the data shown in Figure 3.4 was baseline-corrected by subtracting the change attributable to evaporation (measured before the lamp was turned on):

$$f_{corrected}(t) = f(t) - \left(\frac{df}{dt}\right)_{dark} \times t \qquad \textbf{(3.4)}$$

For the 254 nm and 305 nm experiments, the rate of change in the frequency due to the SOA evaporation was much smaller than that due to photolysis. The effect of photolysis became much smaller in 365 nm experiments and would be difficult to ascertain without the baseline correction of Eq. (3.4).

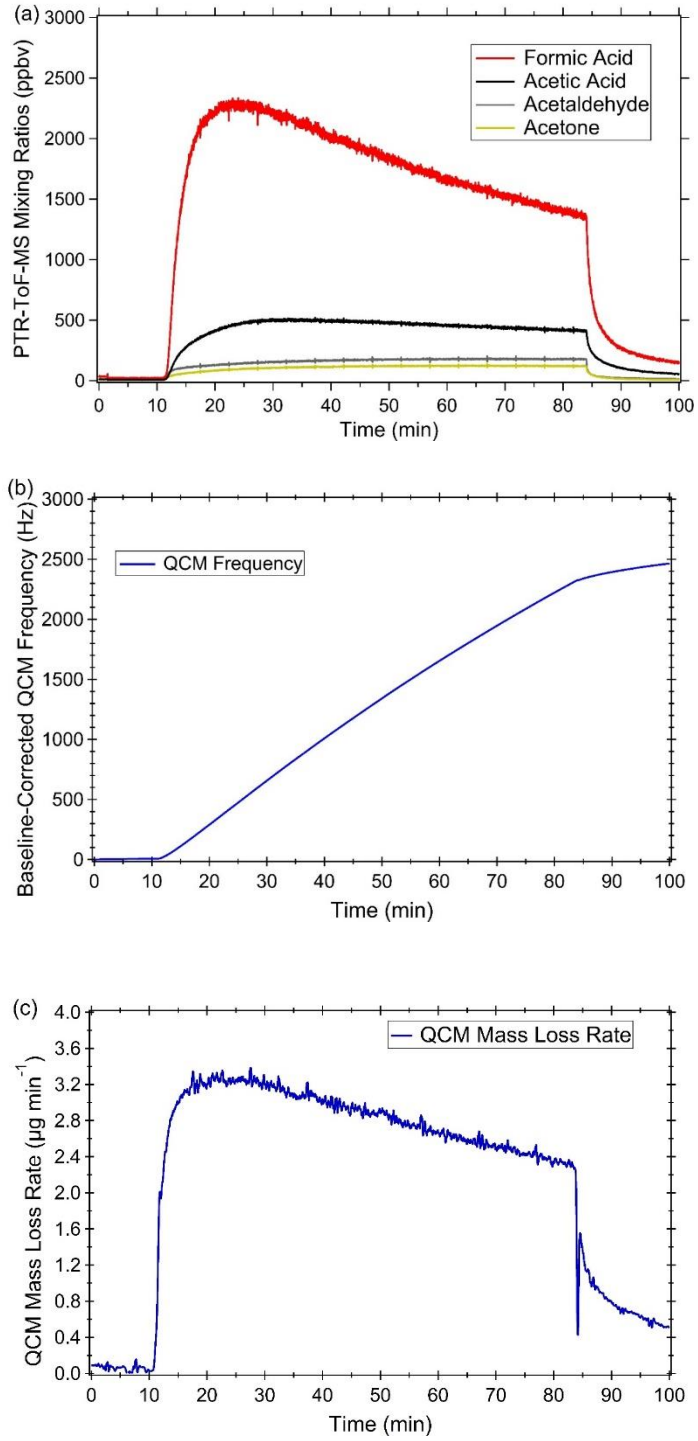

Figure 3.4. (a) Photoproduction of OVOCs observed during 254 nm irradiation of LIM/O_3 SOA. The lamp is turned on at ~10 min and turned off at ~85 min for this sample. (b) The baseline-corrected QCM frequency increases during irradiation because of the SOA material is losing mass. (c) The QCM frequency's mass loss rate, which was determined by taking the derivative of the frequency change with respect to time and then divided by C_f (Eq. 3.1), is also plotted.

The increase in the QCM frequency was accompanied by the photoproduction of a variety of OVOCs. The selected OVOCs plotted in Figure 3.4 include formic acid, acetic acid, acetaldehyde, and acetone – the same OVOCs that were shown to be produced during photodegradation in our previous studies.[150, 160]

These observed changes in the PTR-ToF-MS traces and QCM frequency occurred readily for both the 254 nm and 305 nm radiation; however, the baseline-subtracted 365 nm data, despite the larger photon flux, showed very small mass losses from both the PTR-ToF-MS and the QCM. This is consistent with photolysis yields and absorption cross sections of most molecules decreasing rapidly at longer wavelengths.[4, 13]

3.4.2 Comparing the PTR-ToF-MS and QCM Data

The PTR-ToF-MS data were analyzed as described previously to calculate the mass loss rate attributable to OVOCs.[150] Briefly, the mass loss for each of the major four detected photoproducts (acetone, acetaldehyde, acetic acid, and formic acid) was calculated during the initial part of the photodegradation (e.g. ~20-30 min for the sample in Figure 3.4) using Eq. (2.2) from Chapter 2. and added together to calculate the total mass loss due to these photoproducts.[150] All data are presented in Table 3.1 As noted earlier, the mass loss is likely underpredicted by the PTR-ToF-MS because it is blind to compounds such as methane and carbon monoxide, which are known to be produced in photodegradation of SOA.[93] Figure 3.5 plots the estimated PTR-ToF-MS data versus the actual QCM mass loss rate. Despite the limitations of the PTR-ToF-MS approach, the data are reasonably correlated. Furthermore, these four OVOCs estimate accounts for ~50% of the mass lost (based on the slope of Figure 3.5a).

Table 3.1. All the SOA samples examined in this study. Colum 3 contains the integrated photon fluxes for each sample. The 254 nm data's integrated flux only contains the emission line at 254 nm (other lines assumed to contribute little to photochemistry). Column 4 contains the mass collected on the QCM crystal after the annealing step mentioned in the main text. The masses were taken in triplicate and averaged. C_f was calculated as per the main text (the product of the mass collected and C_f is equal to the change in QCM frequency between the loaded crystal and clean crystal). The mass loss rates for this study were taken during the initial part of the photodegradation, where the frequency change was linear. The PTR Mass Loss Rate was determined by summing up each of the 4 OVOCs' mass loss rates as discussed in the main text.

Sample	λ (nm)	Integrated Flux (Photons/cm^2 s)	Mass Collected After Anneal (μg)	C_f (Hz/μg)	Time Lamp On (hr)	QCM Mass Loss Rate (μg/hr)	PTR Mass Loss Rate (μg/hr)
APIN/O_3	254	2.5x10^{15}	1090	12.60	2.0	168.9	93.1
APIN/O_3	254	2.5x10^{15}	1037	12.74	2.0	148.9	79.5
APIN/O_3	254	2.5x10^{15}	1897	14.45	65.3	231.5	103.4
APIN/O_3	305	3.8x10^{15}	964	13.26	1.8	10.9	7.0
APIN/O_3	305	3.8x10^{15}	1067	12.74	1.7	35.4	16.2
APIN/O_3	305	3.8x10^{15}	1310	13.44	1.1	40.6	22.3
APIN/O_3	365	2.5x10^{15}	1252	12.81	0.9	1.0	1.1
APIN/O_3	365	2.5x10^{15}	823	13.12	0.8	1.5	0.9
APIN/O_3	365	2.5x10^{15}	862	13.46	0.7	-0.1	0.9
GUA/NO_x	254	2.5x10^{15}	971	7.73	1.8	23.2	2.2
GUA/NO_x	254	2.5x10^{15}	2013	11.49	1.0	25.5	2.5
GUA/NO_x	254	2.5x10^{15}	266	5.96	26.0	18.8	1.9
GUA/NO_x	305	3.8x10^{15}	529	7.35	17.3	3.6	0.6
GUA/NO_x	305	3.8x10^{15}	1929	11.84	20.7	3.7	0.5
GUA/NO_x	305	3.8x10^{15}	398	5.62	66.3	1.5	0.4
LIM/O_3	254	2.5x10^{15}	1365	11.53	1.2	165.3	70.7
LIM/O_3	254	2.5x10^{15}	1021	11.47	1.0	168.2	81.6
LIM/O_3	254	2.5x10^{15}	1667	11.72	1.6	148.5	73.2
LIM/O_3	254	2.5x10^{15}	1667	11.72	18.8	43.1	29.1
LIM/O_3	305	3.8x10^{15}	1546	1.69	0.8	56.1	24.1
LIM/O_3	305	3.8x10^{15}	1633	11.70	1.6	58.5	21.3
LIM/O_3	305	3.8x10^{15}	1616	11.73	1.4	62.7	19.7
LIM/O_3	365	2.5x10^{15}	2787	12.99	4.7	5.1	3.3
LIM/O_3	365	2.5x10^{15}	1802	10.65	1.6	-2.9	0.2
LIM/O_3	365	2.5x10^{15}	2598	13.89	1.4	-0.5	0.2
LIM/O_3	365	2.5x10^{15}	2057	11.26	1.0	2.2	0.2

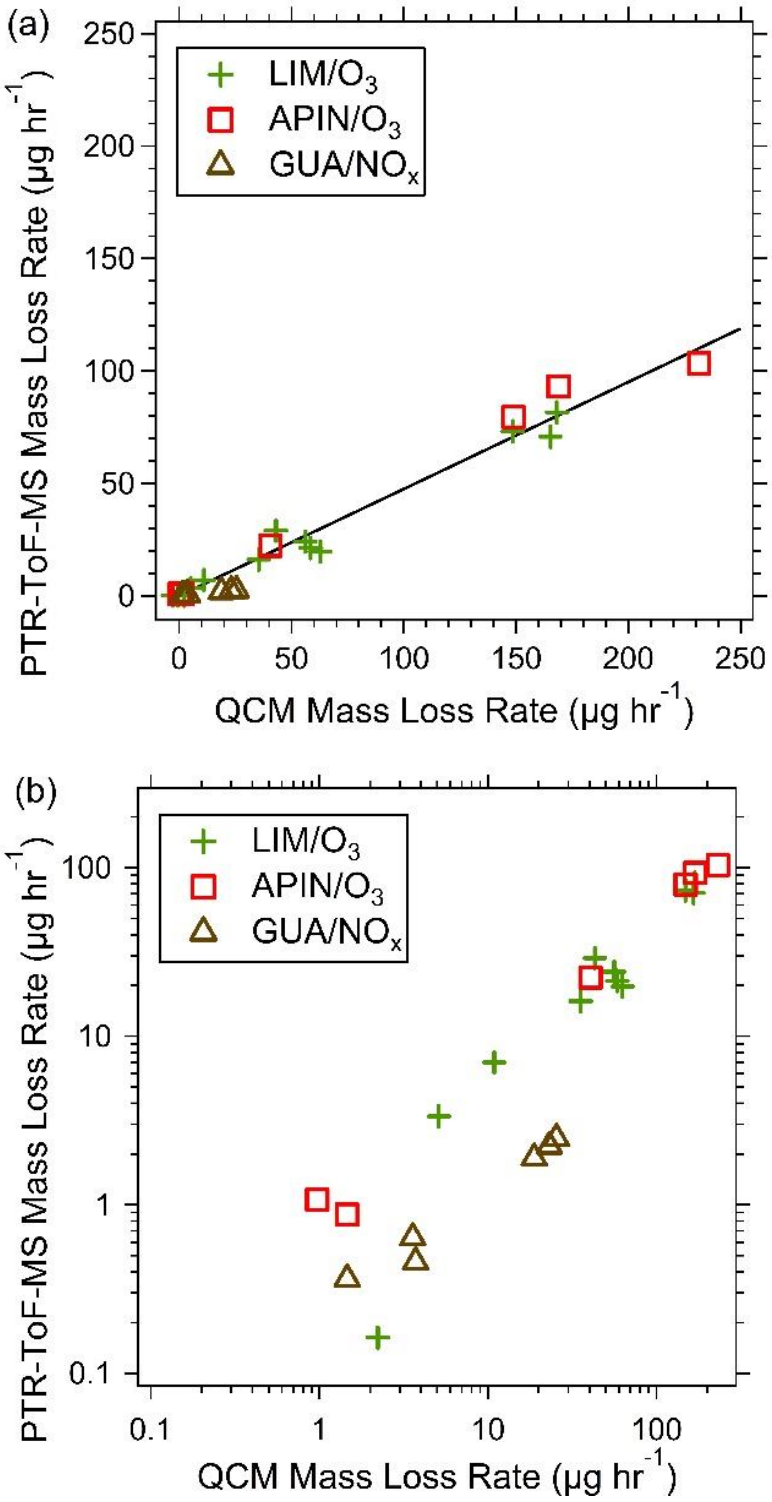

Figure 3.5. (a) The QCM- and PTR-ToF-MS mass loss rates are roughly linearly proportional to one another for all SOA types in this study with the slope being ~0.5. (b) The log-log plot of the same data to zoom in on smaller values.

This study confirmed that the mass loss rates are not correlated to the SOA absorption coefficients. For example, even though the guaiacol samples are the most absorbing[74] (the SOA samples are colored deep brown) they tend to have the lowest mass loss rate. The amount of OVOCs detected by PTR-ToF-MS is close to the detection limit, and only a small mass loss rate is measured with the QCM. The resilience of guaiacol SOA to photodegradation suggests that its compounds must efficiently dispose of the electronic excitation energy. Many of these guaiacol/high NO_x SOA products include derivatives of aromatic species such as nitrophenols, 4-nitroguaiacol, 6-nitroguaiacol, or 4,6-dinotroguaiacol, which have been detected in the condensed phase of the SOA particles.[143, 162-163] The reported photolysis quantum yields of nitrophenols can be high in the gas and aqueous phase (up to 0.3 for 2-nitrophenol).[164-165] However, the yields drop by up to a factor of 10^4 in viscous matrices.[165] The photoexcitation of nitrophenol clusters was shown to result in fast internal conversion mediated by intramolecular hydrogen bonding.[166] These studies suggest that GUA/NO_x SOA compounds may channel most of the excitation energy into heat by internal conversion.

3.4.3 Control Experiments

Several controls were run for this study. The QCM was briefly heated for several minutes with a heat gun to an elevated temperature of 25 °C with the SOA material on it (baseline temperature of 20 °C and maximum UV-LED irradiation temperature of 22 °C), and after an initial drop in QCM frequency, the frequency returned to the initial value, suggesting minimal loss in in the SOA mass due to the heat pulse. A heat control was also run on an empty QCM crystal with similar results. Empty windows were also irradiated with the lamps, and the QCM frequency increased by fewer than 10 Hz to a steady state during irradiation. After the lamp was

shut off, the QCM frequency returned to the same baseline. Finally, a QCM crystal was coated with paraffin wax (assumed to be photostable) and thereafter irradiated. As expected, this sample showed no changes in QCM frequency, suggesting no mass loss of the substrate.

3.4.4 Oxidation Flow Reactor Implications

These measurements have several important implications. We can confirm that the particle mass loss driven by condensed-phase photochemistry is not a serious concern for most OFRs. It is well known that heterogeneous oxidation in OFRs can significantly reduce the size and mass concentration of organic aerosol particles by fragmentation reactions.[82, 167] However, within a 5 min residence time in an OFR reactor less than 1% of particle mass would be lost to the photodegradation processes investigated in this work. It is conceivable that a small fraction of the most photolabile molecules could still undergo photolysis or photoisomerization on this time scale, but these minority compounds would not strongly affect the overall particle mass concentration.

3.4.5 Atmospheric Implications

The mass loss rates discussed in this work could be significant in the atmosphere. The measured fractional mass loss rate (FMLR) was in excess of 10% per hour for the 254 nm irradiation and up to 4% per hour for the 305 nm irradiation (Table 3.1). To estimate FMLR under atmospheric conditions, we assumed that it is proportional to the convolution of the spectral flux of radiation, $F(\lambda)$, and photodegradation efficiency, $E(\lambda)$.

$$FMLR = \frac{1}{m}\frac{dm}{dt} = \int F(\lambda) \bullet E(\lambda) \bullet d\lambda \qquad \textbf{(3.5)}$$

The right hand side of Eq. (3.5) is the convolution of the spectral flux of radiation, $F(\lambda)$, and the efficiency of photodegradation, $E(\lambda)$. The latter is a combination of the effective quantum yield and absorption cross section for the SOA compounds as well as unit conversion constants. Because the lamps in this study have narrow bandwidths, we can determine the efficiency for each of the three irradiation wavelengths by rearranging Eq. (3.5):

$$E(\lambda) = \frac{FMLR_{measured}(\lambda)}{\int F_{lamp}(\lambda) \bullet d\lambda} \tag{3.6}$$

The plots of the efficiency versus wavelength are presented in Figure 3.6 for APIN/O_3 and LIM/O_3 SOA (the mass loss rates for GUA/NO_X SOA samples were too small and could not be measured reliably at all wavelengths). Because the absorption cross section of many molecules decay exponentially in wavelength in this wavelength range,[4, 13] the efficiency was fitted to an empirical exponential function of wavelength as shown in Figure 3.6. The resulting function was inserted into Eq. (3.6) to predict the fractional mass loss rate in the atmosphere

$$FMLR_{atmosphere} = \int F_{sun}(\lambda) \bullet E(\lambda) \bullet d\lambda \tag{3.7}$$

The solar photon fluxes used in the estimate correspond to the Summer solstice in Los Angeles at 0 km and 40 km above sea level (representative of the lower troposphere and upper stratosphere, respectively) derived from the quick TUV calculator.[144]

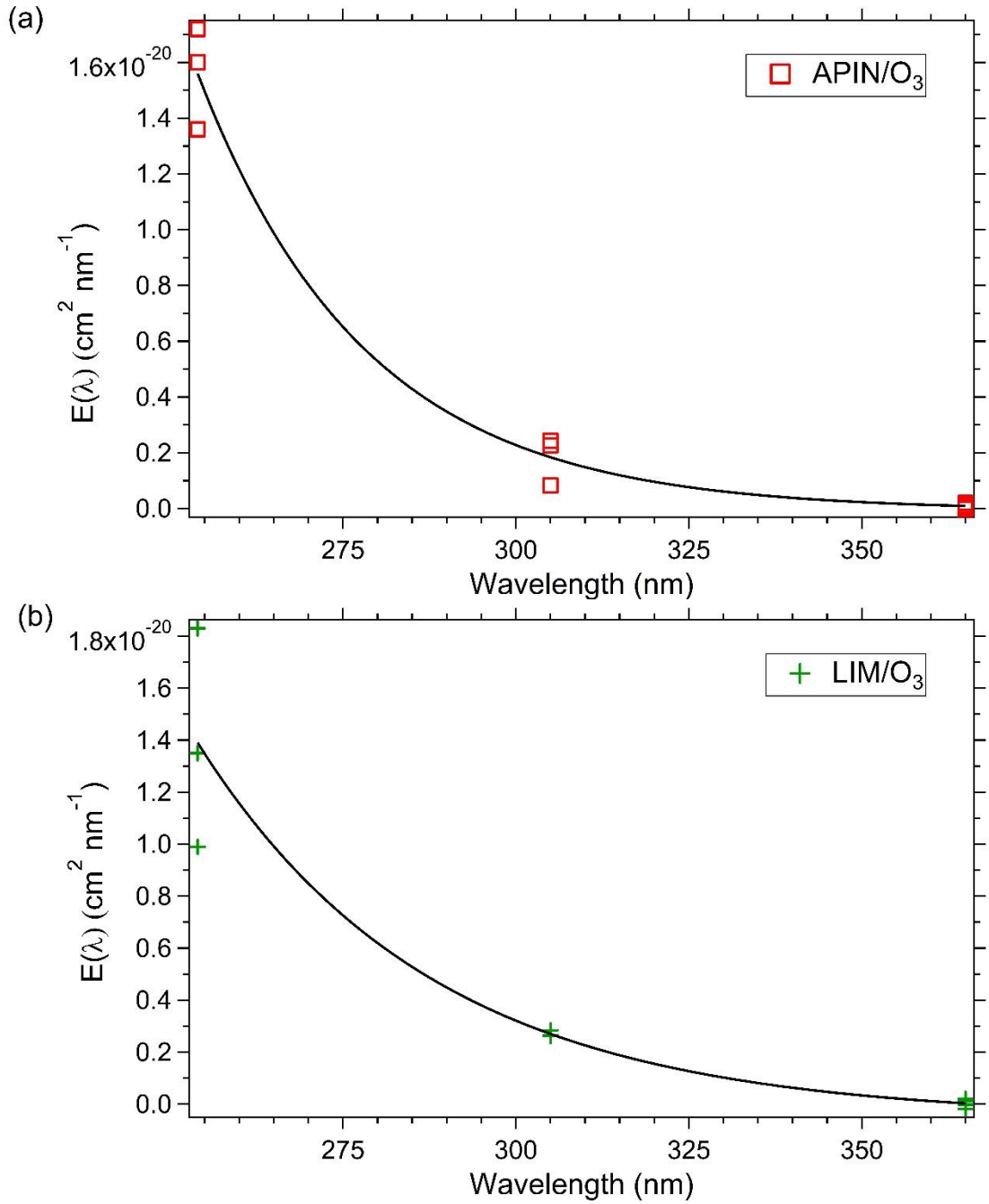

Figure 3.6. The efficiency factor is plotted for the (a) APIN/O_3 and (b) LIM/O_3 data. Each curve is fit to an exponential decay (solid line).

With this approach, the FMLR values during the summer solstice in Los Angeles were found to be 3.8×10^{-6} s^{-1} for APIN/O_3 SOA at 0 km, $1.1\text{x}10^{-5}$ s^{-1} for APIN/O_3 SOA at 40 km, 6.2×10^{-6} s^{-1} for LIM/O_3 SOA at 0 km, and 1.6×10^{-5} s^{-1} for LIM/O_3 at 40 km. These rates would imply up to a 1% mass lost in one hour in the troposphere and a 4% mass lost in one hour in the stratosphere for the APIN/O_3 SOA. This may not seem like much, but 1% per hour translates into 40% mass loss after 50 hours of peak exposure, suggesting that particles can lose a large fraction of their mass after several days in the atmosphere. This finding supports a modeling conjecture by Hodzic et al.,[91] which predicted that SOA mass would decrease by 40-60% after 10 days of atmospheric aging if photolysis processes in particles are included in the model.

Third, these photodegradation processes are predicted to efficiently deplete organic particles from the stratosphere. SOA particles can be transported to the stratosphere through deep convective transport,[168] and the photochemistry associated with the 254 nm radiation in this study could then contribute to their aging. The aerosol particle viscosity would increase in these cool, dry areas of the atmosphere,[169] thus slowing down diffusion in the particle and limiting the aging by heterogeneous reactions with OH to the particle surface. However, the photolysis driven aging could still occur throughout the particle volume because UV radiation can penetrate deep inside the particle. It is remarkable that there does not appear to be a limit on the amount of SOA particle material that can be removed by photodegradation. For selected experiments, the APIN/O_3 particles were subjected to many days of continuous 254 nm irradiation. Nearly 100% of the mass was lost during this time for the APIN/O_3 sample (Figure 3.7); the QCM crystal had almost no visible traces of the organic film after the irradiation. Figure 3.7 contains QCM data from a very long exposure of the substrate to continuous radiation. The APIN/O_3 data were irradiated with 254 nm light starting right before the 2 hr mark and was left on until right before the end of this plot.

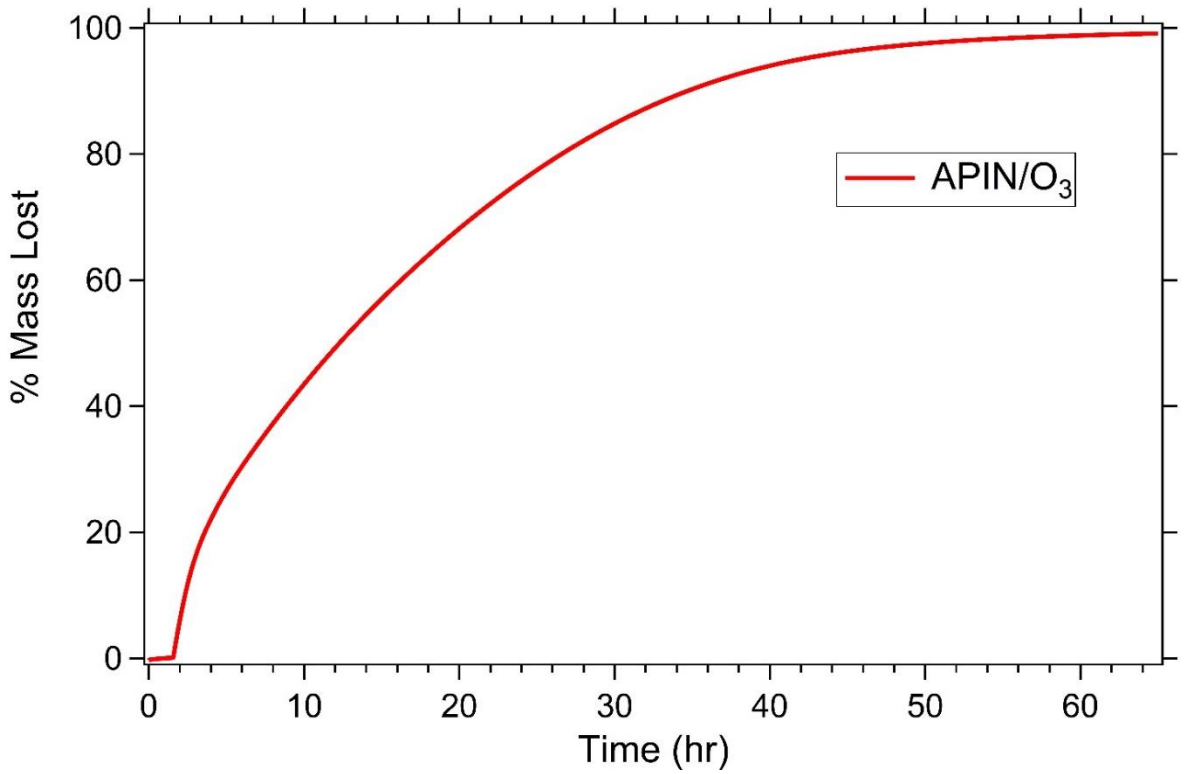

Figure 3.7. The present of mass lost for the APIN/O_3 SOA during long 254 nm irradiation. Nearly all the APIN/O_3 SOA sample mass was lost during this long irradiation period.

The UV photodegradation is thus likely responsible for the low fraction of particulate organics above the tropopause, with only the most photostable organics surviving in this environment.[170]

Chapter 4: Feasibility of Photosensitized Reactions with Secondary Organic Aerosol Particles in the Presence of Volatile Organic Compounds

Portions of this chapter are reproduced with permission from Malecha, K. T.; Nizkorodov, S. A. "Feasibility of Photosensitized Reactions with Secondary Organic Aerosol Particles in the Presence of Volatile Organic Compounds." Journal of Physical Chemistry A 2017, 121, 4961-4967; DOI: 10.1021/acs.jpca.7b04066.
Copyright 2017 by the American Chemical Society.

4.1 Abstract

The ability of a complex mixture of organic compounds found in SOA to act as a photosensitizer in the oxidation of VOCs was investigated. Different types of SOA were produced in a smog chamber by oxidation of various biogenic and anthropogenic VOCs. The SOA particles were collected from the chamber onto an inert substrate, and the resulting material was exposed to 365 nm radiation in an air flow containing ~200 ppbv of limonene vapor. The mixing ratio of limonene and other VOCs in the flow was observed with PTR-ToF-MS. The photosensitized uptake of limonene was observed for several SOA materials, with a lower limit for the reactive uptake coefficient on the scale of ~10^{-5}. The lower limit for the uptake coefficient under conditions of Los Angeles, California on the summer solstice at noon was estimated to be on the order of ~10^{-6}. Photoproduction of OVOCs resulting from photodegradation of the SOA material also occurred in parallel with the photosensitized uptake of limonene. The estimated photosensitized limonene uptake rates by atmospheric SOA particles and vegetation surfaces appear to be too small to compete with the atmospheric oxidation of limonene by the hydroxyl radical or ozone. However, these processes could play a role in the leaf boundary layer where concentrations of oxidants are depleted, and concentrations of VOCs are enhanced relative to the free atmosphere.

4.2 Introduction

Atmospheric SOA is produced when atmospheric oxidants react with biogenic or anthropogenic VOCs.[16] These reactions lead to successively lower volatility organics, which eventually partition into particles.[16] Further aging of the SOA particles can involve a variety of chemical and physical changes. For example, UV-induced photodegradation can reduce the average size and volatility of SOA compounds and serve as a source of small oxygenated VOCs, such as formic acid.[67, 73, 95, 129, 139, 150] Alternatively, certain photochemical processes occurring at surfaces of aerosol particles and other environmental interfaces can also increase the average size and complexity of particulate organics.[171]

Recent work has suggested an additional pathway to SOA particle growth through a photosensitized process in which VOCs are reactively taken up into particles in the presence of solar radiation and suitable photosenitizers.[111, 149, 172-176] Monge et al.[111] observed a size and mass increase of aerosol particles loaded with photosensitizers in the presence of limonene or isoprene and near-UV radiation. Aregahegn et al.[149] observed a diameter growth of ammonium sulfate/glyoxal particles in the presence of various VOCs, and they attributed this growth to photosensitization processes involving imidazole-2-carboxyaldehyde (IC).[177] In a follow-up study by Rossignol et al.,[174] the authors proposed a mechanism for the photosensitized oxidation of limonene on IC-containing particles, and they detected highly oxidized products of limonene with high-resolution mass spectrometry. Photosensitized oxidation of isoprene by IC was also observed in aqueous solution.[175] All the previous studies involved various atmospheric aerosol proxies, such as IC-containing mixtures, and to the best of our knowledge, there is no published work on photosensitization by SOA.

The main goal of the experiments reported in this chapter is to verify whether similar photosensitized processes can occur in more atmospherically-relevant systems, such as SOA produced by photooxidation of common biogenic and anthropogenic VOCs. With this project, the following questions are posed: (1) Does laboratory-generated SOA material have photosensitization properties? (2) What types of SOA materials show these properties? (3) Can the photosensitized uptake of VOCs into SOA particles and onto environmental surfaces under typical atmospheric conditions compete with oxidation of VOCs by gas-phase processes? To answer these questions, laboratory-generated SOA was collected on an inert substrate, and then it was irradiated in the presence of limonene vapor. We find that photosensitized uptake of limonene is possible on a broad range of SOA types; however, the estimated rate of photosensitized uptake under typical atmospheric conditions is considerably lower than the rates of gas-phase oxidation of limonene by OH and/or ozone. Photosensitized SOA+VOC processes on the vegetation could still play a role, especially in the immediate vicinity of leaves.

4.3 Experimental Section

Figure 4.1 shows an overview of the experimental approach. The SOA was generated in a ~5 m^3 Teflon chamber in the absence of seed particles. The SOA formation was monitored with an SMPS, an NO_y monitor (Thermo Scientific model 42i-Y), an ozone monitor (Thermo Scientific model 49i), and, for select experiments, a PTR-ToF-MS.

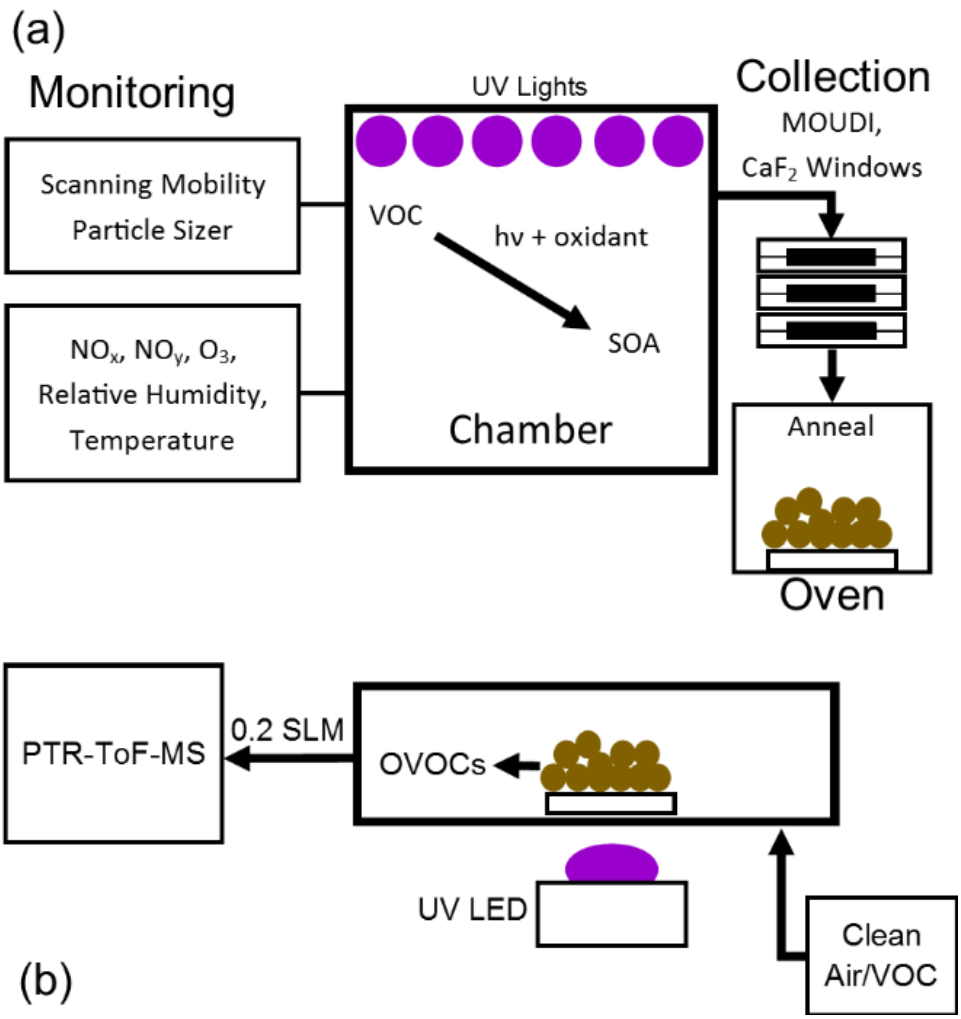

Figure 4.1. An overview of the SOA photosensitization experiments. (a) The SOA is prepared in the chamber, collected on an inert substrate, and annealed to remove volatile SOA components. (b) The sample is irradiated with a UV-LED directly on the substrate in a photolysis flow cell. A collapsible Teflon bag provides either purge air or air containing a known mixing ratio of limonene. The limonene and photoproduced OVOCs are monitored with the PTR-ToF-MS with an inlet flow of 0.2 SLM.

Table 4.1 lists the experimental conditions for the SOA generation. Relatively high mixing ratios of VOCs and oxidants were used in order to collect sufficient amounts of material for analysis. Hydrogen peroxide (H_2O_2) served as the OH precursor in low- and high NO_x photooxidation experiments. H_2O_2 was added to the chamber by evaporating a measured volume of 30 wt % H_2O_2 aqueous solution in a cleaned glass trap with a stream of purge air. For high-

NOx experiments, NO was added from a premixed gas cylinder to achieve a mixing ratio of ~900 ppbv. The VOC was added by evaporating a measured volume of pure VOC liquid or, in the case of naphthalene, a solution of 0.5 g mL^{-1} naphthalene in dichloromethane. The reagents' purity levels are listed in Table 4.2. The injected gases were mixed with a fan for several minutes, and the fan was turned off before turning on the UV lamps to minimize wall loss of particles. Forty-two UV-B lamps (centered at 310 nm; Solar Tec Systems model FS40T12/UVB) surrounding the chamber were turned on, and the aerosol formed for 1.5-4 h until the particle mass concentration reached a maximum as detected by the SMPS.

Table 4.1. Summary of the SOA Samples Prepared for This Work.[a]

precursor	oxidant(s)	no. of repeat chamber runs	precursor (ppmv)	H_2O_2 (ppmv)	NO (ppmv)	reaction time (h)	collection time (h)
NAP	OH, low NO_x	3	0.9	4	0	3.5	4
NAP	OH, high NO_x	3	0.9	4	0.9	3	4
LIM	OH, low NO_x	2	1	5	0	3.5	4.5
LIM	OH, high NO_x	2	1	5	0.9	1.5	3.5
ISO	OH, low NO_x	2	3	18	0	4	3.5
ISO	OH, high NO_x	2	3	18	0.9	3	3.5
GUA	OH, low NO_x	2	0.5	2	0	4	3
GUA	OH, high NO_x	2	0.5	2	0.9	3.5	3

[a]Columns 4-6 correspond to approximate starting mixing ratios of precursors and oxidant(s).

Table 4.2 The reagents used for this study, their CAS registry numbers, their source, and their stated purity.

Reagent Name	**CAS Registry Number**	**Manufacturer**	**Stated Purity**
Hydrogen Peroxide Solution (30 wt%, water balance)	7722-84-1	Fisher	
5086 ppm Nitric Oxide in Nitrogen		Praxair	
Naphthalene	91-20-3	Fisher	98%
Dichloromethane	75-09-2	Fisher	99.9%
d-limonene ((4R)-1-Methyl-4-(1-methylethenyl)-cyclohexene	5989-27-5	Sigma Aldrich	97%
Isoprene (2-Methybuta-1,3-diene)	78-79-5	Sigma Aldrich	99%
Guaiacol (2-methoxyphenol)	90-05-1	Spectrum	99%

The SOA particles were collected with a MOUDI, which was modified to accommodate uncoated CaF_2 windows (Edmund Optics 25 mm diameter, 3 mm thickness) as substrates. Hundreds of micrograms of SOA material per window were collected, with stage 7 (0.32-0.56 μm particle size range) typically collecting the most mass. Stages 6 (0.56 -1.0 μm) and 8 (0.18-0.32 μm) also usually collected sufficient amounts of material for experiments. The experimental results were found to be independent of the MOUDI collection stage, making it possible to use any of the MOUDI stages with sufficient mass of SOA on them. The windows were annealed overnight in a laboratory oven at 40 °C with ~10 lpm of purge air flowing over the windows to drive off the more volatile species. Typical mass losses were a couple of percent of the total collected mass on a window, as confirmed by a Sartorius ME5-F microbalance (1 μg precision). If the annealing process was not performed, the OVOCs evaporating from the sample would

provide too much background for the photosensitization experiments with the PTR-ToF-MS, which are described next.

A reference system containing a mixture of benzophenone (BP, a well-known photosensitizer)[107] and succinic acid (SA, with no known photosensitization properties) was prepared by casting a solution containing known amounts of these compounds in a 1:1 (v/v) methanol:acetone mixture onto a CaF_2 window, drying it and annealing it in the same way as was done for the SOA samples.

An annealed SOA or reference BP/SA sample window was placed into a custom-built glass flow cell with a connection to a ~100 L Teflon bag that was filled with either purge air or a specified mixing ratio of limonene (typically ~200 ppbv) for control- and photosensitization experiments, respectively. The flow cell (Figure 4.2) represented a 15 mm i.d. tube, with a 30 mm long 15 mm I.D. side arm, which was terminated with a #15 O-ring joint for connecting a CaF_2 window loaded with SOA or BP/SA. A sampling flow from the PTR-ToF-MS instrument was used to withdraw air from the bag and over the sample at 0.2 SLM.

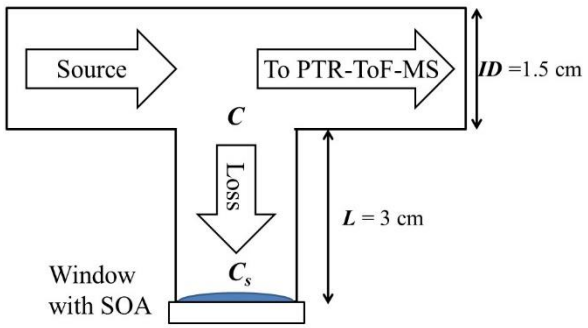

Figure 4.2. Schematic diagram of the flow cell.

A UV-LED and LED driver (Thorlabs, Inc. models M365LP1 and LEDD1B, respectively) with a wavelength centered at ~365 nm, a full width at half-maximum of ~10 nm, and a maximum power of ~480 mW at 1.2 A current (measured with a Coherent Powermax PS19Q power sensor) was used to irradiate the material on the CaF_2 window. The spectral flux density experienced by the SOA sample was also verified using actinometry as described by Bunce et al.[140] The actinometry and direct power measurements agreed with each other to within a factor of 3 (power sensor:actinometry). This level of agreement is still sufficient for the qualitative conclusions reached in this paper.

The limonene signal and the OVOCs resulting from the SOA material photodegradation were detected with the PTR-ToF-MS (drift tube voltage of 600 V, field strength of ~135 Td, drift temperature of 60 °C, inlet flow of 0.2 SLM, and resolving power of $m/\Delta m \sim 5 \times 10^3$). The OVOC and limonene mixing ratios flowing over the sample and resulting from the irradiation were estimated using the built-in calculations of the PTR-ToF-MS Viewer software from Ionicon Analytik (v.3.2.4.0), transmission curves created from a calibrated "TO-14" aromatics mix (Linde), and rate constants between the hydronium ion and the OVOCs/limonene from Zhao and Zhang.[141] The PTR-ToF-MS was calibrated for four VOCs analyzed for this study (acetaldehyde, acetone, acetic acid, and limonene) by evaporating a known amount of a given VOC into the cleaned 5 m^3 chamber and monitoring the [M+1] peak, corresponding to the protonated VOC. The VOC was added to the chamber in small increments, and the corresponding PTR-ToF-MS signal was measured after each successive addition. The inlet line through which the VOC was injected into the chamber was heated throughout the experiment to 60 °C, and the PTR-ToF-MS inlet line was also heated to the same temperature to prevent losses of VOC on the steel surfaces of the inlets. (However, we could not account for losses happening on the surface of the Teflon

chamber.) We created a calibration plot for each VOC comparing the actual amount of VOC in the chamber (assuming no wall losses) with that reported by the PTR-ToF-MS instrument (Figure 4.3). The resulting calibration factors, representing the ratio of measured to actual VOC mixing ratios, ranged from 1.2 to 6.2. Confidence intervals were calculated at the 95% level based on the uncertainty in the injection, the PTR-ToF-MS traces, and the resulting linear regression. These values are reported in Table 4.3.

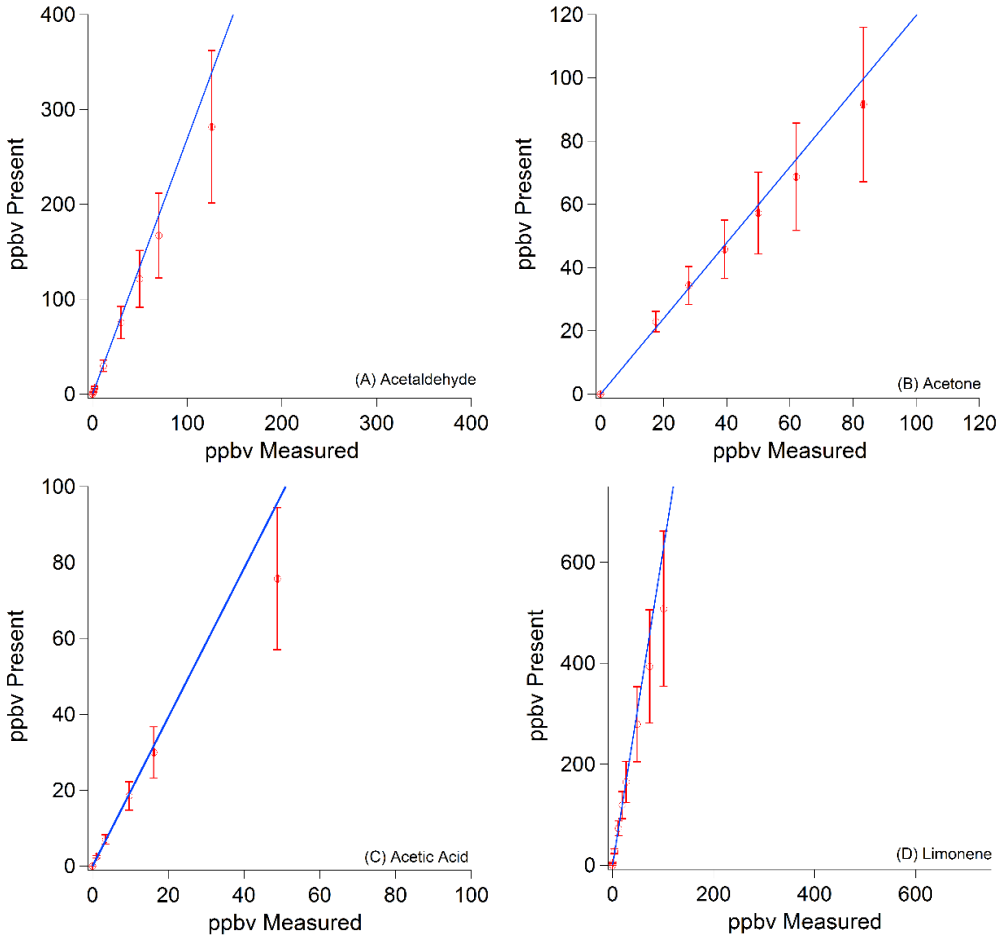

Figure 4.3. The PTR-ToF-MS calibration plots for (A) acetaldehyde, (B) acetone, (C) acetic acid, and (D) d-limonene. The horizontal axis is the PTR-ToF-MS measured mixing ratio and the vertical axis is the known amount that was injected into the chamber. Each data point has vertical and horizontal error bars corresponding to 95% confidence intervals of the amount of VOC present and measured, respectively. The vertical error bars increase with the VOC amount because of the accumulation of errors in the successive injections of the VOC in the chamber.

Table 4.3. The resulting calibration factors for each VOC. For the SOA photodegradation experiments, we multiplied the mixing ratios measured by the PTR-ToF-MS by this factor for each VOC in the main text analysis. The subscripts show the first digit that is not significant.

VOC	Calibration Factor	95% Confidence Interval
Acetaldehyde	2.6_9	0.5_4
Acetone	1.2_0	0.2_7
Acetic Acid	1.9_6	0.5_3
Limonene	$6._2$	$1._1$

4.4 Results and Discussion

4.4.1 Loss of Limonene and Formation of OVOCs

Figure 4.4 shows a result of a typical irradiation experiment in which selected OVOCs and limonene are observed in the PTR-ToF-MS before, during, and after irradiation with the presence of background limonene in the system. For each of these experiments, the window was inserted just before the 0-minute mark, and a baseline count of the OVOCs (and the limonene) was recorded before the UV-LED was turned on. The UV-LED was turned off after observing a steady signal for the OVOCs (and limonene). The signal reached the baseline before inserting a new window. The limonene mixing ratio reproducibly decreased when the UV-LED was on and returned to the previous level after the UV-LED was turned off. During the irradiation period, several OVOCs' mixing ratios increased when the UV-LED was on.

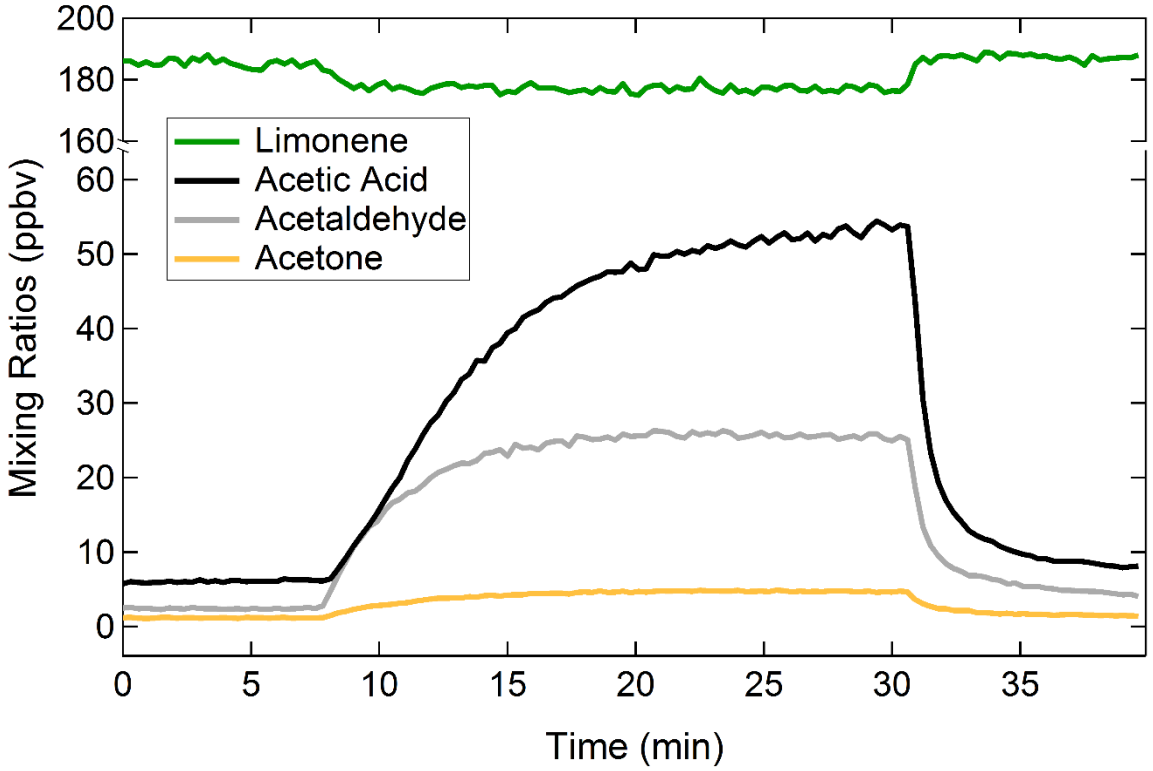

Figure 4.4. An example of photoinduced uptake of limonene and photoproduction of various OVOCs from the NAP/NO_x SOA observed with the PTR-ToF-MS. The UV-LED was turned on at ~8 min and turned off at ~30 min.

Most of the increase in OVOCs can be attributed to photodegradation of the SOA material.[150] In our previous experiments, which had a similar design, but did not have limonene flowing over the SOA, the SOA photodegradation from 305 nm radiation was readily observed. In control experiments with the 365 nm light source, in the absence of limonene, the same nominal masses increased in abundance during irradiation in the PTR-ToF-MS traces as previously observed.[150] However, due to the much larger intensity of the 365 nm LED, the increase in the OVOC signals was considerably higher. Formic acid was observed as the major SOA photodegradation product, similar to the findings of our previous work.[92, 100, 150] In this

work, the increase in formic acid from SOA photodegradation was so large that it often saturated the PTR-ToF-MS detector. Therefore, the formic acid signal is not shown in Figure 4.4.

In addition to the photodegradation of SOA resulting in OVOCs, there was evidence for photosensitized uptake of limonene on SOA. Specifically, it was observed that for selected SOA systems, there was a decrease in the counts of limonene to a steady state when the UV-LED was turned on. The decrease in signal was only a few percent, as shown in Figure 4.4. Table 4.4 lists the SOA systems probed in this work and the effective uptake coefficients (γ_{eff}) for limonene, which are defined as the fraction of limonene collisions with the surface that lead to a photosensitized reaction. Note that the uptake coefficients in Table 4.4 correspond to UV-LED power of 480 mW, and they scale linearly with the power. The next section describes the derivation of the uptake coefficients used for this work.

4.4.2 Uptake Coefficients

The geometry of the experiment is schematically shown in Figure 4.2. The flow of air containing 200 ppbv limonene goes through a cylindrical tube with *i.d.* = 1.5 *cm* at a volume flow rate of $F = 200\ cm^3\ s^{-1}$. The SOA sample is located on a CaF_2 window at the bottom of a cylindrical side tube with length $L = 3\ cm$ and inner diameter $ID = 1.5\ cm$. The PTR-ToF-MS measures the concentration of limonene exiting from the cell, C [$molec\ cm^{-3}$]. For the mixing ratio of 200 ppbv used in these experiments, $C = 4.9\text{x}10^{12}\ molec\ cm^{-3}$. When the UV-LED is on, the reduction in the measured concentration is only a few percent, so the inlet and outlet concentrations of limonene can be regarded as approximately the same. A small amount of limonene is lost onto the SOA coated window establishing a gradient of concentration along the side tube. The concentration in the immediate vicinity of the surface is C_s [$molec\ cm^{-3}$]. The transfer of limonene to the SOA coated window is not purely diffusive - we verified this by

drastically changing the flow geometry and getting the same final result for the uptake coefficient. Nevertheless, we attempt to model the diffusion through the side tube with normal diffusion equations below.

The number of molecules delivered by the air flow per second, *Source* [*molec* s^{-1}], can be related to the volume flow rate set by the mass flow controller, *F*, and the limonene concentration in the inlet flow as follows:

$$Source = F \times C \tag{4.1}$$

Under the steady state conditions, the net flux of limonene molecules through the flow, *J* [*molec* cm^{-2} s^{-1}], and the absolute loss rate due to the surface reaction, *Loss* [*molec* s^{-1}], can be calculated as follows:

$$J = \frac{Loss}{Area} = \frac{\gamma_{eff} \times \upsilon \times C}{4} = \frac{\gamma_{corrected} \times \upsilon \times C_s}{4} \tag{4.2}$$

In this equation, γ_{eff} is the effective uptake coefficient measured in the experiment, $\gamma_{corrected}$ is the actual uptake coefficient, *Area* [cm^2] is the area of the sample that is irradiated (about 1 cm^2), and *v* [*cm* s^{-1}] is the average speed of limonene (*MW* is the molecular weight of limonene, *R* is the gas constant, *T* is the absolute temperature):

$$\upsilon = \sqrt{\frac{8RT}{\pi MW}} = 2.15 \times 10^4 \frac{cm}{s} \tag{4.3}$$

Equation (4.4) shows that the effective and true uptake coefficient are related

$$\gamma_{corrected} = \gamma_{eff} \times \frac{C}{C_s} \tag{4.4}$$

The fractional reduction in the limonene that we observe in the flow with the PTR-ToF-MS is:

$$\frac{Ion_{UVoff} - Ion_{UVon}}{Ion_{UVoff}} = \frac{Loss}{Source} = \frac{\gamma_{eff} \times \upsilon \times Area}{4 \times F} \tag{4.5}$$

We can rearrange and substitute measured values of PTR-ToF-MS ion currents into Eq. (4.5) to calculate γ_{eff}. We show an example of this calculation for the GUA/OH SOA system below, in which the limonene signal dropped by 1.2% during the irradiation:

$$\gamma_{eff} = \frac{Ion_{UVoff} - Ion_{UVon}}{Ion_{UVoff}} \times \frac{4 \times F}{\upsilon \times Area} = 0.012 \times \frac{4 \times 3.33 \frac{cm^3}{s}}{2.15 \times 10^4 \frac{cm}{s} \times 1 cm^2} = 7.4 \times 10^{-6} \tag{4.6}$$

This uptake coefficient is reasonably large, so the diffusion gradient may be substantial (if the limonene transfer to the SOA substrate is controlled by diffusion). If we assume that the concentration gradient in the tube is linear, the diffusion flux can be approximated as:

$$J = D \times \frac{(C - C_s)}{L} \tag{4.7}$$

$D \approx 0.2\ cm^2\ s^{-1}$ is the estimated diffusion coefficient of limonene at ambient temperature and pressure.[178] From this, the concentration near the SOA surface can be estimated as follows:

$$C_s = C - \frac{J \times L}{D} = C\left(1 - \frac{\gamma_{eff} \times \upsilon \times L}{4D}\right) \tag{4.8}$$

And the corrected uptake coefficient becomes

$$\gamma_{corrected} = \gamma_{eff} \times \frac{1}{\left(1 - \frac{\gamma_{eff} \times \upsilon \times L}{4D}\right)} \tag{4.9}$$

For the GUA/OH SOA example, the corrected uptake coefficient is

$$\gamma_{corrected} = 7.4 \times 10^{-6} \times \frac{1}{(1 - 0.60)} = 1.9 \times 10^{-5} \tag{4.10}$$

The correction is quite large even for this smallest observed uptake coefficient. For the rest of the SOA systems studied in this work the effective uptake coefficient becomes too large for making the diffusion correction reliably (the linear gradient approximation breaks down). Therefore, the effective uptake coefficients listed in Table 4.4 should be interpreted as the lower limits for the actual uptake coefficients. Nevertheless, as we discuss in the text, the actual values of the uptake coefficients are not likely to be much higher than the effective values listed in Table 4.4. Therefore, the main conclusion of this work (that these uptake coefficients are too small to play a role in controlling loss rates of VOCs on SOA particles) is not likely to be affected by the diffusion limitations in some of our experiments.

As previously described, diffusion limitations on the observed uptake rate could be possible with the flow cell geometry and experimental conditions used in this work. To minimize possible diffusion limitations, the flow pattern was intentionally changed in selected experiments so that the flow was supplied directly onto the window with a bent 3mm I.D. tube inserted inside the flow cell. This modification did not change the observed uptake coefficient suggesting that there was sufficient turbulent mixing in the flow cell, making diffusion limitations less important. The fact that the γ_{eff} values are reproducibly different for a variety of SOA types also suggests that the diffusion limitations are minimal.

It is important to note that the loss of gas-phase carbon in limonene in Figure 4.4 is not balanced by the gain of gas-phase carbon in OVOC production; therefore, there is both photodegradation of SOA and a photosensitized uptake of limonene occurring simultaneously. For all SOA systems, the amount of carbon in the OVOCs produced was more than an order of magnitude larger than that in the reacted limonene. It is certainly possible that the photosensitized uptake produces similar OVOCs compared to the ones produced by SOA

photodegradation, but photodegradation of SOA is a far more important source of OVOCs than the photosensitized reactions. We attempted to determine the mass lost (or gained) by the SOA sample by recording its change in mass; however, the change in mass was small and not reproducible.

Table 4.4. Summary of the results of the photosensitization experiments.[a]

SOA system	effective uptake coefficient (γ_{eff})
BP/SA Reference System	5.7×10^{-5}
NAP/OH, Low NO_x	1.3×10^{-5}
NAP/OH, High NO_x	3.1×10^{-5}
LIM/OH, Low NO_x	-
LIM/OH, High NO_x	2.0×10^{-5}
ISO/OH, Low NO_x	-
ISO/OH, High NO_x	2.4×10^{-5}
GUA/OH, Low NO_x	7.4×10^{-6}
GUA/OH, High NO_x	1.1×10^{-5}

[a]The effective uptake coefficient, γ_{eff}, is listed for each system that exhibited measurable photosensitization. Because of the possible diffusion limitations in the experiments, the values of γ_{eff} may represent the lower limits for the actual uptake coefficients. The γ_{eff} are calculated for an LED power of 480 mW; when scaled to more typical atmospheric conditions γ_{eff} would be a factor of ~17 smaller. If γ_{eff} is not listed, the decrease in limonene was not detectable. BP/SA stands for the benzophenone/succinic acid mixture, the reference system, which is expected to have photosensitization properties.

All the high-NO_x SOA samples, and all naphthalene and guaiacol SOA samples exhibited photosensitization capabilities in these experiments. These capabilities are likely from nitrogen-containing photosensitizers and aromatics, and these are produced during high-NO_x SOA formation (except for the reference BP/SA system, which already has a known photosensitizer).

Previous studies have shown that lab-generated SOA under high-NO_x conditions and urban particulate matter contain nitrogen-containing species, carbonyls and nitroaromatics.[179-180] The guaiacol high-NO_x samples likely formed substituted nitroaromatic species during the SOA generation,[162] and nitroaromatics are capable of photosensitization.[9, 181] On the other hand, the naphthalene- and guaiacol low-NO_x samples may have formed ring-substituted products during SOA formation,[143, 182] which are likely photosensitizers.[9, 181]

The reference BP/SA system with the known BP photosensitizer is important, as it strongly suggests that the loss of limonene is driven by photosensitization. An alternative explanation for the loss of limonene would be secondary gas-phase photochemical processes involving free radicals. For example, acetaldehyde, acetone, and other OVOCs produced by SOA photodegradation could potentially photolyze in the gas-phase creating free radicals that then attack limonene. Based on our estimates, the 365 nm absorption cross sections and photolysis quantum yields for acetaldehyde, acetone, and other observed OVOCs are far too small to account for the observed loss rate of limonene. However, we cannot rule out the possibility that free radicals are produced on the surface and then escape in the gas-phase as observed in recent experiments with the IC photosensitizer by González Palacios et al.[176]

In the photosensitized reaction of particles containing IC and gaseous limonene, Rossignol et al.[174] were able to detect a number of oxidation products of limonene in the particles by high-resolution electrospray ionization mass spectrometry. Some of the same compounds were also detected in the gas-phase in this study. For example, protonated masses corresponding to $C_8H_{12}O_3$, $C_{10}H_{16}O_2$, $C_9H_{14}O_3$, $C_{10}H_{14}O_3$, and $C_9H_{12}O_4$ were detected across multiple SOA systems, with $C_{10}H_{14}O_3$ often being the compound that increased the most during irradiation. The

results suggest that photosensitized reactions of limonene on SOA particles likely occur by a similar mechanism to the reaction of limonene in IC.

4.4.3 Absorption Spectra of Limonene Reaction Products

VOCs that react in photosensitized reactions could potentially result in products that are light-absorbing, and therefore contribute to the burden of brown carbon.[108, 183] When the reference BP/SA system was exposed to both limonene and 365 nm radiation, a visual browning of the sample occurred reproducibly. The resulting brown film was dissolved in methanol and examined with UV-visible spectrophotometry (Figure 4.5). Another window containing BP/SA was exposed to just 365 nm radiation without limonene vapor, and no visual browning occurred. Each separate window for this control had the same amount of material deposited onto it, and each window's material was dissolved in the same amount of methanol. Even though no drastic changes in shape of the absorption spectrum were observed (Figure 4.5), the increase in the strength of the absorbance and the visual browning of the sample was reproducible. The change in the absorbance and browning of the sample suggests that some of the products of the photosensitized reaction of limonene with BP/SA remained on the surface, in agreement with observations of Rossignol et al.[174] for the limonene+IC photosensitized reactions. Because the amount of the deposited limonene reaction products is unknown, it is not possible to estimate the mass absorption coefficient from these data. However, such a small absorbance change in the visible range suggests that the mass absorption coefficient is too small for the limonene photosensitized reaction products to act as efficient absorbers of visible solar radiation. The SOA samples exposed to UV radiation and limonene vapor showed no discernible change in optical properties (data not shown). This does not rule out the possibility that limonene photosensitized

reaction products remain on the surface of SOA; all that it shows is that these products are not strongly light-absorbing.

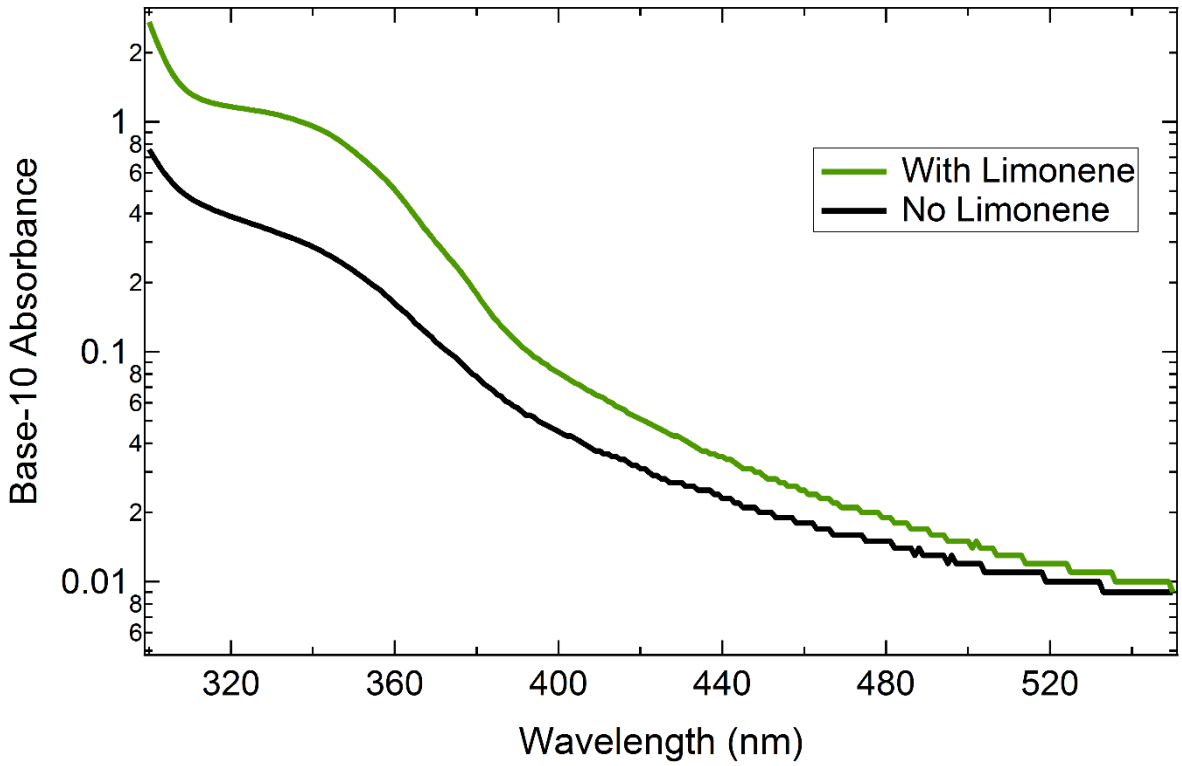

Figure 4.5. A comparison of the absorption spectra of the BP/SA reference system after irradiation for samples irradiated in the presence of limonene and without the presence of limonene.

4.4.4 Control Experiments

Several control experiments were performed in this study. A cleaned CaF_2 window was placed into the system and was irradiated while purge air was flowing through the system. There was no reduction in the limonene signal and only a minimal (< 4% relative to the baseline) increase in each OVOC's signal. The same experiment was performed with a film of paraffin wax (which is not expected to contain any photosensitizers) on a cleaned CaF_2 window, and a similar result to the cleaned CaF_2 was observed.

The power output of the UV-LED was varied, and it was noted that the reduction in limonene signal during irradiation of the high NO_x SOA samples was linearly related to the power output of the UV-LED (Figure 4.6). This suggests that nonlinear processes, such as two-photon absorption by the SOA material, are not likely to be responsible for the observations. This observation makes it possible to rescale the measured uptake coefficients listed in Table 4.4 to ambient conditions.

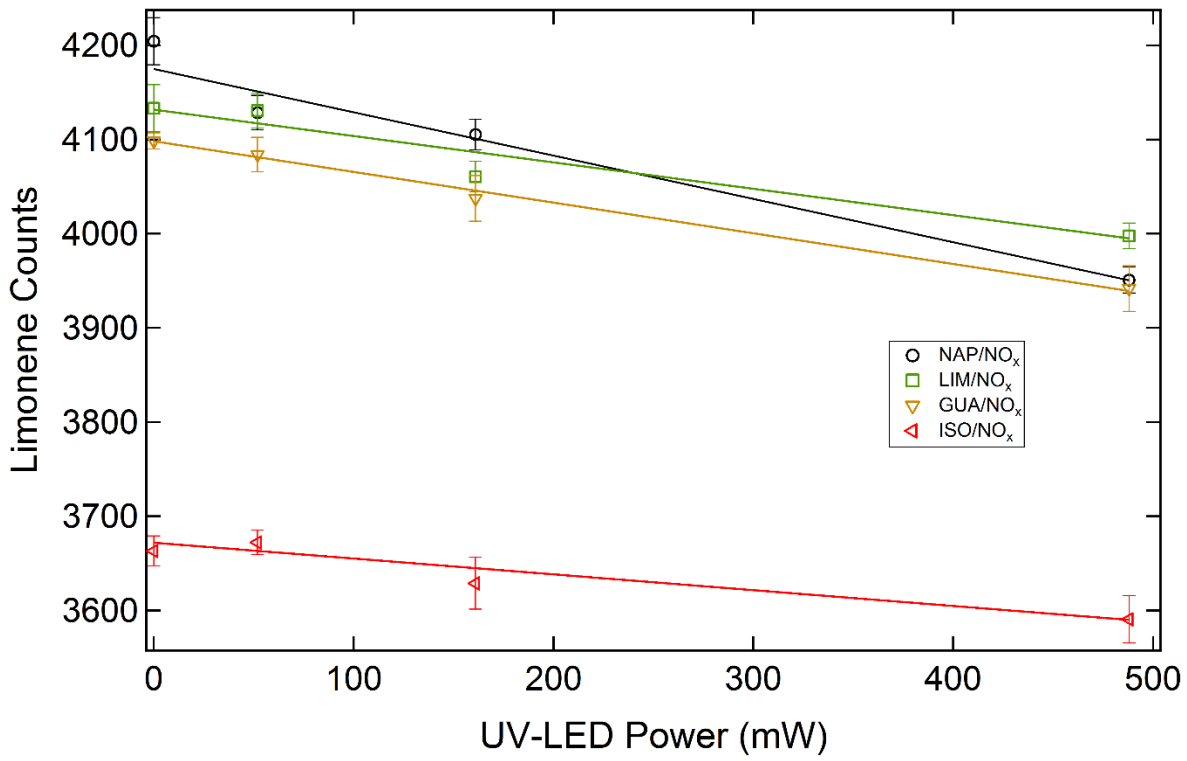

Figure 4.6. A regression plot of the limonene PTR-ToF-MS signal versus the UV-LED power for the high-NO_x SOA systems. Error bars correspond to the 95% confidence level for the ion counts of protonated limonene. The reduction in the ion counts is linear with respect to the power of the UV-LED.

Finally, the background mixing ratio of the limonene flowing over the system was varied over 3 orders of magnitude from ~1 ppbv to ~500 ppbv of limonene. The uptake coefficient was independent of the limonene mixing ratio consistent with a first-order process with respect to limonene.

4.4.5 Atmospheric Implications

The experiments described above were carried out at a relatively high power density of the 365 nm radiation (up to 480 mW/cm^2). The effective uptake coefficients listed in Table 4.4 correspond to the highest power density used in the experiments. Because the uptake of limonene by the irradiated SOA has a linear power dependence (Figure 4.4), we can estimate the uptake coefficient under more typical conditions by scaling the lamp's flux at 365 nm to that of the sun in the near UV range (300-400 nm). In this estimation, we are assuming that visible and near-IR radiation (λ > 400 nm) do not contribute to the photosensitized chemistry because the SOA materials do not absorb strongly at these wavelengths.

This estimation was done for $\gamma_{eff} = 3\times10^{-5}$, which may represent the best-case scenario for photosensitized removal of limonene on SOA particles based on the data listed in Table 4.4. The sun's flux was calculated using the Quick TUV Calculator[144] with parameters corresponding to Los Angeles, California on the summer solstice at noon. A comparison of the sun and lamp's spectral flux densities and the parameters used for the TUV output is below (Figure 4.7). We used the following parameters from the Quick TUV calculator: Latitude/Longitude (34°/-118°), Overhead Ozone (300 du), Surface Albedo (0.1), Ground and Measured Altitude (0 km), Clouds Optical Depth/Base/Top (0.00/4.00/5.00), Aerosols Optical Depth/S-S Albedo/Alpha (0.235/0.990/1.000), Sunlight Direct Beam/Diffuse Down/Diffuse Up (1.0/1.0/0.0) and 4 streams transfer model. Figure 4.7 shows a comparison of the spectral flux densities for the sun and the lamp in the near-UV region (300-400 nm). Each flux density is integrated over this wavelength range. The resulting scaling factor (Lamp/Sun = 17) translates to an effective $\gamma_{ambient}$ of 2×10^{-6} under these atmospheric conditions.

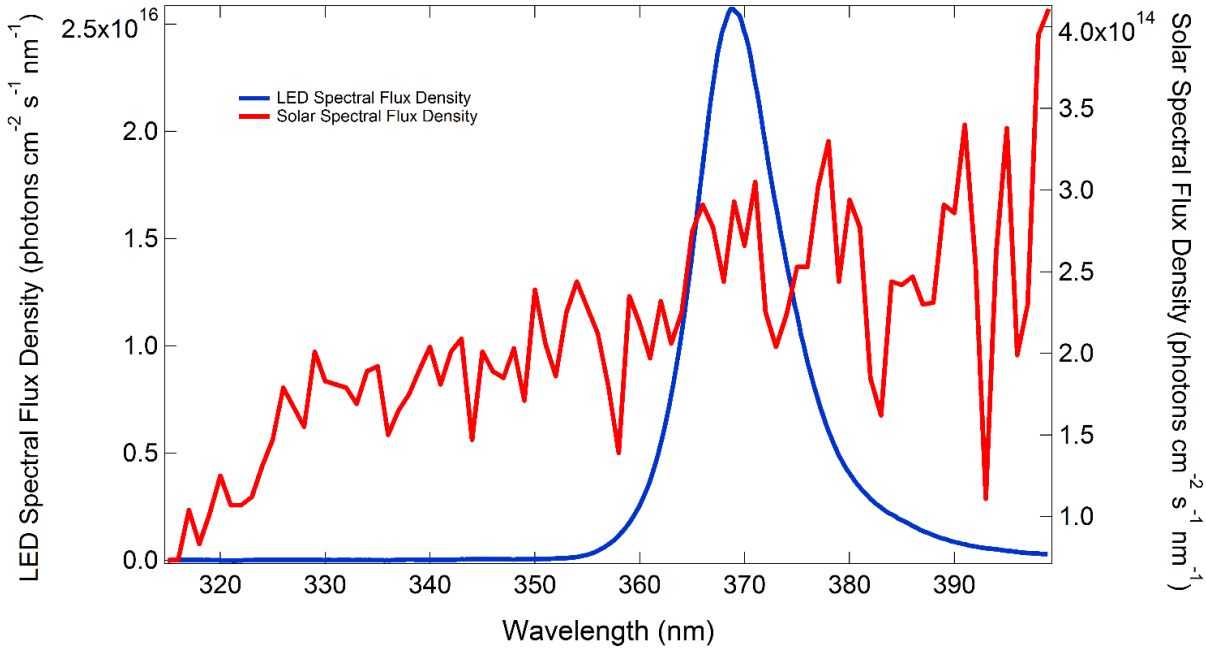

Figure 4.7. The spectral flux densities over the near-UV range of the electromagnetic spectrum of the LED (in blue) and the sun (in red) on the summer solstice in Los Angeles, California. The left axis corresponds to the LED, and the right axis represents the sun's flux density.

Would the estimated value of $\gamma_{ambient} = 2\times10^{-6}$ make the photosensitized loss of limonene on aerosol particles and ground surfaces competitive with gas-phase oxidation processes? To answer this question, the lifetime of limonene with respect to different loss processes was estimated (Table 4.5). The loss rate for limonene under typical ambient conditions is derived below.

Table 4.5. The lifetimes of limonene with respect to different atmospheric sinks.[a]

scenario	estimated lifetime
τ_{SOA}	>1 yr
τ_{OH}	100 min
τ_{Ozone}	170 min
$\tau_{Surface}$	26 hr

[a]The subscripts correspond to: "SOA" = deposition onto 300 nm monodisperse SOA particles at [SOA] = 15 μg m^{-3}, "OH" gas-phase reaction the hydroxyl radical at [OH] = 10^6 molec cm^{-3}, "Ozone" = gas phase reaction with ozone at $[O_3] = 4.8\times10^{11}$ molec cm^{-3}, and "Surface" = deposition onto a vegetation surface.

We now derive the lifetimes of limonene with respect to deposition on atmospheric particles under typical atmospheric conditions (with assumed effective ambient uptake coefficient $\gamma_{ambient} = 2\times10^{-6}$). Our calculations assume monodisperse particles with particle diameter, $d = 3\times10^{-7}$ m, a particle material density, $\rho = 1400$ kg/m^3, and the particle mass concentration in air, $C_{mass} = 15$ μg/m^3. The area to volume ratio (A/V) for such particles is 2×10^7 m^{-1}. Possible diffusion limitations for the uptake are neglected in this estimation.

The combined volume of particulate matter per volume of air is (m^3_{air} is the unit for the volume of air and m^3_p is the unit for the volume of a particle):

$$C_{volume}\left[\frac{m_p^3}{m_{air}^3}\right] = \frac{C_{mass}\left[\frac{\mu g}{m_{air}^3}\right]\times10^{-9}\left[\frac{kg}{\mu g}\right]}{\rho\left[\frac{kg}{m_p^3}\right]} = \frac{15\frac{\mu g}{m_{air}^3}\times10^{-9}\frac{kg}{\mu g}}{1400\frac{kg}{m_p^3}} = 1.07\times10^{-11}\frac{m_p^3}{m_{air}^3} \qquad \textbf{(4.11)}$$

The combined area of particulate matter per volume of air is (where A/V is the area to volume ratio for one particle, per assumptions above):

$$C_{area}\left[\frac{m_p^2}{m_{air}^3}\right]=C_{volume}\left[\frac{m_p^3}{m_{air}^3}\right]\times\frac{A}{V}\left[m_p^{-1}\right]=1.07\times10^{-11}\frac{m_p^3}{m_{air}^3}\times2\times10^7 m_p^{-1}=2.14\times10^{-4}\frac{m_p^2}{m_{air}^3} \quad \textbf{(4.12)}$$

We can also define the loss rate per unit volume air:

$$Loss\left[\frac{molec}{m_{air}^3\cdot s}\right]=\gamma\times\frac{\upsilon\left[\frac{m}{s}\right]\times C_{area}\left[\frac{m_p^2}{m_{air}^3}\right]}{4}\times C_{VOC}\left[\frac{molec}{m_{air}^3}\right] \quad \textbf{(4.13)}$$

The effective first order rate constant for limonene is then:

$$k\left[s^{-1}\right]=\frac{Loss\left[\frac{molec}{m_{air}^3\cdot s}\right]}{C_{VOC}\left[\frac{molec}{m_{air}^3}\right]}=\gamma\times\frac{\upsilon\left[\frac{m}{s}\right]\times C_{area}\left[\frac{m_p^2}{m_{air}^3}\right]}{4} \quad \textbf{(4.14)}$$

Using the effective ambient $\gamma = 2\times10^{-6}$, we get:

$$k\left[s^{-1}\right]=2\times10^{-6}\times\frac{215\frac{m}{s}\times2.14\times10^{-4}\left[\frac{m_p^2}{m_{air}^3}\right]}{4}=2.3\times10^{-8}s^{-1} \quad \textbf{(4.15)}$$

This corresponds to lifetime of limonene with respect to the deposition on SOA particles of:

$$\tau\left[s\right]=\frac{1}{k\left[s^{-1}\right]}=\frac{1}{2.3\times10^{-8}s^{-1}}=4.3\times10^7 s>1yr \quad \textbf{(4.16)}$$

If we compare this lifetime to that of limonene reacting with OH and limonene reacting with O_3 in the gas phase, we arrive at the following. We assume that the typical [OH] is 10^6 molecules/cm^3 and the typical [O_3] is ~4.8 x 10^{11} molecules/cm^3. Rate constants are from Atkinson.[184]

$$k_{OH}\left[s^{-1}\right] = k_{OH+LIM} \times [OH] = 1.7\times10^{-10}\,\frac{cm^3}{molec\cdot s}\times10^{6}\,\frac{molec}{cm^3} = 1.7\times10^{-4}\,s^{-1} \qquad \textbf{(4.17)}$$

$$\tau_{OH}\left[s\right] = \frac{1}{k_{OH}\left[s^{-1}\right]} = \frac{1}{1.7\times10^{-4}\,s^{-1}} = 5.9\times10^{3}\,s = 98\,\text{min} \qquad \textbf{(4.18)}$$

$$k_{O_3}\left[s^{-1}\right] = k_{O_3+LIM} \times [O_3] = 2.0\times10^{-16}\,\frac{cm^3}{molec\cdot s}\times4.8\times10^{11}\,\frac{molec}{cm^3} = 9.6\times10^{-5}\,s^{-1} \qquad \textbf{(4.19)}$$

$$\tau_{O_3}\left[s\right] = \frac{1}{k_{O_3}\left[s^{-1}\right]} = \frac{1}{9.5\times10^{-5}\,s^{-1}} = 1.0\times10^{4}\,s = 174\,\text{min} \qquad \textbf{(4.20)}$$

We now consider the lifetime of limonene with respect to uptake onto urban surfaces. In this case, the first term in Eq. 4.21 is the ratio of the actual surface area to the geometric surface area over 1 m^2 of ground (we set it to 50 as per the maximum discussed by Asner et al.[185]) and the second term is the height of the boundary layer where species mix freely (we set it to 500 m). The surface concentration is now considerably larger than it was estimated for the particles:

$$C_{area}\left[\frac{m^2_{surface}}{m^3_{air}}\right] = \frac{S_{actual}}{S_{geometric}}\times\frac{1}{h_{boundary}\left[m\right]} = 0.1m^{-1} \qquad \textbf{(4.21)}$$

If we substitute the result from Eq. (4.21) into Eq. (4.14), we arrive at the rate of limonene loss and lifetime of limonene as:

$$k\left[s^{-1}\right] = 2\times10^{-6}\times\frac{215\,\frac{m}{s}\times0.1\left[\frac{m^2_{surface}}{m^3_{air}}\right]}{4} = 1.1\times10^{-5}\,s^{-1} \qquad \textbf{(4.22)}$$

$$\tau\left[s\right] = \frac{1}{k\left[s^{-1}\right]} = \frac{1}{1.1\times10^{-5}\,s^{-1}} = 9.3\times10^{4}\,s = 26hr \qquad \textbf{(4.23)}$$

This lifetime is considerably shorter but still not short enough to be competitive with the oxidation of limonene by OH or ozone in the gas phase.

The predicted lifetimes of limonene with respect to the reactions with the hydroxyl radical and ozone are 100 min and 170 min, respectively. The lifetime with respect to the photosensitized loss to SOA particles is orders of magnitude longer. As such, the photosensitized reaction of limonene with SOA particles cannot kinetically compete with the gas-phase oxidation processes. In terms of the rate with which mass is added to the particle, the SOA+VOC photosensitization process similarly cannot compete with the gas-phase oxidation followed by deposition, at least for VOCs that have high SOA yield. Because gas-phase oxidation of limonene produces SOA particles in high yields,[123] the rate of particle growth will be determined by the rate of limonene oxidation, which is faster in the gas phase. The situation may be different for VOCs that have low SOA yield, such as isoprene. But for VOCs with high SOA yields, the photosensitized growth of particles proposed by Monge et al.,[111] might be too slow compared to the growth from the normal gas-to-particle partitioning of limonene gas-phase oxidation products.

Based on our estimations, the uptake of limonene onto vegetation surfaces (τ~26 hr) may be more competitive with atmospheric gas-phase oxidation because of the higher available surface area provided by the vegetation surfaces. Because the uptake coefficients estimated in this study represent a lower limit for the actual uptake coefficients, the photosensitized uptake could be even faster. Such photosensitized reactions could be more relevant in the leaf boundary layer, where the concentrations of VOCs are higher and concentrations of oxidants are lower,[186] making the vegetation surface driven photosensitized processes potentially important. This is a

research avenue that should be explored, as it may be another possible sink for freshly-emitted VOCs in the atmosphere.

This study explored the possibility of photosensitized reactions with SOA particles; however, a number important questions remain: (a) What is the influence of relative humidity on the SOA and photosensitized reactions? The viscosity of the SOA matrix is lowered[187] when the relative humidity is increased, and this could lead to different uptake coefficients and therefore lifetimes of VOCs partitioning into aerosols. (b) Does this photosensitization process occur for VOCs other than limonene? Isoprene was also tested in preliminary experiments, and it exhibited similar behavior to limonene. (c) Which other irradiation wavelengths show photosensitization capabilities for SOA particles? It would be interesting to try other wavelengths to create a so-called photochemical action spectrum in which the effective uptake coefficient is plotted on the y-axis and the wavelength of irradiation is on the x-axis; however, that is beyond the scope of this work. (d) Running experiments with urban surfaces and/or plant materials would help elucidate the degree of uptake of VOCs onto them. If this uptake is kinetically competitive with the previously-mentioned gas-phase oxidants, it could help improve climate models for sinks of VOCs.

4.5 Conclusions

This exploratory study on the feasibility of photosensitized reactions involving SOA particles in the presence of gas-phase VOCs has shown that photoinduced uptake of VOCs is indeed experimentally observable on a variety of types of SOA particles. While previous observations of photosensitized loss of VOCs exist, they relied on simple model mixtures containing known photosensitizers. To the best of the authors' knowledge, this is the first time

photosensitized loss of VOCs on surfaces has been observed for more atmospherically-relevant SOA. The experimentally determined lower limits for the effective uptake coefficients for the photosensitized loss of limonene on SOA particles are on the order of ~10^{-5} under laboratory conditions or ~10^{-6} under solar irradiation conditions corresponding to Los Angeles, California on the summer solstice at noon. The relatively small size of the uptake coefficient and insufficient surface area presented by ambient SOA particles make the resulting rate of the photosensitized loss of limonene on SOA particles considerably slower than the rate of the gas-phase oxidation of limonene by OH and O_3. However, the rate of photosensitized loss of limonene on vegetation surfaces coated with SOA material could be higher and potentially competitive with the gas-phase oxidation.

Chapter 5: Photochemical Reactions on Tree Surfaces

5.1 Abstract

The photodegradation and photoinduced uptake experiments we previously discussed in Chapters 2, 3, and 4 are now probed for a Scots pine sapling. A given isolated sapling is exposed to doses of ultraviolet light and ozone in an attempt to form SOA from the tree emissions and coat the needle surfaces with some SOA material. A second ultraviolet light dose is then given to the tree to induce photochemical reactions in the SOA material sitting on the needles. The results of these measurements are not conclusive, due to complications associated with VOCs being emitted by the plant itself and the dependence of these emissions on the irradiation level. However, secondary photochemical reactions could still occur in other parts of the atmosphere for the SOA that does not coat the pine needle surfaces.

5.2 Introduction

Boreal forests (also known as the "taiga") are located in the extreme northern hemisphere,[188] comprise nearly 30% of the forest cover on Earth,[189] and are known to emit large amounts (hundreds Tg/year) of monoterpenes.[190-191] Therefore, they make a large contribution to global SOA formation. A common characteristic of these forests is the presence of coniferous trees, and in Finland, the Scots pine (*Pinus sylvestris* L.) is a dominant species.[192] Recently, it was suggested that forests can serve as a large source of formic acid in the atmosphere through secondary atmospheric processing.[146, 193-196] Formic acid contributes to acid rain, particularly in remote atmospheres.[145]

In order to understand tree emission VOC profiles and the subsequent reactions involving the VOCs emitted by the trees, there have been many previous studies on trees isolated in indoor vessels. For example, trees have been isolated and exposed to a variety of stressors, such as simulated herbivory,[197] pine weevil feeding,[198] ozone exposure,[199-200] mechanical wounding,[201]

and elevated ultraviolet light exposure.[202-204] Additionally, photodegradation studies have been carried out on pesticides[205] and organic pollutants[206] that were deposited onto plant surfaces. However, the chemistry of SOA material that presumably deposits on trees in significant quantities has not been explored.[207] We previously showed that photodegradation of SOA is efficient and occurs on atmospherically-relevant time scales.[150] We did see evidence for photosensitized uptake of VOCs into SOA, but the rate of VOC deposition was not as atmospherically relevant as the competing production of VOC in photodegradation of SOA.[160]

We wanted to test if photochemical reactions on surfaces of vegetation (in this case Scots pine saplings) could serve as a source and/or sink of VOCs. We isolated trees in Teflon bags and probed the photochemical reactions after they were coated with SOA formed from the tree volatiles. Our primary motivation was to see how these reactions would occur in the vicinity of these trees for a more "atmospherically realistic" system. For these preliminary experiments, we observed more complicated behavior compared to the isolated SOA that we studied in previous chapters.

5.3 Experimental Section

Approximately 7-year-old Scots pine saplings were used for this study. The saplings were approximately 1.5 m in height. Before experiments began, the saplings were kept in a greenhouse and watered regularly. This study was done in June in Kuopio, Finland, so the trees were exposed to nearly 21 hours of daylight per day. A selected sapling was brought into the laboratory, and a 150 L Teflon bag was placed around the tree and zip tied closed at the trunk. The airflow into the bag was ~100 sccm more than the instruments required, so that the bag would inflate slightly and not touch as many plant surfaces. The tree was allowed to equilibrate to the indoor environment for at least 12 hours. Eight visible, full spectrum lamps (Ikea) were

placed around the sapling and were kept on at all times during the experiment in order to simulate the greenhouse conditions. The room where the experiment was done was kept between 20 and 22 °C.

During the equilibration and experiment, a humidified zero air stream was passed through a Nafion exchange system (Perma Pure PD-100T) to create ~60% RH in the Teflon bag. The total incoming air was set at 1 SLM. A relative humidity and temperature probe was placed inside the bag as well (Vaisala model HMP60).

Ozone was generated during specific stages of the experiment as well. The ozone was generated via oxygen ("6.0 purity," AGA Company) being passed over a 254 nm lamp setup (UVP model 506-2). The ozone levels were monitored with an ozone monitor (Thermo Scientific model 49i).

UV lamps surrounded the side and top of the tree when it was in the experiment phase. Four were on the side and 3 were on the top at distances of 8 cm and 20 cm, respectively from the Teflon bag. UV-B lamps were predominately used (Philips TL-40W-12-RS), and control studies were done with UV-A lamps (Philips TL-K-40W-1SL). A figure containing the irradiance of the lamps (measured with a Gooch & Housego OL 756 Spectroradiometer) is found below (Figure 5.1). The lamps are also compared to the solar irradiance at noon on the Summer solstice in Kuopio, Finland with data from the Quick TUV calculator.[144] The following parameters were employed:

- Latitude/Longitude: 63°N, 28°E
- Date: 20170621
- Time (GMT): 14:00:00
- Overhead Ozone: 300 du

- Surface Albedo: 0.1
- Ground/Measured Altitude: 0 km
- Clouds: 0/4/5
- Aerosols: 0.235/0.990/1
- Sunlight: 1/1/0

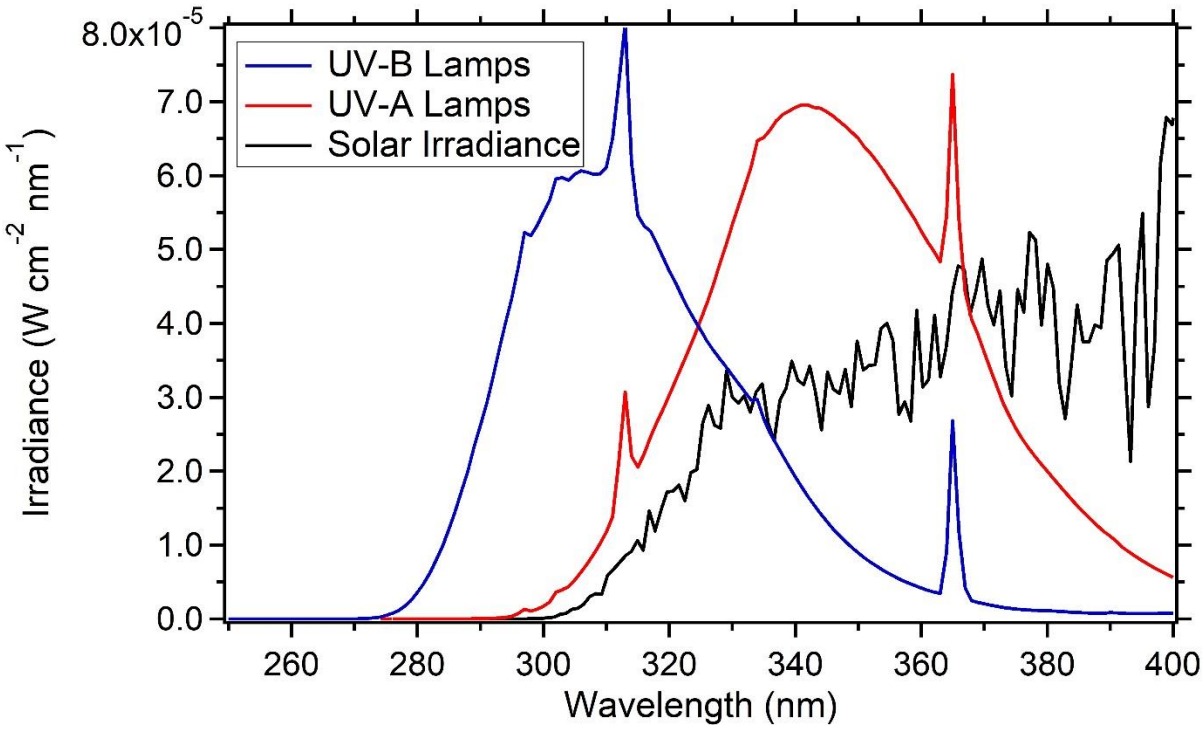

Figure 5.1. The irradiance of the set of UV-B lamps (in blue), UV-A lamps (in red), and the solar irradiance at noon on the Summer solstice in Kuopio, Finland are compared between 250 and 400 nm.

Detection was performed with a suite of on-line instruments. A PTR-ToF-MS was used to detect volatile organic compounds (with a higher proton affinity than that of water) at 200 sccm inlet flow and 130 Td drift field strength. Because “stickier” species such as formic acid

can be lost in tubing to the PTR-ToF-MS inlet, the inlet was placed directly into the bottom of the Teflon bag during the experiment. An SMPS with a model 3775 condensation particle sizer and a model 3082 electrostatic classifier was used to determine the size-resolved mass concentration of generated particles. An Aerosol Mass Spectrometer (AMS; Aerodyne, Inc.) was hooked up for select experiments to ascertain the degree of oxidation of the aerosol. Finally, for select experiments an Iodide CIMS was used for detection of SVOCs. The CIMS used for this study is described elsewhere.[208]

An overview of the experiment is shown below in Figure 5.2, Figure 5.3, and Table 5.1. After a tree was equilibrated, the experiment began at approximately the same time every morning (within 15 minutes start time). Five hundred mL of tap water was fed to the tree right before the experiment began. The PTR-ToF-MS monitored the biogenic VOCs coming from the tree inside the bag. Before the tree was even inserted into the bag, background VOC mixing ratios in the bag were recorded. After the background signal with the plant was attained, the UV-B lamps were turned on for several hours in order to stress the plant and to make it produce more biogenic VOCs. The UV-B lamps were turned off and the plant was allowed to equilibrate for ~20 minutes. (If we waited long enough (i.e., hours) after the UV-B lamps were turned off, the levels of the biogenic VOCs decreased to the earlier baseline.) Next, the ozone was fed to the Teflon bag to achieve ~100 ppbv of ozone inside the bag. Previous studies show that this mixing ratio of ozone is not likely to stress the plant,[199, 209] but it does produce SOA. The ozone was fed to the bag for 1.5 hr. During this time, 75-250 $\mu g\ m^{-3}$ of particles were present inside the Teflon bag (as detected by the SMPS). After the ozone was no longer supplied to the bag, the plant was allowed to sit for a couple of hours to allow the SOA to coat the needles of the tree (and partition

to the walls of the bag). Finally, the UV-B lamps were turned on a second time to irradiate the SOA particles that were on the needles and monitor the behavior of the VOCs.

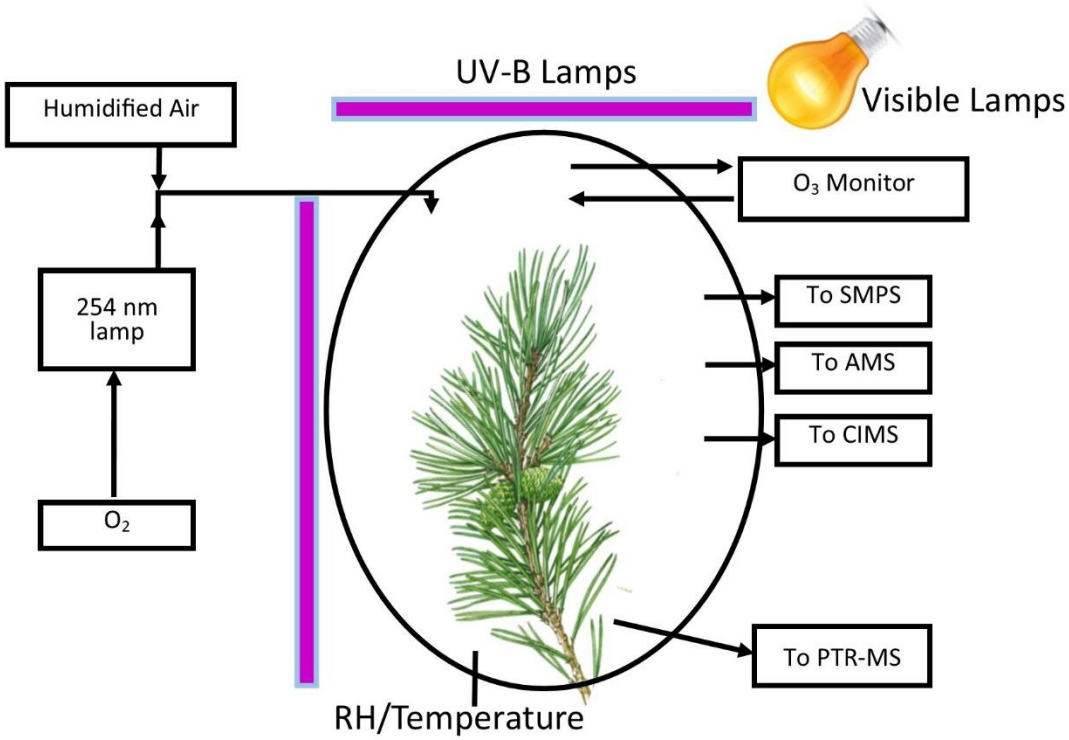

Figure 5.2. An overview of the experimental setup used for the scots pine saplings. A stream of humidified air that can optionally contain ozone is fed to the Teflon bag containing the tree. Relative humidity and temperature are also measured in real time with a probe. UV-B lamps are turned on during specific stages of the experiment to initiate either stress of the tree or photochemistry of the SOA. Visible lamps are on at all times. A variety of instruments on the right-hand side of this figure are used for detection of species. The PTR-ToF-MS is connected directly to the bottom of the bag for reasons mentioned in the main text. The tree branch image is from the public domain.

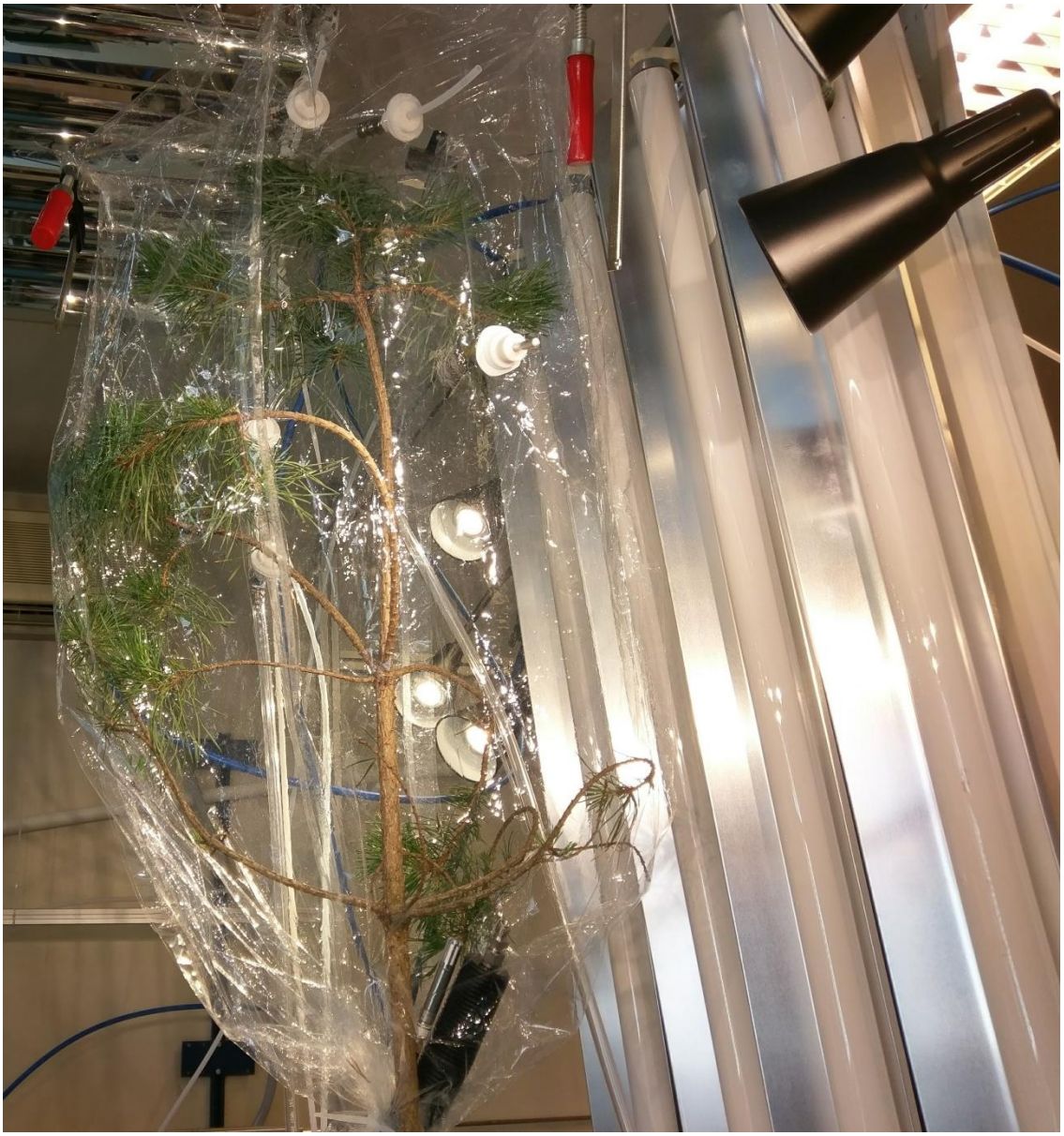

Figure 5.3. A photograph of the experimental setup wherein a tree sapling is placed inside the Teflon bag. The visible lights are turned on in this example.

Table 5.1. An overview of the experimental parameters used for these experiments. The X in each column corresponds to which parameters were employed at the given section of the experiment. The experiment progresses from top to bottom of this table.

Parameter	**Visible Light**	**Ozone**	**UV light**
Bag Background	X		
Background with Plant	X		
UV Light	X		X
Background	X		
Ozone Exposure	X	X	
Background	X		
UV Light	X		X
Background	X		

Several controls were also run for this study. The time durations between switching experimental parameters (e.g., the wait time between ozone exposure and the second UV-B irradiation episode) were varied. These experimental results (next section) were consistent with other experiments. UV-A lamps were also used for a control experiment. These lamps made the tree emit fewer quantities of biogenic VOCs, and the photolysis section of the experiment was consistent with the UV-B lamp data. The temperature experienced inside the Teflon bag increased by 2 °C during irradiation experiments. Therefore, a control was run where the inlet air was heated to make the tree experience the same temperature effect. The results of this specific control experiment showed only a negligible amount of biogenic VOC emission increase. An empty, clean Teflon bag was exposed to the UV-B radiation, and it was determined that a

majority of the signal from acetaldehyde during irradiation was actually from irradiation of the air in the bag, which complicated interpretation of the experiments. Finally, after exposure to the ozone, the UV-B lamps were cycled on and off for several hour periods. The given tree emitted successively fewer quantities of biogenic VOCs during this control.

5.4 Results and Discussion

Figure 5.4 shows the PTR-ToF-MS results of a typical experimental run. The monoterpenes (e.g., limonene, pinene) are isobars and cannot be resolved with this technique. They are therefore plotted as a single trace (in purple). The other traces selected were either ones that showed significant changes during varying experimental parameters or were ones that were found in high amounts in previous chapters of this dissertation. The preliminary results of this exploratory study show that the behavior of the SOA-coated trees is different from that observed for the condensed-phase aging experiments that were parts of Chapters 2, 3, and 4. A variety of VOCs are produced, but formic acid is not the dominant photoproduced VOC like in the previous studies. In fact, the production amounts of formic acid on the second round of UV-B exposure relative to the initial exposure is not discernable. As mentioned earlier, the control study with an empty Teflon bag actually yielded an appreciable amount of acetaldehyde photoproduction. With this study, the origin of the VOCs is not clear in regard to the photochemistry of the SOA deposited on the trees versus just the UV-B light stressing the plants. Additionally, there is no evidence for uptake of VOCs during the irradiation. Because the PTR-ToF-MS results yielded results that were inconclusive, we did not pursue the full analysis of the Iodide CIMS or the AMS data. Preliminary analysis showed similar results to the PTR-ToF-MS data for the Iodide CIMS data (not shown).

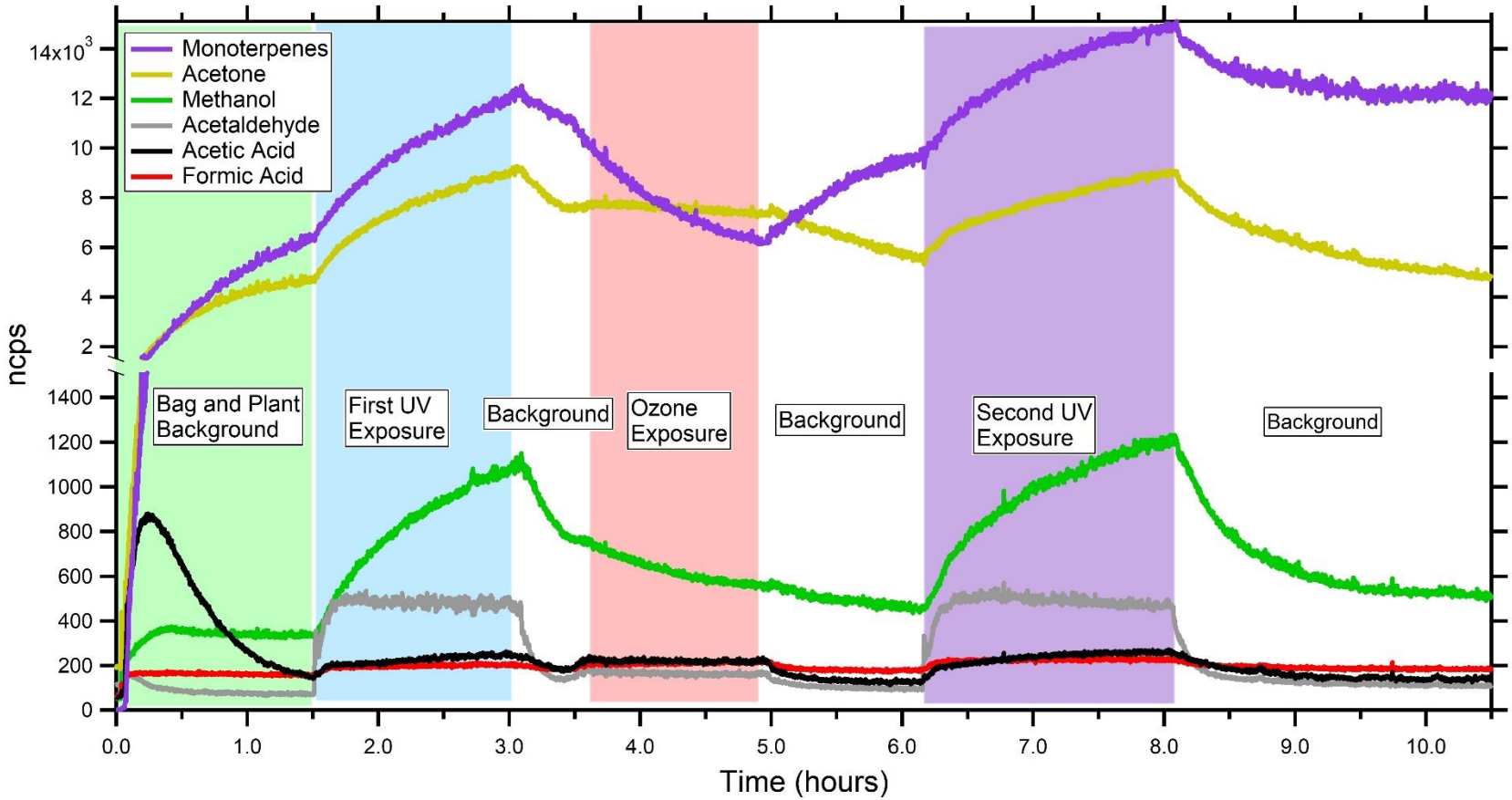

Figure 5.4. The PTR-ToF-MS traces for a typical experiment. The normalized (to the hydronium reagent ion) counts per second are presented on the y-axis and the time (in hr) is presented on the x-axis. Colored background shading corresponds to different experimental parameters. The initial bag and then plant background are presented with green shading. The first UV exposure is shown with blue shading. The next background is presented with no shading. Note that this time was shorter than other backgrounds for reasons mentioned in the experimental section. The ozone exposure is shown in pink shading. The second UV exposure is shown in purple shading. Finally, the background of the plant is shown in white shading at the end of the experiment.

Figure 5.5 shows the results of the SMPS data for right before ozone exposure, during ozone exposure, after ozone exposure, and during the second UV exposure for two different days in which the time before UV exposure was varied.

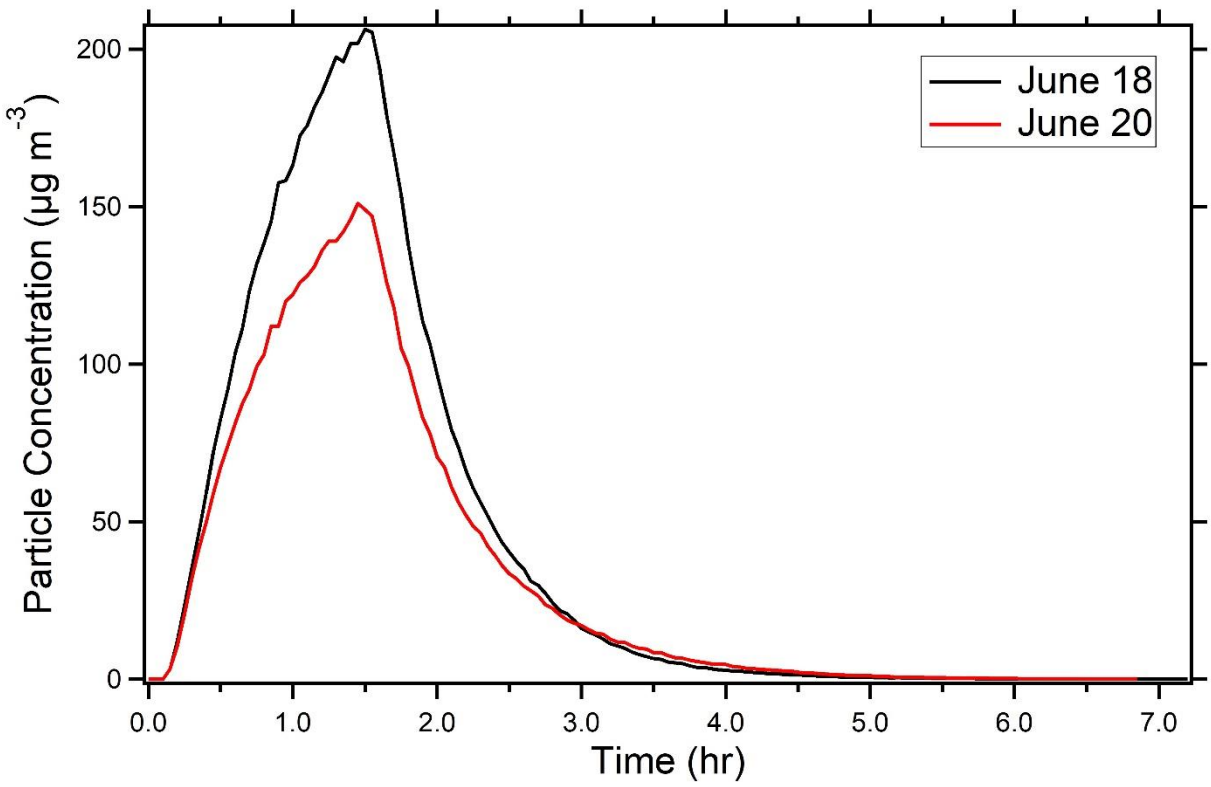

Figure 5.5. The SMPS particle concentration data for two separate days of experiments. The ozone is fed to the bag right after the 0 hr mark. The ozone is stopped at the 1.5 hr mark for each of these days. On June 18, the UV-B lamps were turned on at the 2.5 hr mark, and for June 20, they were turned on at the 4.25 hr mark.

For the SMPS data, waiting to turn the lamps on until a later time showed no effect on the decrease in particle concentration (June 20th relative to June 18th). The decrease asymptotically reached the baseline after a few hours regardless of when the lamps were turned on. Because of the experimental design, it was not possible to determine if the SOA was being deposited on the needles of the tree or partitioning to the walls of the Teflon bag.

The most interesting aspect of this project is that the behavior of the photodegradation is quite different from the isolated SOA particles. However, this is not to say that the photodegradation will not occur. The lamps used for this study may not be strong enough relative to the lamps used in Chapters 2, 3, and 4. As such, the particles may be partitioning away out of the bag before there is a chance for photolysis to occur. Additionally, even though we do not see primary photoproduction of species such as formic acid, they could be formed as secondary photoproducts.[193]

References

1. Saha, K. *The Earth's atmosphere: Its physics and dynamics*. Springer Science & Business Media: 2008.

2. Peixoto, J. P.; Oort, A. H. *Physics of climate*. American Institute of Physics: New York, 1995.

3. Haagen-Smit, A. J. Chemistry and physiology of Los Angeles smog. *Ind. Eng. Chem.* **1952,** *44*, 1342-1346.

4. Calvert, J. A.; Pitts, J. N. *Photochemistry*. John Wiley: New York, 1966.

5. Normand, C. Atmospheric ozone and the upper-air conditions. *Q. J. R. Meteorol. Soc.* **1953,** *79*, 39-50.

6. Stephens, E. R.; Hanst, P. L.; Doerr, R. C.; Scott, W. E. Reactions of nitrogen dioxide and organic compounds in air. *Ind. Eng. Chem.* **1956,** *48*, 1498-1504.

7. Bates, D. R.; Nicolet, M. The photochemistry of atmospheric water vapor. *J. Geophys. Res.* **1950,** *55*, 301-327.

8. Inn, E. C. Y.; Tanaka, Y. Ozone absorption coefficients in the visible and ultraviolet regions. In *Ozone chemistry and technology*, American Chemical Society: 1959; Vol. 21, pp 263-268.

9. Turro, N. J.; Ramamurthy, V.; Scaiano, J. C. *Modern molecular photochemistry of organic molecules*. University Science Books: Sausalito, CA, 2010.

10. Pöschl, U.; Shiraiwa, M. Multiphase chemistry at the atmosphere-biosphere interface influencing climate and public health in the anthropocene. *Chem. Rev.* **2015,** *115*, 4440-4475.

11. Chang, W. L.; Bhave, P. V.; Brown, S. S.; Riemer, N.; Stutz, J.; Dabdub, D. Heterogeneous atmospheric chemistry, ambient measurements, and model calculations of N_2O_5: A review. *Aerosol Sci. Technol.* **2011,** *45*, 665-695.

12. Molina, M. J.; Tso, T. L.; Molina, L. T.; Wang, F. C. Antarctic stratospheric chemistry of chlorine nitrate, hydrogen chloride, and ice: Release of active chlorine. *Science* **1987,** *238*, 1253-1257.

13. Finlayson-Pitts, B. J.; Pitts, J. N. *Chemistry of the upper and lower atmosphere theory, experiments, and applications*. Academic Press: San Diego, CA, 2000.

14. Hallquist, M.; Wenger, J. C.; Baltensperger, U.; Rudich, Y.; Simpson, D.; Claeys, M.; Dommen, J.; Donahue, N. M.; George, C.; Goldstein, A. H.; Hamilton, J. F.; Herrmann,

H.; Hoffmann, T.; Iinuma, Y.; Jang, M.; Jenkin, M. E.; Jimenez, J. L.; Kiendler-Scharr, A.; Maenhaut, W.; McFiggans, G.; Mentel, T. F.; Monod, A.; Prevot, A. S. H.; Seinfeld, J. H.; Surratt, J. D.; Szmigielski, R.; Wildt, J. The formation, properties and impact of secondary organic aerosol: Current and emerging issues. *Atmos. Chem. Phys.* **2009,** *9*, 5155-5236.

15. George, C.; Ammann, M.; D'Anna, B.; Donaldson, D. J.; Nizkorodov, S. A. Heterogeneous photochemistry in the atmosphere. *Chem. Rev.* **2015,** *115*, 4218-4258.

16. Pöschl, U. Atmospheric aerosols: Composition, transformation, climate and health effects. *Angew. Chem. Int. Ed.* **2005,** *44*, 7520-7540.

17. Kanakidou, M.; Seinfeld, J. H.; Pandis, S. N.; Barnes, I.; Dentener, F. J.; Facchini, M. C.; Van Dingenen, R.; Ervens, B.; Nenes, A.; Nielsen, C. J.; Swietlicki, E.; Putaud, J. P.; Balkanski, Y.; Fuzzi, S.; Horth, J.; Moortgat, G. K.; Winterhalter, R.; Myhre, C. E. L.; Tsigaridis, K.; Vignati, E.; Stephanou, E. G.; Wilson, J. Organic aerosol and global climate modelling: A review. *Atmos. Chem. Phys.* **2005,** *5*, 1053-1123.

18. Liousse, C.; Penner, J. E.; Chuang, C.; Walton, J. J.; Eddleman, H.; Cachier, H. A global three-dimensional model study of carbonaceous aerosols. *J. Geophys. Res.: Atmos.* **1996,** *101*, 19411-19432.

19. Koppmann, R. *Volatile organic compounds in the atmosphere*. John Wiley & Sons: Ames, Iowa, 2008.

20. Ng, N. L.; Brown, S. S.; Archibald, A. T.; Atlas, E.; Cohen, R. C.; Crowley, J. N.; Day, D. A.; Donahue, N. M.; Fry, J. L.; Fuchs, H.; Griffin, R. J.; Guzman, M. I.; Herrmann, H.; Hodzic, A.; Iinuma, Y.; Jimenez, J. L.; Kiendler-Scharr, A.; Lee, B. H.; Luecken, D. J.; Mao, J. Q.; McLaren, R.; Mutzel, A.; Osthoff, H. D.; Ouyang, B.; Picquet-Varrault, B.; Platt, U.; Pye, H. O. T.; Rudich, Y.; Schwantes, R. H.; Shiraiwa, M.; Stutz, J.; Thornton, J. A.; Tilgner, A.; Williams, B. J.; Zaveri, R. A. Nitrate radicals and biogenic volatile organic compounds: Oxidation, mechanisms, and organic aerosol. *Atmos. Chem. Phys.* **2017,** *17*, 2103-2162.

21. Lenner, M. Nitrogen-dioxide in exhaust emissions from motor-vehicles. *Atmos. Environ.* **1987,** *21*, 37-43.

22. Sato, K.; Hatakeyama, S.; Imamura, T. Secondary organic aerosol formation during the photooxidation of toluene: NO_x dependence of chemical composition. *J. Phys. Chem. A* **2007,** *111*, 9796-9808.

23. Song, C.; Na, K.; Cocker, D. R. Impact of the hydrocarbon to NO_x ratio on secondary organic aerosol formation. *Environ. Sci. Technol.* **2005,** *39*, 3143-3149.

24. Zhang, J.; Huff Hartz, K. E.; Pandis, S. N.; Donahue, N. M. Secondary organic aerosol formation from limonene ozonolysis: Homogeneous and heterogeneous influences as a function of NO_x. *J. Phys. Chem. A* **2006,** *110*, 11053-11063.

25. Riipinen, I.; Pierce, J. R.; Yli-Juuti, T.; Nieminen, T.; Hakkinen, S.; Ehn, M.; Junninen, H.; Lehtipalo, K.; Petaja, T.; Slowik, J.; Chang, R.; Shantz, N. C.; Abbatt, J.; Leaitch, W. R.; Kerminen, V. M.; Worsnop, D. R.; Pandis, S. N.; Donahue, N. M.; Kulmala, M. Organic condensation: A vital link connecting aerosol formation to cloud condensation nuclei (CCN) concentrations. *Atmos. Chem. Phys.* **2011,** *11*, 3865-3878.

26. Kulmala, M.; Vehkamaki, H.; Petaja, T.; Dal Maso, M.; Lauri, A.; Kerminen, V. M.; Birmili, W.; McMurry, P. H. Formation and growth rates of ultrafine atmospheric particles: A review of observations. *J. Aerosol Sci.* **2004,** *35*, 143-176.

27. Hodzic, A.; Kasibhatla, P. S.; Jo, D. S.; Cappa, C. D.; Jimenez, J. L.; Madronich, S.; Park, R. J. Rethinking the global secondary organic aerosol (SOA) budget: Stronger production, faster removal, shorter lifetime. *Atmos. Chem. Phys.* **2016,** *16*, 7917-7941.

28. Lim, H. J.; Turpin, B. J. Origins of primary and secondary organic aerosol in Atlanta: Results of time-resolved measurements during the Atlanta supersite experiment. *Environ. Sci. Technol.* **2002,** *36*, 4489-4496.

29. Robinson, A. L.; Donahue, N. M.; Shrivastava, M. K.; Weitkamp, E. A.; Sage, A. M.; Grieshop, A. P.; Lane, T. E.; Pierce, J. R.; Pandis, S. N. Rethinking organic aerosols: Semivolatile emissions and photochemical aging. *Science* **2007,** *315*, 1259-1262.

30. Pope, C. A., 3rd; Burnett, R. T.; Thun, M. J.; Calle, E. E.; Krewski, D.; Ito, K.; Thurston, G. D. Lung cancer, cardiopulmonary mortality, and long-term exposure to fine particulate air pollution. *JAMA, J. Am. Med. Assoc.* **2002,** *287*, 1132-1141.

31. Brook, R. D.; Rajagopalan, S.; Pope, C. A., 3rd; Brook, J. R.; Bhatnagar, A.; Diez-Roux, A. V.; Holguin, F.; Hong, Y.; Luepker, R. V.; Mittleman, M. A.; Peters, A.; Siscovick, D.; Smith, S. C., Jr.; Whitsel, L.; Kaufman, J. D. Particulate matter air pollution and cardiovascular disease: An update to the scientific statement from the american heart association. *Circulation* **2010,** *121*, 2331-2378.

32. Pope, C. A., 3rd; Ezzati, M.; Dockery, D. W. Fine-particulate air pollution and life expectancy in the United States. *N. Engl. J. Med.* **2009,** *360*, 376-386.

33. Dockery, D. W.; Pope, C. A., 3rd; Xu, X.; Spengler, J. D.; Ware, J. H.; Fay, M. E.; Ferris, B. G., Jr.; Speizer, F. E. An association between air pollution and mortality in six U.S. cities. *N. Engl. J. Med.* **1993,** *329*, 1753-1759.

34. Nel, A. Atmosphere. Air pollution-related illness: Effects of particles. *Science* **2005,** *308*, 804-806.

35. Huang, R. J.; Zhang, Y.; Bozzetti, C.; Ho, K. F.; Cao, J. J.; Han, Y.; Daellenbach, K. R.; Slowik, J. G.; Platt, S. M.; Canonaco, F.; Zotter, P.; Wolf, R.; Pieber, S. M.; Bruns, E. A.; Crippa, M.; Ciarelli, G.; Piazzalunga, A.; Schwikowski, M.; Abbaszade, G.; Schnelle-Kreis, J.; Zimmermann, R.; An, Z.; Szidat, S.; Baltensperger, U.; El Haddad, I.; Prevot, A. S. High secondary aerosol contribution to particulate pollution during haze events in China. *Nature* **2014,** *514*, 218-222.

36. Charlson, R. J.; Schwartz, S. E.; Hales, J. M.; Cess, R. D.; Coakley, J. A., Jr.; Hansen, J. E.; Hofmann, D. J. Climate forcing by anthropogenic aerosols. *Science* **1992,** *255*, 423-430.

37. Sisler, J. F.; Malm, W. C. The relative importance of soluble aerosols to spatial and seasonal trends of impaired visibility in the United States. *Atmos. Environ.* **1994,** *28*, 851-862.

38. Kaufman, Y. J.; Tanre, D.; Boucher, O. A satellite view of aerosols in the climate system. *Nature* **2002,** *419*, 215-223.

39. Haywood, J.; Boucher, O. Estimates of the direct and indirect radiative forcing due to tropospheric aerosols: A review. *Rev. Geophys.* **2000,** *38*, 513-543.

40. Bond, T. C.; Sun, H. Can reducing black carbon emissions counteract global warming? *Environ. Sci. Technol.* **2005,** *39*, 5921-5926.

41. Ramanathan, V.; Ramana, M. V.; Roberts, G.; Kim, D.; Corrigan, C.; Chung, C.; Winker, D. Warming trends in asia amplified by brown cloud solar absorption. *Nature* **2007,** *448*, 575-578.

42. Intergovernmental Panel on Climate Change. *Climate change 2013 – the physical science basis*; Cambridge University Press: Cambridge, 2014.

43. Romonosky, D. E.; Laskin, A.; Laskin, J.; Nizkorodov, S. A. High-resolution mass spectrometry and molecular characterization of aqueous photochemistry products of common types of secondary organic aerosols. *J. Phys. Chem. A* **2015,** *119*, 2594-2606.

44. Kourtchev, I.; Fuller, S. J.; Giorio, C.; Healy, R. M.; Wilson, E.; O'Connor, I.; Wenger, J. C.; McLeod, M.; Aalto, J.; Ruuskanen, T. M.; Maenhaut, W.; Jones, R.; Venables, D. S.; Sodeau, J. R.; Kulmala, M.; Kalberer, M. Molecular composition of biogenic secondary organic aerosols using ultrahigh-resolution mass spectrometry: Comparing laboratory and field studies. *Atmos. Chem. Phys.* **2014,** *14*, 2155-2167.

45. Noziere, B.; Kalberer, M.; Claeys, M.; Allan, J.; D'Anna, B.; Decesari, S.; Finessi, E.; Glasius, M.; Grgic, I.; Hamilton, J. F.; Hoffmann, T.; Iinuma, Y.; Jaoui, M.; Kahnt, A.; Kampf, C. J.; Kourtchev, I.; Maenhaut, W.; Marsden, N.; Saarikoski, S.; Schnelle-Kreis, J.; Surratt, J. D.; Szidat, S.; Szmigielski, R.; Wisthaler, A. The molecular identification of organic compounds in the atmosphere: State of the art and challenges. *Chem. Rev.* **2015,** *115*, 3919-3983.

46. Forstner, H. J. L.; Flagan, R. C.; Seinfeld, J. H. Secondary organic aerosol from the photooxidation of aromatic hydrocarbons: Molecular composition. *Environ. Sci. Technol.* **1997,** *31*, 1345-1358.

47. Zhang, X.; Lambe, A. T.; Upshur, M. A.; Brooks, W. A.; Gray Be, A.; Thomson, R. J.; Geiger, F. M.; Surratt, J. D.; Zhang, Z.; Gold, A.; Graf, S.; Cubison, M. J.; Groessl, M.; Jayne, J. T.; Worsnop, D. R.; Canagaratna, M. R. Highly oxygenated multifunctional

compounds in α-pinene secondary organic aerosol. *Environ. Sci. Technol.* **2017,** *51*, 5932-5940.

48. D'Ambro, E. L.; Lee, B. H.; Liu, J.; Shilling, J. E.; Gaston, C. J.; Lopez-Hilfiker, F. D.; Schobesberger, S.; Zaveri, R. A.; Mohr, C.; Lutz, A. Molecular composition and volatility of isoprene photochemical oxidation secondary organic aerosol under low-and high-NO_x conditions. *Atmos. Chem. Phys.* **2017,** *17*, 159-174.

49. Henze, D. K.; Seinfeld, J. H.; Ng, N. L.; Kroll, J. H.; Fu, T. M.; Jacob, D. J.; Heald, C. L. Global modeling of secondary organic aerosol formation from aromatic hydrocarbons: High- vs. Low-yield pathways. *Atmos. Chem. Phys.* **2008,** *8*, 2405-2420.

50. Klotz, B.; Volkamer, R.; Hurley, M. D.; Andersen, M. P. S.; Nielsen, O. J.; Barnes, I.; Imamura, T.; Wirtz, K.; Becker, K. H.; Platt, U.; Wallington, T. J.; Washida, N. OH-initiated oxidation of benzene - part II. Influence of elevated NO_x concentrations. *Phys. Chem. Chem. Phys.* **2002,** *4*, 4399-4411.

51. Zhang, Y. J.; Tang, L. L.; Sun, Y. L.; Favez, O.; Canonaco, F.; Albinet, A.; Couvidat, F.; Liu, D. T.; Jayne, J. T.; Wang, Z.; Croteau, P. L.; Canagaratna, M. R.; Zhou, H. C.; Prevot, A. S. H.; Worsnop, D. R. Limited formation of isoprene epoxydiols-derived secondary organic aerosol under NO_x-rich environments in eastern China. *Geophys. Res. Lett.* **2017,** *44*, 2035-2043.

52. Hoffmann, T.; Odum, J. R.; Bowman, F.; Collins, D.; Klockow, D.; Flagan, R. C.; Seinfeld, J. H. Formation of organic aerosols from the oxidation of biogenic hydrocarbons. *J. Atmos. Chem.* **1997,** *26*, 189-222.

53. Lambe, A. T.; Chhabra, P. S.; Onasch, T. B.; Brune, W. H.; Hunter, J. F.; Kroll, J. H.; Cummings, M. J.; Brogan, J. F.; Parmar, Y.; Worsnop, D. R.; Kolb, C. E.; Davidovits, P. Effect of oxidant concentration, exposure time, and seed particles on secondary organic aerosol chemical composition and yield. *Atmos. Chem. Phys.* **2015,** *15*, 3063-3075.

54. Gao, S.; Ng, N. L.; Keywood, M.; Varutbangkul, V.; Bahreini, R.; Nenes, A.; He, J.; Yoo, K. Y.; Beauchamp, J. L.; Hodyss, R. P.; Flagan, R. C.; Seinfeld, J. H. Particle phase acidity and oligomer formation in secondary organic aerosol. *Environ. Sci. Technol.* **2004,** *38*, 6582-6589.

55. Iinuma, Y.; Böge, O.; Gnauk, T.; Herrmann, H. Aerosol-chamber study of the α-pinene/O_3 reaction: Influence of particle acidity on aerosol yields and products. *Atmos. Environ.* **2004,** *38*, 761-773.

56. Altieri, K. E.; Seitzinger, S. P.; Carlton, A. G.; Turpin, B. J.; Klein, G. C.; Marshall, A. G. Oligomers formed through in-cloud methylglyoxal reactions: Chemical composition, properties, and mechanisms investigated by ultra-high resolution FT-ICR mass spectrometry. *Atmos. Environ.* **2008,** *42*, 1476-1490.

57. Heaton, K. J.; Dreyfus, M. A.; Wang, S.; Johnston, M. V. Oligomers in the early stage of biogenic secondary organic aerosol formation and growth. *Environ. Sci. Technol.* **2007,** *41*, 6129-6136.

58. Tolocka, M. P.; Jang, M.; Ginter, J. M.; Cox, F. J.; Kamens, R. M.; Johnston, M. V. Formation of oligomers in secondary organic aerosol. *Environ. Sci. Technol.* **2004,** *38*, 1428-1434.

59. Baltensperger, U.; Kalberer, M.; Dommen, J.; Paulsen, D.; Alfarra, M. R.; Coe, H.; Fisseha, R.; Gascho, A.; Gysel, M.; Nyeki, S.; Sax, M.; Steinbacher, M.; Prevot, A. S.; Sjogren, S.; Weingartner, E.; Zenobi, R. Secondary organic aerosols from anthropogenic and biogenic precursors. *Faraday Discuss.* **2005,** *130*, 265-278.

60. Hallquist, M.; Wangberg, I.; Ljungstrom, E.; Barnes, I.; Becker, K. H. Aerosol and product yields from NO_3 radical-initiated oxidation of selected monoterpenes. *Environ. Sci. Technol.* **1999,** *33*, 553-559.

61. Odum, J. R.; Hoffmann, T.; Bowman, F.; Collins, D.; Flagan, R. C.; Seinfeld, J. H. Gas/particle partitioning and secondary organic aerosol yields. *Environ. Sci. Technol.* **1996,** *30*, 2580-2585.

62. Carrico, C. M.; Petters, M. D.; Kreidenweis, S. M.; Sullivan, A. P.; McMeeking, G. R.; Levin, E. J. T.; Engling, G.; Malm, W. C.; Collett, J. L. Water uptake and chemical composition of fresh aerosols generated in open burning of biomass. *Atmos. Chem. Phys.* **2010,** *10*, 5165-5178.

63. Mikhailov, E.; Vlasenko, S.; Martin, S. T.; Koop, T.; Poschl, U. Amorphous and crystalline aerosol particles interacting with water vapor: Conceptual framework and experimental evidence for restructuring, phase transitions and kinetic limitations. *Atmos. Chem. Phys.* **2009,** *9*, 9491-9522.

64. Zhao, B.; Wang, S.; Donahue, N. M.; Chuang, W.; Hildebrandt Ruiz, L.; Ng, N. L.; Wang, Y.; Hao, J. Evaluation of one-dimensional and two-dimensional volatility basis sets in simulating the aging of secondary organic aerosol with smog-chamber experiments. *Environ. Sci. Technol.* **2015,** *49*, 2245-2254.

65. Ruiz, H. L.; Paciga, A. L.; Cerully, K.; Nenes, A.; Donahue, N. M.; Pandis, S. N. Aging of secondary organic aerosol from small aromatic VOCs: Changes in chemical composition, mass yield, volatility and hygroscopicity. *Atmos. Chem. Phys.* **2014,** *14*, 31441-31481.

66. Riva, M.; Robinson, E. S.; Perraudin, E.; Donahue, N. M.; Villenave, E. Photochemical aging of secondary organic aerosols generated from the photooxidation of polycyclic aromatic hydrocarbons in the gas-phase. *Environ. Sci. Technol.* **2015,** *49*, 5407-5416.

67. Henry, K. M.; Donahue, N. M. Photochemical aging of α-pinene secondary organic aerosol: Effects of OH radical sources and photolysis. *J. Phys. Chem. A* **2012,** *116*, 5932-5940.

68. Henry, K. M.; Lohaus, T.; Donahue, N. M. Organic aerosol yields from α-pinene oxidation: Bridging the gap between first-generation yields and aging chemistry. *Environ. Sci. Technol.* **2012,** *46*, 12347-12354.

69. Rudich, Y.; Donahue, N. M.; Mentel, T. F. Aging of organic aerosol: Bridging the gap between laboratory and field studies. *Annu. Rev. Phys. Chem.* **2007,** *58*, 321-352.

70. Shiraiwa, M.; Poschl, U.; Knopf, D. A. Multiphase chemical kinetics of NO_3 radicals reacting with organic aerosol components from biomass burning. *Environ. Sci. Technol.* **2012,** *46*, 6630-6636.

71. Epstein, S. A.; Nizkorodov, S. A. A comparison of the chemical sinks of atmospheric organics in the gas and aqueous phase. *Atmos. Chem. Phys.* **2012,** *12*, 8205-8222.

72. Kroll, J. H.; Smith, J. D.; Che, D. L.; Kessler, S. H.; Worsnop, D. R.; Wilson, K. R. Measurement of fragmentation and functionalization pathways in the heterogeneous oxidation of oxidized organic aerosol. *Phys. Chem. Chem. Phys.* **2009,** *11*, 8005-8014.

73. Epstein, S. A.; Blair, S. L.; Nizkorodov, S. A. Direct photolysis of α-pinene ozonolysis secondary organic aerosol: Effect on particle mass and peroxide content. *Environ. Sci. Technol.* **2014,** *48*, 11251-11258.

74. Romonosky, D. E.; Ali, N. N.; Saiduddin, M. N.; Wu, M.; Lee, H. J.; Aiona, P. K.; Nizkorodov, S. A. Effective absorption cross sections and photolysis rates of anthropogenic and biogenic secondary organic aerosols. *Atmos. Environ.* **2016,** *130*, 172-179.

75. Surratt, J. D.; Murphy, S. M.; Kroll, J. H.; Ng, N. L.; Hildebrandt, L.; Sorooshian, A.; Szmigielski, R.; Vermeylen, R.; Maenhaut, W.; Claeys, M.; Flagan, R. C.; Seinfeld, J. H. Chemical composition of secondary organic aerosol formed from the photooxidation of isoprene. *J. Phys. Chem. A* **2006,** *110*, 9665-9690.

76. Jang, M.; Czoschke, N. M.; Lee, S.; Kamens, R. M. Heterogeneous atmospheric aerosol production by acid-catalyzed particle-phase reactions. *Science* **2002,** *298*, 814-817.

77. Beilke, S.; Gravenhorst, G. Heterogeneous SO_2-oxidation in the droplet phase. *Atmos. Environ.* **1978,** *12*, 231-239.

78. Dentener, F. J.; Crutzen, P. J. Reaction of N_2O_5 on tropospheric aerosols: Impact on the global distributions of NO_x, O_3, and OH. *J. Geophys. Res.: Atmos.* **1993,** *98*, 7149-7163.

79. Zahardis, J.; Petrucci, G. The oleic acid-ozone heterogeneous reaction system: Products, kinetics, secondary chemistry, and atmospheric implications of a model system–a review. *Atmos. Chem. Phys.* **2007,** *7*, 1237-1274.

80. Donahue, N. M.; Robinson, A. L.; Trump, E. R.; Riipinen, I.; Kroll, J. H. Volatility and aging of atmospheric organic aerosol. In *Atmospheric and aerosol chemistry*, Springer: Berlin, 2012, pp 97-143.

81. Donahue, N. M.; Henry, K. M.; Mentel, T. F.; Kiendler-Scharr, A.; Spindler, C.; Bohn, B.; Brauers, T.; Dorn, H. P.; Fuchs, H.; Tillmann, R.; Wahner, A.; Saathoff, H.; Naumann, K. H.; Mohler, O.; Leisner, T.; Muller, L.; Reinnig, M. C.; Hoffmann, T.; Salo, K.; Hallquist, M.; Frosch, M.; Bilde, M.; Tritscher, T.; Barmet, P.; Praplan, A. P.; DeCarlo, P. F.; Dommen, J.; Prevot, A. S.; Baltensperger, U. Aging of biogenic secondary organic aerosol via gas-phase OH radical reactions. *Proc. Natl. Acad. Sci. U. S. A.* **2012,** *109*, 13503-13508.

82. Kroll, J. H.; Lim, C. Y.; Kessler, S. H.; Wilson, K. R. Heterogeneous oxidation of atmospheric organic aerosol: Kinetics of changes to the amount and oxidation state of particle-phase organic carbon. *J. Phys. Chem. A* **2015,** *119*, 10767-10783.

83. George, I. J.; Abbatt, J. P. Heterogeneous oxidation of atmospheric aerosol particles by gas-phase radicals. *Nat. Chem.* **2010,** *2*, 713-722.

84. Hoffmann, M. R. Homogeneous and heterogeneous photochemistry in the troposphere. In *Environmental photochemistry part II*, Boule, P.; Bahnemann, D. W.; Robertson, P. K. J., Eds. Springer Berlin Heidelberg: Berlin, 2005.

85. Vione, D.; Maurino, V.; Minero, C.; Pelizzetti, E.; Harrison, M. A.; Olariu, R. I.; Arsene, C. Photochemical reactions in the tropospheric aqueous phase and on particulate matter. *Chem. Soc. Rev.* **2006,** *35*, 441-453.

86. Herrmann, H.; Schaefer, T.; Tilgner, A.; Styler, S. A.; Weller, C.; Teich, M.; Otto, T. Tropospheric aqueous-phase chemistry: Kinetics, mechanisms, and its coupling to a changing gas phase. *Chem. Rev.* **2015,** *115*, 4259-4334.

87. Dubowski, Y.; Vieceli, J.; Tobias, D. J.; Gomez, A.; Lin, A.; Nizkorodov, S. A.; McIntire, T. M.; Finlayson-Pitts, B. J. Interaction of gas-phase ozone at 296 K with unsaturated self-assembled monolayers: A new look at an old system. *J. Phys. Chem. A* **2004,** *108*, 10473-10485.

88. Gomez, A. L.; Park, J.; Walser, M. L.; Lin, A.; Nizkorodov, S. A. UV photodissociation spectroscopy of oxidized undecylenic acid films. *J. Phys. Chem. A* **2006,** *110*, 3584-3592.

89. Park, J.; Gomez, A. L.; Walser, M. L.; Lin, A.; Nizkorodov, S. A. Ozonolysis and photolysis of alkene-terminated self-assembled monolayers on quartz nanoparticles: Implications for photochemical aging of organic aerosol particles. *Phys. Chem. Chem. Phys.* **2006,** *8*, 2506-2512.

90. Ruiz, L. H.; Paciga, A. L.; Cerully, K. M.; Nenes, A.; Donahue, N. M.; Pandis, S. N. Formation and aging of secondary organic aerosol from toluene: Changes in chemical composition, volatility, and hygroscopicity. *Atmos. Chem. Phys.* **2015,** *15*, 8301-8313.

91. Hodzic, A.; Madronich, S.; Kasibhatla, P. S.; Tyndall, G.; Aumont, B.; Jimenez, J. L.; Lee-Taylor, J.; Orlando, J. Organic photolysis reactions in tropospheric aerosols: Effect on secondary organic aerosol formation and lifetime. *Atmos. Chem. Phys.* **2015,** *15*, 9253-9269.

92. Walser, M. L.; Park, J.; Gomez, A. L.; Russell, A. R.; Nizkorodov, S. A. Photochemical aging of secondary organic aerosol particles generated from the oxidation of d-limonene. *J. Phys. Chem. A* **2007,** *111*, 1907-1913.

93. Mang, S. A.; Henricksen, D. K.; Bateman, A. P.; Andersen, M. P.; Blake, D. R.; Nizkorodov, S. A. Contribution of carbonyl photochemistry to aging of atmospheric secondary organic aerosol. *J. Phys. Chem. A* **2008,** *112*, 8337-8344.

94. Hung, H. M.; Chen, Y. Q.; Martin, S. T. Reactive aging of films of secondary organic material studied by infrared spectroscopy. *J. Phys. Chem. A* **2013,** *117*, 108-116.

95. Wong, J. P.; Zhou, S.; Abbatt, J. P. Changes in secondary organic aerosol composition and mass due to photolysis: Relative humidity dependence. *J. Phys. Chem. A* **2015,** *119*, 4309-4316.

96. Yu, L.; Smith, J.; Laskin, A.; George, K. M.; Anastasio, C.; Laskin, J.; Dillner, A. M.; Zhang, Q. Molecular transformations of phenolic SOA during photochemical aging in the aqueous phase: Competition among oligomerization, functionalization, and fragmentation. *Atmos. Chem. Phys.* **2016,** *16*, 4511-4527.

97. Zhao, R.; Aljawhary, D.; Lee, A. K. Y.; Abbatt, J. P. D. Rapid aqueous-phase photooxidation of dimers in the α-pinene secondary organic aerosol. *Environ. Sci. Technol. Lett.* **2017,** *4*, 205-210.

98. Fan, Z. H.; Kamens, R. M.; Hu, J. X.; Zhang, J. B.; McDow, S. Photostability of nitro polycyclic aromatic hydrocarbons on combustion soot particles in sunlight. *Environ. Sci. Technol.* **1996,** *30*, 1358-1364.

99. Jang, M.; McDow, S. R. Benz[a]anthracene photodegradation in the presence of known organic constituents of atmospheric aerosols. *Environ. Sci. Technol.* **1995,** *29*, 2654-2660.

100. Pan, X.; Underwood, J. S.; Xing, J. H.; Mang, S. A.; Nizkorodov, S. A. Photodegradation of secondary organic aerosol generated from limonene oxidation by ozone studied with chemical ionization mass spectrometry. *Atmos. Chem. Phys.* **2009,** *9*, 3851-3865.

101. Vlasenko, A.; George, I. J.; Abbatt, J. P. Formation of volatile organic compounds in the heterogeneous oxidation of condensed-phase organic films by gas-phase OH. *J. Phys. Chem. A* **2008,** *112*, 1552-1560.

102. Shiraiwa, M.; Ammann, M.; Koop, T.; Pöschl, U. Gas uptake and chemical aging of semisolid organic aerosol particles. *Proc. Natl. Acad. Sci. U. S. A.* **2011,** *108*, 11003-11008.

103. Perraud, V.; Bruns, E. A.; Ezell, M. J.; Johnson, S. N.; Yu, Y.; Alexander, M. L.; Zelenyuk, A.; Imre, D.; Chang, W. L.; Dabdub, D.; Pankow, J. F.; Finlayson-Pitts, B. J. Nonequilibrium atmospheric secondary organic aerosol formation and growth. *Proc. Natl. Acad. Sci. U. S. A.* **2012,** *109*, 2836-2841.

104. Donaldson, D. J.; Vaida, V. The influence of organic films at the air-aqueous boundary on atmospheric processes. *Chem. Rev.* **2006,** *106*, 1445-1461.

105. Gilman, J. B.; Vaida, V. Permeability of acetic acid through organic films at the air-aqueous interface. *J. Phys. Chem. A* **2006,** *110*, 7581-7587.

106. McNaught, A. D.; McNaught, A. D. *Compendium of chemical terminology*. Blackwell Science: Oxford, 1997; Vol. 1669.

107. Choudhry, G. G.; Roof, A. A. M.; Hutzinger, O. Mechanisms in sensitized photochemistry of environmental chemicals. *Toxicol. Environ. Chem. Rev.* **1979,** *2*, 259-302.

108. Laskin, A.; Laskin, J.; Nizkorodov, S. A. Chemistry of atmospheric brown carbon. *Chem. Rev.* **2015,** *115*, 4335-4382.

109. Teich, M.; van Pinxteren, D.; Kecorius, S.; Wang, Z.; Herrmann, H. First quantification of imidazoles in ambient aerosol particles: Potential photosensitizers, brown carbon constituents, and hazardous components. *Environ. Sci. Technol.* **2016,** *50*, 1166-1173.

110. Hamilton, J. F.; Webb, P. J.; Lewis, A. C.; Hopkins, J. R.; Smith, S.; Davy, P. Partially oxidised organic components in urban aerosol using GCXGC-TOF/MS. *Atmos. Chem. Phys.* **2004,** *4*, 1279-1290.

111. Monge, M. E.; Rosenorn, T.; Favez, O.; Muller, M.; Adler, G.; Abo Riziq, A.; Rudich, Y.; Herrmann, H.; George, C.; D' Anna, B. Alternative pathway for atmospheric particles growth. *Proc. Natl. Acad. Sci. U. S. A.* **2012,** *109*, 6840-6844.

112. Geron, C.; Rasmussen, R.; Arnts, R. R.; Guenther, A. A review and synthesis of monoterpene speciation from forests in the United States. *Atmos. Environ.* **2000,** *34*, 1761-1781.

113. Guenther, A.; Karl, T.; Harley, P.; Wiedinmyer, C.; Palmer, P. I.; Geron, C. Estimates of global terrestrial isoprene emissions using MEGAN (model of emissions of gases and aerosols from nature). *Atmos. Chem. Phys.* **2006,** *6*, 3181-3210.

114. Braddock, R. J.; Cadwallader, K. R. Bioconversion of citrus d-limonene. In *Fruit flavors*, American Chemical Society: 1995; Vol. 596, pp 142-148.

115. McDonald, J. D.; Zielinska, B.; Fujita, E. M.; Sagebiel, J. C.; Chow, J. C.; Watson, J. G. Fine particle and gaseous emission rates from residential wood combustion. *Environ. Sci. Technol.* **2000,** *34*, 2080-2091.

116. Kidd, J. Observations on naphthaline, a peculiar substance resembling a concrete essential oil, which is apparently produced during the decomposition of coal tar, by exposure to a red heat. *Philos. Trans. R. Soc. London* **1821,** *111*, 209-221.

117. Kim, Y. M.; Harrad, S.; Harrison, R. M. Concentrations and sources of VOCs in urban domestic and public microenvironments. *Environ. Sci. Technol.* **2001,** *35*, 997-1004.

118. Graedel, T. *Chemical compounds in the atmosphere*. Academic Press, Inc.: New York, 1978.

119. Alegbeleye, O. O.; Opeolu, B. O.; Jackson, V. A. Polycyclic aromatic hydrocarbons: A critical review of environmental occurrence and bioremediation. *Environ. Manage.* **2017,** *60*, 758-783.

120. Sindelarova, K.; Granier, C.; Bouarar, I.; Guenther, A.; Tilmes, S.; Stavrakou, T.; Muller, J. F.; Kuhn, U.; Stefani, P.; Knorr, W. Global data set of biogenic VOC emissions calculated by the MEGAN model over the last 30 years. *Atmos. Chem. Phys.* **2014,** *14*, 9317-9341.

121. Guenther, A.; Geron, C.; Pierce, T.; Lamb, B.; Harley, P.; Fall, R. Natural emissions of non-methane volatile organic compounds; carbon monoxide, and oxides of nitrogen from north america. *Atmos. Environ.* **2000,** *34*, 2205-2230.

122. Guenther, A.; Hewitt, C. N.; Erickson, D.; Fall, R.; Geron, C.; Graedel, T.; Harley, P.; Klinger, L.; Lerdau, M.; Mckay, W. A.; Pierce, T.; Scholes, B.; Steinbrecher, R.; Tallamraju, R.; Taylor, J.; Zimmerman, P. A global-model of natural volatile organic-compound emissions. *J. Geophys. Res.: Atmos.* **1995,** *100*, 8873-8892.

123. Griffin, R. J.; Cocker, D. R.; Flagan, R. C.; Seinfeld, J. H. Organic aerosol formation from the oxidation of biogenic hydrocarbons. *J. Geophys. Res.: Atmos.* **1999,** *104*, 3555-3567.

124. Atkinson, R.; Arey, J. Atmospheric degradation of volatile organic compounds. *Chem. Rev.* **2003,** *103*, 4605-4638.

125. Pandis, S. N.; Paulson, S. E.; Seinfeld, J. H.; Flagan, R. C. Aerosol formation in the photooxidation of isoprene and β-pinene. *Atmos. Environ., Part A* **1991,** *25*, 997-1008.

126. Cocker, D. R.; Mader, B. T.; Kalberer, M.; Flagan, R. C.; Seinfeld, J. H. The effect of water on gas–particle partitioning of secondary organic aerosol: II. m-xylene and 1,3,5-trimethylbenzene photooxidation systems. *Atmos. Environ.* **2001,** *35*, 6073-6085.

127. Paulsen, D.; Dommen, J.; Kalberer, M.; Prevot, A. S.; Richter, R.; Sax, M.; Steinbacher, M.; Weingartner, E.; Baltensperger, U. Secondary organic aerosol formation by irradiation of 1,3,5-trimethylbenzene-NO_x-H_2O in a new reaction chamber for atmospheric chemistry and physics. *Environ. Sci. Technol.* **2005,** *39*, 2668-2678.

128. Sax, M.; Zenobi, R.; Baltensperger, U.; Kalberer, M. Time resolved infrared spectroscopic analysis of aerosol formed by photo-oxidation of 1,3,5-trimethylbenzene and α-pinene. *Aerosol Sci. Technol.* **2005,** *39*, 822-830.

129. Kroll, J. H.; Ng, N. L.; Murphy, S. M.; Flagan, R. C.; Seinfeld, J. H. Secondary organic aerosol formation from isoprene photooxidation. *Environ. Sci. Technol.* **2006,** *40*, 1869-1877.

130. Carlton, A. G.; Wiedinmyer, C.; Kroll, J. H. A review of secondary organic aerosol (SOA) formation from isoprene. *Atmos. Chem. Phys.* **2009,** *9*, 4987-5005.

131. Marple, V. A.; Rubow, K. L.; Behm, S. M. A microorifice uniform deposit impactor (MOUDI) - description, calibration, and use. *Aerosol Sci. Technol.* **1991,** *14*, 434-446.

132. Bones, D. L.; Henricksen, D. K.; Mang, S. A.; Gonsior, M.; Bateman, A. P.; Nguyen, T. B.; Cooper, W. J.; Nizkorodov, S. A. Appearance of strong absorbers and fluorophores in limonene-O_3 secondary organic aerosol due to NH_4^+-mediated chemical aging over long time scales. *J. Geophys. Res.* **2010,** *115*.

133. Hansel, A.; Jordan, A.; Holzinger, R.; Prazeller, P.; Vogel, W.; Lindinger, W. Proton transfer reaction mass spectrometry: On-line trace gas analysis at the ppb level. *Int. J. Mass Spectrom. Ion Processes* **1995,** *149-150*, 609-619.

134. Blake, R. S.; Monks, P. S.; Ellis, A. M. Proton-transfer reaction mass spectrometry. *Chem. Rev.* **2009,** *109*, 861-896.

135. Sauerbrey, G. Verwendung von schwingquarzen zur wägung dünner schichten und zur mikrowägung. *Z. Phys.* **1959,** *155*, 206-222.

136. Henderson, J. *Electronic devices: Concepts and applications*. Prentice-Hall, Inc.: 1991.

137. Rodahl, M.; Höök, F.; Krozer, A.; Brzezinski, P.; Kasemo, B. Quartz crystal microbalance setup for frequency and q-factor measurements in gaseous and liquid environments. *Rev. Sci. Instrum.* **1995,** *66*, 3924-3930.

138. Shiraiwa, M.; Yee, L. D.; Schilling, K. A.; Loza, C. L.; Craven, J. S.; Zuend, A.; Ziemann, P. J.; Seinfeld, J. H. Size distribution dynamics reveal particle-phase chemistry in organic aerosol formation. *Proc. Natl. Acad. Sci. U. S. A.* **2013,** *110*, 11746-11750.

139. Daumit, K. E.; Carrasquillo, A. J.; Sugrue, R. A.; Kroll, J. H. Effects of condensed-phase oxidants on secondary organic aerosol formation. *J. Phys. Chem. A* **2016,** *120*, 1386-1394.

140. Bunce, N. J.; Lamarre, J.; Vaish, S. P. Photorearrangement of azoxybenzene to 2-hydroxyazobenzene - a convenient chemical actinometer. *Photochem. Photobiol.* **1984,** *39*, 531-533.

141. Zhao, J.; Zhang, R. Y. Proton transfer reaction rate constants between hydronium ion (H_3O^+) and volatile organic compounds. *Atmos. Environ.* **2004,** *38*, 2177-2185.

142. Chen, Q.; Heald, C. L.; Jimenez, J. L.; Canagaratna, M. R.; Zhang, Q.; He, L. Y.; Huang, X. F.; Campuzano-Jost, P.; Palm, B. B.; Poulain, L.; Kuwata, M.; Martin, S. T.; Abbatt, J.

P. D.; Lee, A. K. Y.; Liggio, J. Elemental composition of organic aerosol: The gap between ambient and laboratory measurements. *Geophys. Res. Lett.* **2015,** *42*, 4182-4189.

143. Lauraguais, A.; Coeur-Tourneur, C.; Cassez, A.; Deboudt, K.; Fourmentin, M.; Choel, M. Atmospheric reactivity of hydroxyl radicals with guaiacol (2-methoxyphenol), a biomass burning emitted compound: Secondary organic aerosol formation and gas-phase oxidation products. *Atmos. Environ.* **2014,** *86*, 155-163.

144. Madronich, S. Tropospheric ultraviolet and visible (TUV) radiation model. https://www2.acom.ucar.edu/modeling/tropospheric-ultraviolet-and-visible-tuv-radiation-model (accessed November 27, 2017).

145. Chameides, W. L.; Davis, D. D. Aqueous-phase source of formic-acid in clouds. *Nature* **1983,** *304*, 427-429.

146. Stavrakou, T.; Müller, J. F.; Peeters, J.; Razavi, A.; Clarisse, L.; Clerbaux, C.; Coheur, P. F.; Hurtmans, D.; De Mazière, M.; Vigouroux, C.; Deutscher, N. M.; Griffith, D. W. T.; Jones, N.; Paton-Walsh, C. Satellite evidence for a large source of formic acid from boreal and tropical forests. *Nat. Geosci.* **2011,** *5*, 26-30.

147. Lignell, H.; Hinks, M. L.; Nizkorodov, S. A. Exploring matrix effects on photochemistry of organic aerosols. *Proc. Natl. Acad. Sci. U. S. A.* **2014,** *111*, 13780-13785.

148. Hinks, M. L.; Brady, M. V.; Lignell, H.; Song, M.; Grayson, J. W.; Bertram, A. K.; Lin, P.; Laskin, A.; Laskin, J.; Nizkorodov, S. A. Effect of viscosity on photodegradation rates in complex secondary organic aerosol materials. *Phys. Chem. Chem. Phys.* **2016,** *18*, 8785-8793.

149. Aregahegn, K. Z.; Noziere, B.; George, C. Organic aerosol formation photo-enhanced by the formation of secondary photosensitizers in aerosols. *Faraday Discuss.* **2013,** *165*, 123-134.

150. Malecha, K. T.; Nizkorodov, S. A. Photodegradation of secondary organic aerosol particles as a source of small, oxygenated volatile organic compounds. *Environ. Sci. Technol.* **2016,** *50*, 9990-9997.

151. Kang, E.; Root, M. J.; Toohey, D. W.; Brune, W. H. Introducing the concept of potential aerosol mass (PAM). *Atmos. Chem. Phys.* **2007,** *7*, 5727-5744.

152. Peng, Z.; Day, D. A.; Stark, H.; Li, R.; Lee-Taylor, J.; Palm, B. B.; Brune, W. H.; Jimenez, J. L. HO_x radical chemistry in oxidation flow reactors with low-pressure mercury lamps systematically examined by modeling. *Atmos. Meas. Tech.* **2015,** *8*, 4863-4890.

153. Peng, Z.; Day, D. A.; Ortega, A. M.; Palm, B. B.; Hu, W. W.; Stark, H.; Li, R.; Tsigaridis, K.; Brune, W. H.; Jimenez, J. L. Non-OH chemistry in oxidation flow reactors for the study of atmospheric chemistry systematically examined by modeling. *Atmos. Chem. Phys.* **2016,** *16*, 4283-4305.

154. Liu, P.; Li, Y. J.; Wang, Y.; Gilles, M. K.; Zaveri, R. A.; Bertram, A. K.; Martin, S. T. Lability of secondary organic particulate matter. *Proc. Natl. Acad. Sci. U. S. A.* **2016,** *113*, 12643-12648.

155. Grant, J. S.; Shaw, S. K. A model system to mimic environmentally active surface film roughness and hydrophobicity. *Chemosphere* **2017,** *185*, 772-779.

156. Thomas, E.; Rudich, Y.; Trakhtenberg, S.; Ussyshkin, R. Water adsorption by hydrophobic organic surfaces: Experimental evidence and implications to the atmospheric properties of organic aerosols. *J. Geophys. Res.: Atmos.* **1999,** *104*, 16053-16059.

157. Rudich, Y.; Benjamin, I.; Naaman, R.; Thomas, E.; Trakhtenberg, S.; Ussyshkin, R. Wetting of hydrophobic organic surfaces and its implications to organic aerosols in the atmosphere. *J. Phys. Chem. A* **2000,** *104*, 5238-5245.

158. Demou, E.; Visram, H.; Donaldson, D. J.; Makar, P. A. Uptake of water by organic films: The dependence on the film oxidation state. *Atmos. Environ.* **2003,** *37*, 3529-3537.

159. Molina, M. J.; Ivanov, A. V.; Trakhtenberg, S.; Molina, L. T. Atmospheric evolution of organic aerosol. *Geophys. Res. Lett.* **2004,** *31*.

160. Malecha, K. T.; Nizkorodov, S. A. Feasibility of photosensitized reactions with secondary organic aerosol particles in the presence of volatile organic compounds. *J. Phys. Chem. A* **2017,** *121*, 4961-4967.

161. Li, R.; Palm, B. B.; Ortega, A. M.; Hlywiak, J.; Hu, W.; Peng, Z.; Day, D. A.; Knote, C.; Brune, W. H.; de Gouw, J. A.; Jimenez, J. L. Modeling the radical chemistry in an oxidation flow reactor: Radical formation and recycling, sensitivities, and the OH exposure estimation equation. *J. Phys. Chem. A* **2015,** *119*, 4418-4432.

162. Chhabra, P. S.; Ng, N. L.; Canagaratna, M. R.; Corrigan, A. L.; Russell, L. M.; Worsnop, D. R.; Flagan, R. C.; Seinfeld, J. H. Elemental composition and oxidation of chamber organic aerosol. *Atmos. Chem. Phys.* **2011,** *11*, 8827-8845.

163. Kitanovski, Z.; Cusak, A.; Grgic, I.; Claeys, M. Chemical characterization of the main products formed through aqueous-phase photonitration of guaiacol. *Atmos. Meas. Tech.* **2014,** *7*, 2457-2470.

164. Sangwan, M.; Zhu, L. Absorption cross sections of 2-nitrophenol in the 295-400 nm region and photolysis of 2-nitrophenol at 308 and 351 nm. *J. Phys. Chem. A* **2016,** *120*, 9958-9967.

165. Barsotti, F.; Bartels-Rausch, T.; De Laurentiis, E.; Ammann, M.; Brigante, M.; Mailhot, G.; Maurino, V.; Minero, C.; Vione, D. Photochemical formation of nitrite and nitrous acid (HONO) upon irradiation of nitrophenols in aqueous solution and in viscous secondary organic aerosol proxy. *Environ. Sci. Technol.* **2017,** *51*, 7486-7495.

166. Grygoryeva, K.; Kubecka, J.; Pysanenko, A.; Lengyel, J.; Slavicek, P.; Farnik, M. Photochemistry of nitrophenol molecules and clusters: Intra- vs intermolecular hydrogen bond dynamics. *J. Phys. Chem. A* **2016,** *120*, 4139-4146.

167. Ortega, A. M.; Hayes, P. L.; Peng, Z.; Palm, B. B.; Hu, W.; Day, D. A.; Li, R.; Cubison, M. J.; Brune, W. H.; Graus, M.; Warneke, C.; Gilman, J. B.; Kuster, W. C.; de Gouw, J.; Gutiérrez-Montes, C.; Jimenez, J. L. Real-time measurements of secondary organic aerosol formation and aging from ambient air in an oxidation flow reactor in the Los Angeles area. *Atmos. Chem. Phys.* **2016,** *16*, 7411-7433.

168. Yu, P.; Rosenlof, K. H.; Liu, S.; Telg, H.; Thornberry, T. D.; Rollins, A. W.; Portmann, R. W.; Bai, Z.; Ray, E. A.; Duan, Y.; Pan, L. L.; Toon, O. B.; Bian, J.; Gao, R. S. Efficient transport of tropospheric aerosol into the stratosphere via the asian summer monsoon anticyclone. *Proc. Natl. Acad. Sci. U. S. A.* **2017,** *114*, 6972-6977.

169. Shiraiwa, M.; Li, Y.; Tsimpidi, A. P.; Karydis, V. A.; Berkemeier, T.; Pandis, S. N.; Lelieveld, J.; Koop, T.; Poschl, U. Global distribution of particle phase state in atmospheric secondary organic aerosols. *Nat. Commun.* **2017,** *8*, 15002.

170. Murphy, D. M.; Cziczo, D. J.; Hudson, P. K.; Thomson, D. S. Carbonaceous material in aerosol particles in the lower stratosphere and tropopause region. *J. Geophys. Res.: Atmos.* **2007,** *112*.

171. Rapf, R. J.; Vaida, V. Sunlight as an energetic driver in the synthesis of molecules necessary for life. *Phys. Chem. Chem. Phys.* **2016,** *18*, 20067-20084.

172. Handley, S. R.; Clifford, D.; Donaldson, D. J. Photochemical loss of nitric acid on organic films: A possible recycling mechanism for NO_x. *Environ. Sci. Technol.* **2007,** *41*, 3898-3903.

173. De Laurentiis, E.; Socorro, J.; Vione, D.; Quivet, E.; Brigante, M.; Mailhot, G.; Wortham, H.; Gligorovski, S. Phototransformation of 4-phenoxyphenol sensitised by 4-carboxybenzophenone: Evidence of new photochemical pathways in the bulk aqueous phase and on the surface of aerosol deliquescent particles. *Atmos. Environ.* **2013,** *81*, 569-578.

174. Rossignol, S.; Aregahegn, K. Z.; Tinel, L.; Fine, L.; Noziere, B.; George, C. Glyoxal induced atmospheric photosensitized chemistry leading to organic aerosol growth. *Environ. Sci. Technol.* **2014,** *48*, 3218-3227.

175. Li, W. Y.; Li, X.; Jockusch, S.; Wang, H.; Xu, B.; Wu, Y.; Tsui, W. G.; Dai, H. L.; McNeill, V. F.; Rao, Y. Photoactivated production of secondary organic species from isoprene in aqueous systems. *J. Phys. Chem. A* **2016,** *120*, 9042-9048.

176. González Palacios, L.; Corral Arroyo, P.; Aregahegn, K. Z.; Steimer, S. S.; Bartels-Rausch, T.; Nozière, B.; George, C.; Ammann, M.; Volkamer, R. Heterogeneous photochemistry of imidazole-2-carboxaldehyde: HO_2 radical formation and aerosol growth. *Atmos. Chem. Phys.* **2016,** *16*, 11823-11836.

177. Tinel, L.; Dumas, S.; George, C. A time-resolved study of the multiphase chemistry of excited carbonyls: Imidazole-2-carboxaldehyde and halides. *C. R. Chim.* **2014,** *17*, 801-807.

178. Estimated diffusion coefficients in air and water - extended version. https://www3.epa.gov/ceampubl/learn2model/part-two/onsite/estdiffusion-ext.html (accessed June 7, 2017).

179. Nguyen, T. B.; Laskin, J.; Laskin, A.; Nizkorodov, S. A. Nitrogen-containing organic compounds and oligomers in secondary organic aerosol formed by photooxidation of isoprene. *Environ. Sci. Technol.* **2011,** *45*, 6908-6918.

180. Kawamura, K.; Yasui, O. Diurnal changes in the distribution of dicarboxylic acids, ketocarboxylic acids and dicarbonyls in the urban tokyo atmosphere. *Atmos. Environ.* **2005,** *39*, 1945-1960.

181. Klán, P.; Wirz, J. Chemistry of excited molecules. In *Photochemistry of organic compounds*, John Wiley & Sons, Ltd: 2009, pp 227-453.

182. Kautzman, K. E.; Surratt, J. D.; Chan, M. N.; Chan, A. W.; Hersey, S. P.; Chhabra, P. S.; Dalleska, N. F.; Wennberg, P. O.; Flagan, R. C.; Seinfeld, J. H. Chemical composition of gas- and aerosol-phase products from the photooxidation of naphthalene. *J. Phys. Chem. A* **2010,** *114*, 913-934.

183. Andreae, M. O.; Gelencser, A. Black carbon or brown carbon? The nature of light-absorbing carbonaceous aerosols. *Atmos. Chem. Phys.* **2006,** *6*, 3131-3148.

184. Atkinson, R. Gas-phase tropospheric chemistry of volatile organic compounds .1. Alkanes and alkenes. *J. Phys. Chem. Ref. Data* **1997,** *26*, 215-290.

185. Asner, G. P.; Scurlock, J. M. O.; Hicke, J. A. Global synthesis of leaf area index observations: Implications for ecological and remote sensing studies. *Global. Ecol. Biogeogr.* **2003,** *12*, 191-205.

186. Holopainen, J. K. Multiple functions of inducible plant volatiles. *Trends Plant Sci.* **2004,** *9*, 529-533.

187. Renbaum-Wolff, L.; Grayson, J. W.; Bateman, A. P.; Kuwata, M.; Sellier, M.; Murray, B. J.; Shilling, J. E.; Martin, S. T.; Bertram, A. K. Viscosity of α-pinene secondary organic material and implications for particle growth and reactivity. *Proc. Natl. Acad. Sci. U. S. A.* **2013,** *110*, 8014-8019.

188. Shugart, H. H.; Leemans, R.; Bonan, G. B. *A systems analysis of the global boreal forest*. Cambridge University Press: Cambridge, 1992.

189. Day, T. *Taiga*. Infobase Publishing: Chicago, 2006.

190. Janson, R.; de Serves, C. Acetone and monoterpene emissions from the boreal forest in northern Europe. *Atmos. Environ.* **2001,** *35*, 4629-4637.

191. Rinne, J.; Back, J.; Hakola, H. Biogenic volatile organic compound emissions from the Eurasian taiga: Current knowledge and future directions. *Boreal Environ. Res.* **2009,** *14*, 807-826.

192. de Rigo, D.; Caudullo, G.; Houston Durrant, T.; San-Miguel-Ayanz, J. The european atlas of forest tree species: Modelling, data and information on forest tree species. *European Atlas of Forest Tree Species* **2016**.

193. Schobesberger, S.; Lopez-Hilfiker, F. D.; Taipale, D.; Millet, D. B.; D'Ambro, E. L.; Rantala, P.; Mammarella, I.; Zhou, P. T.; Wolfe, G. M.; Lee, B. H.; Boy, M.; Thornton, J. A. High upward fluxes of formic acid from a boreal forest canopy. *Geophys. Res. Lett.* **2016,** *43*, 9342-9351.

194. Millet, D. B.; Baasandorj, M.; Farmer, D. K.; Thornton, J. A.; Baumann, K.; Brophy, P.; Chaliyakunnel, S.; de Gouw, J. A.; Graus, M.; Hu, L.; Koss, A.; Lee, B. H.; Lopez-Hilfiker, F. D.; Neuman, J. A.; Paulot, F.; Peischl, J.; Pollack, I. B.; Ryerson, T. B.; Warneke, C.; Williams, B. J.; Xu, J. A large and ubiquitous source of atmospheric formic acid. *Atmos. Chem. Phys.* **2015,** *15*, 6283-6304.

195. Paulot, F.; Wunch, D.; Crounse, J. D.; Toon, G. C.; Millet, D. B.; DeCarlo, P. F.; Vigouroux, C.; Deutscher, N. M.; Abad, G. G.; Notholt, J.; Warneke, T.; Hannigan, J. W.; Warneke, C.; de Gouw, J. A.; Dunlea, E. J.; De Maziere, M.; Griffith, D. W. T.; Bernath, P.; Jimenez, J. L.; Wennberg, P. O. Importance of secondary sources in the atmospheric budgets of formic and acetic acids. *Atmos. Chem. Phys.* **2011,** *11*, 1989-2013.

196. Yatavelli, R. L. N.; Mohr, C.; Stark, H.; Day, D. A.; Thompson, S. L.; Lopez-Hilfiker, F. D.; Campuzano-Jost, P.; Palm, B. B.; Vogel, A. L.; Hoffmann, T.; Heikkinen, L.; Aijala, M.; Ng, N. L.; Kimmel, J. R.; Canagaratna, M. R.; Ehn, M.; Junninen, H.; Cubison, M. J.; Petaja, T.; Kulmala, M.; Jayne, J. T.; Worsnop, D. R.; Jimenez, J. L. Estimating the contribution of organic acids to northern hemispheric continental organic aerosol. *Geophys. Res. Lett.* **2015,** *42*, 6084-6090.

197. Faiola, C. L.; Jobson, B. T.; VanReken, T. M. Impacts of simulated herbivory on volatile organic compound emission profiles from coniferous plants. *Biogeosciences* **2015,** *12*, 527-547.

198. Blande, J. D.; Turunen, K.; Holopainen, J. K. Pine weevil feeding on norway spruce bark has a stronger impact on needle VOC emissions than enhanced ultraviolet-B radiation. *Environ. Pollut.* **2009,** *157*, 174-180.

199. Heiden, A. C.; Hoffmann, T.; Kahl, J.; Kley, D.; Klockow, D.; Langebartels, C.; Mehlhorn, H.; Sandermann, H.; Schraudner, M.; Schuh, G.; Wildt, J. Emission of volatile organic compounds from ozone-exposed plants. *Ecological Applications* **1999,** *9*, 1160-1167.

200. Vuorinen, T.; Nerg, A. M.; Holopainen, J. K. Ozone exposure triggers the emission of herbivore-induced plant volatiles, but does not disturb tritrophic signalling. *Environ. Pollut.* **2004,** *131*, 305-311.

201. Loreto, F.; Barta, C.; Brilli, F.; Nogues, I. On the induction of volatile organic compound emissions by plants as consequence of wounding or fluctuations of light and temperature. *Plant, Cell Environ.* **2006,** *29*, 1820-1828.

202. Prado, F. E.; Rosa, M.; Prado, C.; Podazza, G.; Interdonato, R.; González, J. A.; Hilal, M. UV-B radiation, its effects and defense mechanisms in terrestrial plants. In *Environmental adaptations and stress tolerance of plants in the era of climate change*, Ahmad, P.; Prasad, M. N. V., Eds. Springer New York: New York, NY, 2012, pp 57-83.

203. Verdaguer, D.; Jansen, M. A.; Llorens, L.; Morales, L. O.; Neugart, S. UV-a radiation effects on higher plants: Exploring the known unknown. *Plant Sci.* **2017,** *255*, 72-81.

204. Harley, P.; Deem, G.; Flint, S.; Caldwell, M. Effects of growth under elevated UV-B on photosynthesis and isoprene emission in quercus gambelii and mucuna pruriens. *Global Change Biol.* **1996,** *2*, 149-154.

205. Katagi, T. Photodegradation of pesticides on plant and soil surfaces. In *Reviews of environmental contamination and toxicology: Continuation of residue reviews*, Ware, G. W., Ed. Springer New York: New York, NY, 2004, pp 1-78.

206. Dolinova, J.; Klanova, J.; Klan, P.; Holoubek, I. Photodegradation of organic pollutants on the spruce needle wax surface under laboratory conditions. *Chemosphere* **2004,** *57*, 1399-1407.

207. Holopainen, J. K.; Kivimaenpaa, M.; Nizkorodov, S. A. Plant-derived secondary organic material in the air and ecosystems. *Trends Plant Sci.* **2017,** *22*, 744-753.

208. Lee, B. H.; Lopez-Hilfiker, F. D.; Mohr, C.; Kurten, T.; Worsnop, D. R.; Thornton, J. A. An iodide-adduct high-resolution time-of-flight chemical-ionization mass spectrometer: Application to atmospheric inorganic and organic compounds. *Environ. Sci. Technol.* **2014,** *48*, 6309-6317.

209. Holopainen, J. K.; Gershenzon, J. Multiple stress factors and the emission of plant VOCs. *Trends Plant Sci.* **2010,** *15*, 176-184.